博士論文

Nonlinear dynamics in a parsimonious structured neural network
（非一様な結合が神経回路の非線形ダイナミクスに及ぼす影響について）

五十嵐　康彦

Abstract

Perception is highly robust to the presence of sensory noise. How to be robust to the external stimulus and to optimize neuronal performance have been intensely debated. As single neurons are not very informative, to obtain accurate information about sensory or motor variables some sort of population averaging must be performed. Moreover, how population codes are used in computations depend on whether or not the noise is correlated. If the noise is uncorrelated, meaning the fluctuations in the response of one neuron around its average are not correlated with the fluctuations of other neurons, population coding is relatively well understood. However, noise in the brain is correlated, which is mainly a consequence of interactions between two neurons and shared presynaptic input. We then have to take into consideration both mean firing rates and neural correlation of neural activities.

Not only sensory noise but also rapidly changes in incoming stimuli affect sensory coding. How to be robust and adapt rapidly to the external stimulus and to optimize neuronal performance have been intensely debated. To provide information about how the nervous system can implement the computation among sensory adaptation, we assume that a possible mechanism is short-term synaptic depression, which is local computation in each neuron, and investigate the relationship in short-term synaptic depression linking the role of information processing. We expanded the previous theoretical framework in this study to spiking neuron models with short-term synaptic depression and found that synaptic depression reduces neural correlation, which could be beneficial for sensory coding.

Electrophysiological experiments conducted in the field of neuroscience have recently shown that the manner in which information is represented using specific spiking and silence patterns over a group of neurons, is also understood both by the pairwise and higher-order correlated neural activities. However, very little is known about the relationships in the higher order correlations linking the role of information processing. To investigate the role of higher order correlations, we have studied whether higher-order correlations, especially 3rd-order correlations among neural activities, have the information of external inputs. We used a parsimonious network structure with common inputs and spiking nonlinearities, which can provide not only a firing rate tuning curve but also the relationship among the statistics gathered from neuronal response of primary visual cortex to a random stimulus. We found that the heterogeneous structure of this network

can dynamically control the structure of the higher-order correlations and can generate both sparse and synchronized neural activity. The 3rd-order correlations resulting from visual stimulation can carry stimulus-specific information these dynamics based on these dynamics.

These theory enables us to analytically calculate how local computations in each neuron, such as synaptic depression and spiking non-linearities, affect on neural activities. Based on the theory, we investigate how these local computations and the structured connectivity coordinate effects on information procession, especially sensory coding in primary visual cortex. Our study should open up the way for theoretical studies on information processing in structured neural network.

Acknowledgement

I am very grateful to my supervisor Prof. Masato Okada. He not only advised me on technical matters, but he also taught me how to plan work, and how to present my studies fluently. Because of the training he gave me, I have studied well and published two papers in the master's course. I thank my collaborator, Dr. Masafumi Oizumi, for Chapter 2 and 3. He gave me a insightful commenst, discussion, and taught me how to write and present my work when I start from ground zero. In heated discussions, he taught me what is important for theoretical neuroscience. I thank my laboratory members for enjoyable discussions and supporting my laboratory life. Especially, I thank Dr. Toshiaki Omori for beneficial comments about theoretical neuroscience and revising my paper. I collaborate on studies not included in but related to this theisi: Prof. Kazuyuki Aihara, Prof. Kazuo Okanoya, Dr. Kenji Nagata, Dr. Yuichi Katori, Dr. Kentro Katahira, Mr. Itsuki Yamashita, Mr. Ryo Karakida, Mr. Kenji Tanaka. Collaborating and discussing with them not just expanded my research interests and skills but deepened my views of each research themes. I acknowledge Mr. Kairi Mashio for publishing his excellent pictures, which are included in Fig.2.1. Finally, I wish to thank my family and soon-to-be wife for encouraging me in my everyday life. I will reply their favor for long periods.

Contents

Acknowledgement iii

Chapter 1 Introduction 1

Chapter 2 Theory of firing rates in stochastic neural network models with synaptic depression 6
2.1 Background 6
2.2 Model 8
2.3 Mean field theory 9
2.4 Network with uniform connections 12
2.5 Ring attractor network with Mexican hat type connectivity 18
2.6 Summary 33

Chapter 3 Theory of correlations in stochastic neural network models with synaptic depression 34
3.1 Background 34
3.2 Model 35
3.3 Theory of correlations 36
3.4 Ring attractor network with Mexican hat type connectivity 46
3.5 Discussion 56

Chapter 4 Higher-order correlation in a feed-forward network with inhomogeneous connectivity 60
4.1 Background 60
4.2 Model 61
4.3 Theory of higher-order correlations 63
4.4 Stimulus-specific decomposition of the mutual information (SSI) . . . 65
4.5 Results: Response to a random stimulus 67

4.6 Results: Prediction of responses to a grating stimulus 70
4.7 Results: Information theory for higher order correlations 73
4.8 Summary 75

Chapter 5 Conclusion 76

Appendix A Dimensionality reduction for stability analysis 80

Appendix B The order of input correlations 83
B.1 Equal-time correlation functions 83
B.2 Adjustment of external inputs 86

Bibliography 88

Chapter 1

Introduction

Perception is highly robust to the presence of sensory noise and adapt rapidly to changes in incoming stimuli. How to be robust and adapt rapidly to the external stimulus and to optimize neuronal performance have been intensely debated. A possible mechanism is local computation in each neuron, such as short-term synaptic plasticity and threshold non-linearity, because it is local computation and does not need to sum up their individual information. While short-term synaptic plasticity, that is activity-dependent changes over milliseconds to minutes in synaptic transmission, could allow adaptive computations in neural circuits (Zucker and Regehr 2002), threshold non-linearity produces higher-order correlations and could induce synchronous firing and temporal train-patterns (Amari et al., 2003). However, because of their dynamical synapses, it is difficult to evaluate their macroscopic effects on information processing.

Here, we propose a theoretical framework for neural network models with two types of local computation, that is, synaptic depression and threshold non-linearity. To evaluate clearly the functional role of these local computations, we compare the results of homogeneous network model and parsimonious structured network model, which is observed in various brain regions (Ko et al., 2011), and study how the structured connectivity modulate neural dynamics and the estimation of information.

Neural encoding is an algorithms to predict a given stimulus or behaviour from the pattern of neuronal responses, that is spike trains (Dayan and Abbott 2001). We can catalog how neural respond to a wide variety of stimuli, and then construct models that attempt to predict response to other stimuli. Neural coding thus refers to the map from stimulus to response. Neural decoding refers to the reverse map, from response to stimulus, and the challenge is to reconstruct a stimulus, or certain aspects of that stimulus, from the spike sequences it evokes.

The most important characteristic of the encoding process in the brain is that neurons stochastically respond to stimuli. The same visual stimulus does not evoke the same response of neurons. This means that the brain must confront with the uncertainty of stimuli due to the noise inherent in the nervous system. As single neurons are not very informative, to obtain accurate information about sensory or motor variables some sort of population averaging must be performed. Individual neurons thus count for little; it is population activity that matters. For example, as with control of eye (Lee et al. 1988) and arm (Georgopoulos et al. 1986) movements, visual discrimination in the primary visual cortex (V1) is much more accurate than would be predicted from the responses of single neurons (Paradiso 1988). If the encoding process is noisy and imperfect, the decoding process in the brain also has to be imperfect and perceptual misinterpretation in difficult cognitive tasks originate in the stochastic firing of neurons (Newsome et al. 1989, Britten et al. 1992, Salzman et al. 1992, Celebrini and Newsome 1994).

Exactly how this averaging is carried out in the brain, however, and especially how population codes are used in computations (such as reaching for an object on the basis of visual cues, an action that requires a transformation from population codes in visual areas to those in motor areas), is not fully understood. Part of the difficulty in understanding population coding is the nature of the the neuronal noise, and especially on whether or not the noise is correlated. If the noise is uncorrelated, meaning the fluctuations in the response of one neuron around its average are not correlated with the fluctuations of other neurons, population coding is relatively well understood (Averbeck, Latham and Pouget 2006). Unfortunately, noise in the brain is correlated (Zohary et al 1994), which is mainly a consequence of interactions between two neurons (Perkel et al. 1967, Singer 1999) and shared presynaptic input (Shadlen and Newsome 1998, Kriener et al. 2008, Ecker et al. 2010, Renart et al. 2010). Because of the correlated noise, we need to take a second look at the results that have been obtained under the assumption of independent noise. This means extending the theories to take into account correlated noise.

As discussed previously, a possible mechanism to adapt rapidly to changes in incoming stimuli and percept the environment is short-term synaptic plasticity. It is clear that we cannot understand neural coding or information processing in perception of the environment without taking synaptic dynamics into account. Here, we investigate how short-term synaptic plasticity affects information processing and discuss their implications for neuronal coding and signaling. In Chapter 2 and 3, Here, using mean field analysis, we propose a theoretical framework for neural network models with short-term synaptic

plasticity to evaluate how short-term synaptic plasticity affects firing rates, neural correlations and Fisher information. We then investigate parameter regions where synaptic depression increases the Fisher information by systematically changing the strengths of the homogeneous and lateral-inhibitory synaptic connection and discuss the mechanism of belief adaptation effects in primary visual cortex.

In Chapter 2, we investigated the effects of synaptic depression on a macroscopic behavior of stochastic neural networks, namely the firing rate. Dynamical mean field equations were derived for such networks by taking the average of two stochastic variables: a firing-state variable and a synaptic variable. In these equations, the average product of these variables is decoupled as the product of their averages because synaptic depression is activity-dependent and leads to the Independence of the two stochastic variable. We proved the independence of these two stochastic variables assuming that the synaptic weight J_{ij} is of the order of $1/N$ with respect to the number of neurons N. Using these equations, we derived macroscopic steady-state equations for a network with uniform connections and for a ring attractor network with Mexican hat type connectivity, which is used as a model of the primary visual cortex and prefrontal cortex (Ben-Yishai et al. 1995, Compte et al. 2000), and investigated the stability of the steady-state solutions. An oscillatory uniform state was observed in the network with uniform connections owing to a Hopf instability. For the ring network, high-frequency perturbations were shown not to affect system stability. Two mechanisms destabilize the inhomogeneous steady state, leading to two oscillatory states. A Turing instability leads to a rotating bump state, while a Hopf instability leads to an oscillatory bump state, which was previously unreported. Various oscillatory states take place in a network with synaptic depression depending on the strength of the interneuron connections.

Synaptic depression affects not only firing rates of neurons, but also mean and variability of neural correlations, which affects efficacy of population coding. Even small correlations between neurons can have greatly affect the efficiency of a population of neurons to encode information. Although previous studies constructed such a theory of correlation in a spiking neuron model including the time course of postsynaptic potential and refractory properties by using the framework of mean-field theory (Ginzburg and Sompolinsky 1994, Meyer and van Vreeswijk 2002), synaptic depression has not been taken into consideration. In Chapter 3, we extended the previous theoretical framework to spiking neuron models with short-term synaptic depression. On the basis of this theory, we analytically calculated neural correlations for a ring attractor network with Mexican hat type connectivity and found that synaptic depression greatly reduces neural correlation, which can

improve population coding accuracy (Abbott and Dayan 1999).

The reduction of both firing rates and rate correlation due to synaptic depression, which is previously discussed in Chapter 2 and 3, have the opposite effects on the accuracy of population coding. Whether the Fisher information increases or not as a combinational effect is determined by which effects are stronger. However, it is unknown how both changes in firing rates and neural correlations due to synaptic depression affect on the accuracy of a population code. In the latter part of Chapter 3, by taking into consideration both changes, we aim to analytically compute the Fisher information to evaluate the effects of synaptic depression on an upper bound to the accuracy that any decoder can achieve (Seung and Sompolinsky 1993, Abbott and Dayan 1999). We then investigate parameter regions where synaptic depression increases the Fisher information by systematically changing the strengths of the homogeneous and lateral-inhibitory synaptic connection and discuss the mechanism of belief adaptation effects in primary visual cortex.

So far, we discuss only about the sensory information transmitted by firing rates and pair-wise correlations between neurons. However, the widely observed complex features of population activity, such as synchronization and concentration patterns of suspension, can be captured not only by pairwise correlations but also by higher-order correlations, which have significant effects on complicated physical processes and information processing. In neuroscience, electrophysiological experiments have recently shown that the manner in which information is represented by specific patterns of spiking and silence over a group of neurons, is also understood both by the pairwise and higher-order correlated neural activities. But, very little is known about the relationships the higher-order correlations linking the role of information procening, that is, whether higher-order correlations between neuronal activities could allow neurons to robustly and rapidly transmit sensory or motion information.

In Chapter 4, we investigated a parsimonious structured network with common inputs and spiking non-linearities to investigate the effects of structured connectivities on higher-order correlations, which are recently observed in various brain regions. Although in the previous chapter we derive neural correlations based on the fluctuation-dissipation theory for investigating changes in the equilibrium order parameters, due to sufficiently weak externally applied perturbations (Ginzburg and Sompolinsky 1994), this network model cannot reproduce there are no equilibrium order parameters and we cannot apply the fluctuation-dissipation theory to network model (Amari et al., 2003, Macke et al., 2011). We then constructed a parsimonious structured network with common inputs and spiking non-linearities as a model of orientation selectivity and theoretically investigate the effects

of structured connectivity on higher-order correlations.

This thesis is organized as follows. In Chapter 2, [*1] we have explored the macroscopic properties of two types of stochastic binary neural networks with synaptic depression: a network with homogeneous connectivity and a ring attractor network with Mexican hat type connectivity. Comparing the macroscopic properties, especially firing rates, between the two types network model, we investigate the effects of structured connectivities on the neural dynamics induced by synaptic depression. Synaptic depression affects not only the mean responses of neurons but also the correlation of response variability in neural populations. In Chapter 3, [*2] we investigated how synaptic depression affects neural correlations in a ring attractor network with Mexican- hat- type connectivity. In Chapter 4, we investigated a parsimonious structured network with common inputs and spiking non-linearities. Whether or not structured connectivity are important for higher-order correlations, which are recently observed in various brain regions. In Chapter 5, we present a summary of this thesis and discuss future directions.

[*1] Preliminary results for the present work have been published elsewhere (Igarashi et al. 2009, Igarashi et al. 2010). Published under licence in *Statistical mechanics of attractor neural network models with synaptic depression* by IOP Publishing Ltd, and *Mean Field Analysis of Stochastic Neural Network Models with Synaptic Depression* by the Physical Society of Japan. Content from this work may be used under the terms of the Creative Commons Attribution 3.0 licence. Any further distribution of this work must maintain attribution to the authors and the title of the work, journal citation and DOI.

[*2] Preliminary results for the present work also have been published elsewhere (Igarashi et al. 2012). Published under licence in *Theory of correlation in a network with synaptic depression* by APS Publishing Ltd. Content from this work may be used under the terms of the Creative Commons Attribution 3.0 licence. Any further distribution of this work must maintain attribution to the authors and the title of the work, journal citation and DOI.

Chapter 2

Theory of firing rates in stochastic neural network models with synaptic depression

2.1 Background

Neurophysiological experiments have shown that high-frequency inputs reduce the efficacy of signal transmission owing to the exhaustion of neurotransmitters (Thomson and Deuchars 1994). This phenomenon, called "synaptic depression", enables dynamic gain control by reducing presynaptic inputs (Abbott et al. 1997, Tsodyks and Markram 1997, Rothman et al. 2009). Synaptic depression not only affects the activity of a single neuron but also the overall activity in neural networks (Abbott and Regehr 2004). Synaptic depression can allow synapses to perform critical computational functions in neural circuits such as adaptation to external stimuli and short-term memory (Abbott and Regehr 2004, Tsodyks and Gilbert 2004, Kohn 2007). However, systems with synaptic depression cannot be analyzed by the conventional equilibrium statistical-mechanical approach owing to the asymmetry of connections. Thus, we propose a dynamical mean field theory for a stochastic binary neural network model with synaptic depression to explore the effects of synaptic depression on the macroscopic behavior of stochastic neural networks. Preliminary results for the present work have been published elsewhere (Igarashi et al. 2009, Igarashi et al. 2010).

To observe the macroscopic behavior of the network, we reduced the stochastic neural network model with synaptic depression to microscopic dynamical mean field

equations by taking the average of two stochastic variables, a firing-state variable and a synaptic variable, over different realizations of stochastic spikes. Because in the equations the averaged product of the two stochastic variables is decoupled as the product of their averages, they must be independent. We demonstrated such independence for a non frustrated system and derived microscopic dynamical mean field equations for a stochastic binary neural network model with synaptic depression. The derived equations coincide with those of an analog neural network with synaptic depression(Abbott et al. 1997, Tsodyks and Markram 1997, Tsodyks et al. 1998). Using these microscopic equations, we derived macroscopic steady-state equations and analyzed their stability for two types of neural network: one with uniform connections and one with Mexican hat type connections(York and van Rossum 2009, Kilpatrick and Bressloff 2010, Kilpatrick and Bressloff 2010). A network with uniform connections is the simplest type of network, for which the effect of synaptic depression has been previously studied(Tsodyks et al. 1998). A ring neural network with Mexican hat type connections has nonuniform connectivity and has been used as a model of the primary visual cortex and prefrontal cortex(Ben-Yishai et al. 1995, Compte et al. 2000). Although several researchers have reported that synaptic depression in the ring network leads to an oscillatory state, which is called a "rotating bump" (RB) state or a "traveling wave" state, little is known about the cause of the oscillation(York and van Rossum 2009, Kilpatrick and Bressloff 2010, Kilpatrick and Bressloff 2010).

We assume that oscillatory instability is caused by synaptic depression because a neural network with synaptic depression can be considered as an activator-inhibitor system in which firing rate is an activator and synaptic variable is an inhibitor. As discussed by Kuramoto et al., the activator-inhibitor system can induce an oscillatory instability (a Hopf instability) (Kuramoto 2003). To test the assumption, we first discuss a network with uniform connections. Owing to its simplicity, we can reduce the network to a model with only two components in which an oscillatory instability (a Hopf instability) can exist. This reduction enables us to easily understand why synaptic depression causes oscillatory instability. We first show that an oscillatory uniform (OU) state appears owing to the presence of synaptic depression. Although it has been reported that synaptic depression leads to an oscillatory state in a network with non uniform connections(York and van Rossum 2009, Kilpatrick and Bressloff 2010, Kilpatrick and Bressloff 2010), an oscillatory state has not been reported for a network with uniform connections.

Next, we show that, in a ring network with Mexican hat type connections, synaptic depression leads to three oscillatory states: the OU state, the RB state, and an oscillatory

bump (OB) state, which was previously unreported. To investigate the mechanisms of steady-state destabilization that lead to these oscillatory states, we analyzed the stability of the steady-state solutions when there are frequency perturbations. In §2.5, we show that high-frequency perturbations do not affect the system stability and that two mechanisms destabilize an inhomogeneous steady state, leading to the two oscillatory states, i.e., the RB and OB states. Analytical and numerical investigation of the ring network with synaptic depression revealed a phase diagram in which a wealth of states and multistable regimes can be discerned.

2.2 Model

We used a recurrent neural network with N neurons. The state of the ith neuron at time t is represented by $s_i(t)$. The state takes either a resting state, $s_i(t) = 0$, or a firing-state, $s_i(t) = 1$. Each neuron follows a probabilistic dynamic:

$$\mathrm{Prob}[s_i(t+1) = 1] \equiv g_\beta[h_i(t)], \tag{2.1}$$

$$g_\beta[h_i(t)] = \frac{1}{2}\left\{1 + \tanh[\beta h_i(t)]\right\}, \tag{2.2}$$

where $h_i[= \sum_{j\neq i}^{N} J_{ij}[2x_j(t)s_j(t) - 1]]$ represents the total synaptic current arriving at neuron i, and $1/\beta(= T)$ is the level of noise due to the stochastic synaptic activity. At each time step, all neurons are updated in parallel. J_{ij} is a fixed synaptic weight from the jth neuron to the ith neuron. $x_j(t)(0 < x_j(t) \leq 1)$ denotes the efficacy of signal transmission at the jth neuron, which dynamically changes with synaptic depression. $x_j(t)$ is determined by the corresponding neuron state and itself at the preceding time $t-1$:

$$x_j(t) = x_j(t-1) + \frac{1 - x_j(t-1)}{\tau} - U_{\mathrm{se}} x_j(t-1)s_j(t-1). \tag{2.3}$$

In this model, the synaptic connection $J_{ij}(t)(= J_{ij}x_j(t))$ dynamically changes with the efficacy of signal transmission $x_j(t)$. The phenomenological model of synaptic depression described by eq. (2.3) was proposed by several researchers(Abbott et al. 1997, Tsodyks and Markram 1997). A schematic of this model is shown in Fig. 2.1. Information from one neuron (presynaptic neuron) flows to another neuron (postsynaptic neuron) across a synapse. A synapse is a small gap separating neurons and consists of a presynaptic ending that contains neurotransmitters stored in synaptic vesicles, a postsynaptic ending containing receptor sites for neurotransmitters, and a synaptic cleft, or space, between the presynaptic and postsynaptic endings [Fig. 2.1(a)]. An action potential cannot cross the

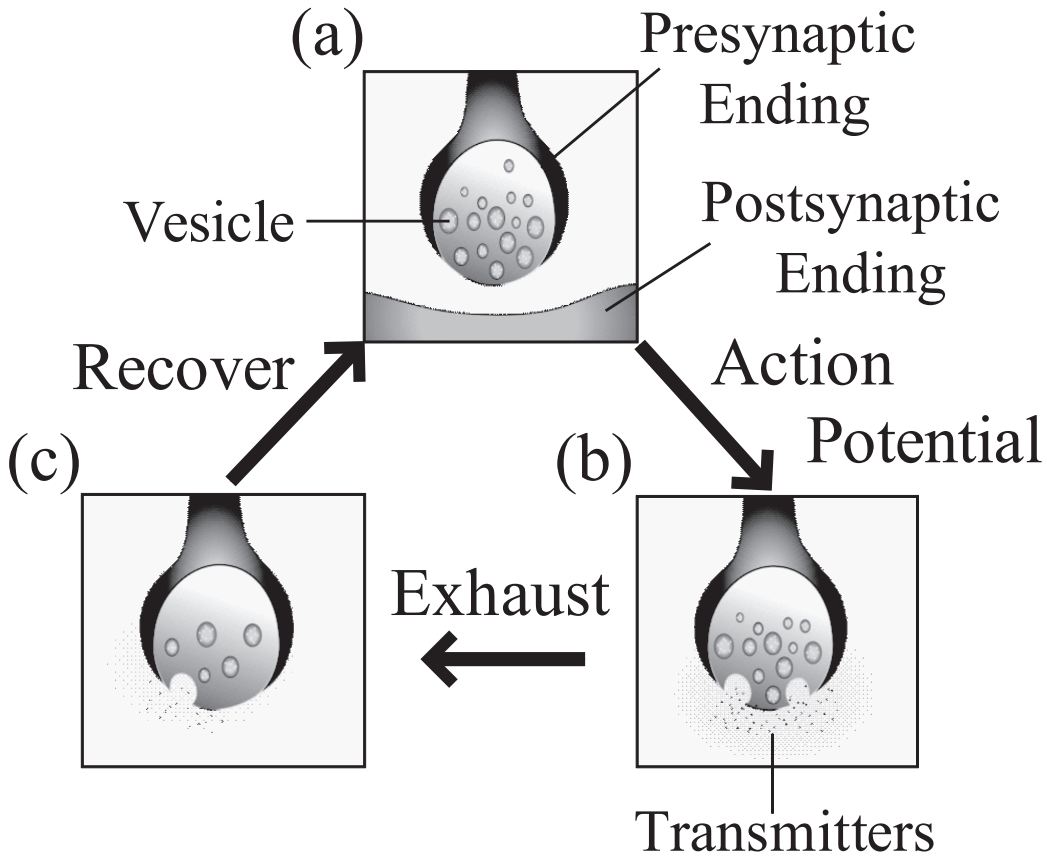

Fig. 2.1. Schematic of phenomenological model of synaptic depression.

synaptic cleft between neurons. Instead, the nerve impulse is carried by chemicals called neurotransmitters [Fig. 2.1(b)]. The cell receiving the nerve impulse (the postsynaptic neuron) has chemical-gated ion channels, called neuroreceptors, in its membrane. The presynaptic neurons exhaust neurotransmitters when they transmit signals. The efficacy of signal transmission at presynaptic neuron j at time t decreases by a certain fraction, $U_{\rm se}x_j(t-1)(0 < U_{\rm se} \leq 1)$, after the firing of the presynaptic neuron, $s_j(t-1) = 1$ [Fig. 2.1(c)], and recovers with time constant $\tau(\tau \geq 1)$, as shown in eq. (2.3).

2.3 Mean field theory

We propose a dynamical mean field theory for a stochastic binary neural network model with synaptic depression assuming that synaptic weight J_{ij} is of the order of $1/N$ with respect to the number of neurons, N.

2.3.1 Microscopic mean field theory

We derived microscopic dynamical mean field equations by first taking the noise average of the firing-state variable at time t:

$$\langle s_i(t+1)\rangle = g_\beta[\langle h_i(t)\rangle], \tag{2.4}$$

$$\langle h_i(t)\rangle = \sum_{j\neq i}^{N} J_{ij}[2\langle x_j(t)s_j(t)\rangle - 1]. \tag{2.5}$$

Similarly, we consider the noise average of eq. (2.3) for the synaptic variable:

$$\langle x_j(t+1)\rangle = \langle x_j(t)\rangle + \frac{1-\langle x_j(t)\rangle}{\tau} - U_{\rm se}\langle x_j(t)s_j(t)\rangle. \tag{2.6}$$

It is evident that $x_i(t+\tau)$ and $s_i(t)$ are correlated when $\tau > 0$. However, equal time correlations between $s_i(t)$ and $x_i(t)$ are of the order of $1/N$; that is, $x_i(t)$ and $s_i(t)$ become independent when $N \to \infty$, as we will show below.

Here, we define $\delta x_i(t) = x_i(t) - \langle x_i(t)\rangle$ and $\delta s_i(t) = s_i(t) - \langle s_i(t)\rangle$. Substituting eq. (2.1) for $\langle \delta x_i(t)\delta s_i(t)\rangle$, we obtain

$$\langle \delta x_i(t)\delta s_i(t)\rangle = \langle \delta x_i(t) g_\beta\left[h_i(t-1)\right]\rangle. \tag{2.7}$$

Taylor expansion gives

$$g_\beta\left[h_i(t-1)\right] = g_\beta\left[\langle h_i(t-1)\rangle\right] + g'_\beta\left[\langle h_i(t-1)\rangle\right]\delta\left[h_i(t-1)\right] + \ldots. \tag{2.8}$$

Neglecting the higher-order terms yields

$$\langle \delta x_i(t)\delta s_i(t)\rangle = g'_\beta\left[\langle h_i(t-1)\rangle\right]\langle \delta h_i(t-1)\delta x_i(t)\rangle \tag{2.9}$$

$$= g'_\beta\left[\langle h_i(t-1)\rangle\right]\sum_{j\neq i}^{N} J_{ij}\langle \delta\left[x_j(t-1)s_j(t-1)\right]\delta x_i(t)\rangle. \tag{2.10}$$

We evaluate the order of the right-hand side of eq. (2.10):

$$\langle \delta\left[x_j(t-1)s_j(t-1)\right]\delta x_i(t)\rangle = \langle x_j(t-1)\rangle\langle \delta s_j(t-1)\delta x_i(t)\rangle + \langle s_j(t-1)\rangle\langle \delta x_j(t-1)\delta x_i(t)\rangle + \langle \delta x_j(t-1)\delta s_j(t-1)\delta x_i(t)\rangle. \tag{2.11}$$

$\langle \delta(x_j(t-1)s_j(t-1))\delta x_i(t)\rangle$ is of the order of $1/N$ because the time-delayed cross-correlation is of the order of $1/N$(Ginzburg and Sompolinsky 1994). Since we have assumed $J_{ij} \sim$

$O(1/N)$, we obtain

$$\sum_{j\neq i}^{N} J_{ij}\langle\delta\left[x_j(t-1)s_j(t-1)\right]\delta x_i(t)\rangle \sim O(1/N), \tag{2.12}$$

and the equal-time correlations between $s_i(t)$ and $x_i(t)$, $\langle\delta x_i(t)\delta s_i(t)\rangle$, disappear in the limit of large networks, $N\to\infty$:

$$\left\langle x_i(t)s_i(t)\right\rangle = \langle x_i(t)\rangle\langle s_i(t)\rangle. \tag{2.13}$$

Taking advantage of the independence of $x_i(t)$ and $s_i(t)$, we obtained the dynamical mean field equations for $m_i(t)$ and $X_i(t)$:

$$m_i(t+1) = g_\beta\left\{\sum_{j\neq i}^{N} J_{ij}\left[2m_j(t)X_j(t)-1\right]\right\}, \tag{2.14}$$

$$X_i(t+1) = X_i(t) + \frac{1-X_i(t)}{\tau} - U_{\rm se}X_i(t)m_i(t), \tag{2.15}$$

where $m_i(t)\equiv\langle s_i(t)\rangle$ and $X_i(t)\equiv\langle x_i(t)\rangle$. These equations for the stochastic neural network model coincide with those for an analog neural network with synaptic depression(Tsodyks et al. 1998). The steady-state equation for noise average $X_j = X_j(\infty)$ is

$$X_j = \frac{1}{1+\gamma m_j}, \quad \gamma = \tau U_{\rm se}, \tag{2.16}$$

which is a finite-temperature version obtained in the $T=0$ case(Matsumoto et al. 2007). Finally, we obtain the microscopic steady-state equation for $m_i[=m_i(\infty)]$ for a network with synaptic depression:

$$m_i = g_\beta\left[\sum_{j\neq i}^{N} J_{ij}\left(\frac{2m_j}{1+\gamma m_j}-1\right)\right]. \tag{2.17}$$

According to eq. (2.17), the steady state depends on $\gamma(=\tau U_{\rm se})$(Tsodyks et al. 1998).

2.3.2 Stability analysis

To examine the stability of the steady state obtained with eq. (2.17), we consider small deviations around a fixed point(Tsodyks et al. 1998, York and van Rossum 2009, Hansel and Sompolinsky 1998):

$$m_i(t) = m_i + \delta m_i(t), \quad X_i(t) = X_i + \delta X_i(t), \tag{2.18}$$

where $X_i = \frac{1}{1+\gamma m_i}$. We linearize eqs. (2.14) and (2.15) about the steady-state solution. Neglecting the higher-order terms, we obtain

$$\delta m_i(t+1) = \sum_{j \neq i} \left[\frac{\partial g_\beta(h_i)}{\partial m_j} \delta m_j(t) + \frac{\partial g_\beta(h_i)}{\partial X_j} \delta X_j(t) \right], \tag{2.19}$$

$$h_i = \sum_{j \neq i} J_{ij} \left(2 m_j X_j - 1\right). \tag{2.20}$$

Similarly,

$$\delta X_i(t+1) = -U_{\mathrm{se}} X_i \delta m_i(t) + \left(1 - \frac{1}{\tau} - U_{\mathrm{se}} m_i\right) \delta X_i(t). \tag{2.21}$$

Next we calculate the partial differential coefficients $\frac{\partial g_\beta(h_i)}{\partial m_j}$ and $\frac{\partial g_\beta(h_i)}{\partial X_j}$ of eq. (2.19) in more detail.

$$\frac{\partial g_\beta(h_i)}{\partial m_j} = \frac{\partial g_\beta(h_i)}{\partial h_i} \frac{\partial h_i}{\partial m_j} \tag{2.22}$$

$$= \beta J_{ij} X_j \left\{ 1 - \left[\tanh \beta(h_i)\right]^2 \right\} \tag{2.23}$$

Substituting the steady-state equation. (2.17) into eq. (2.23), we obtain

$$\frac{\partial g_\beta(h_i)}{\partial m_j} = 4\beta J_{ij} X_j \left(m_i - m_i^2\right). \tag{2.24}$$

Similarly, we have

$$\frac{\partial g_\beta(h_i)}{\partial X_j} = 4\beta J_{ij} m_j \left(m_i - m_i^2\right). \tag{2.25}$$

Substituting eqs. (2.24) and (2.25) into eq. (2.19) yields

$$\delta m_i(t+1) = \sum_{j \neq i} 4\beta J_{ij} \left(m_i - m_i^2\right) \left[X_j \delta m_j(t) + m_j \delta X_j(t)\right]. \tag{2.26}$$

From the relations for the coefficients of eqs. (2.21) and (2.26), we obtain the Jacobian matrix for the system (York and van Rossum 2009). The Jacobian matrix K has a size of $2N \times 2N$ with the following matrix:

$$K^{ij} \equiv \begin{pmatrix} K^{ij}_{mm} & K^{ij}_{mX} \\ K^{ij}_{Xm} & K^{ij}_{XX} \end{pmatrix}, \quad \begin{pmatrix} \delta m_i(t+1) \\ \delta X_i(t+1) \end{pmatrix} = K^{ij} \begin{pmatrix} \delta m_j(t) \\ \delta X_j(t) \end{pmatrix}, \tag{2.27}$$

$$K^{ij}_{mm} = 4\beta J_{ij}(m_i - m_i^2) X_j, \quad K^{ij}_{mX} = 4\beta J_{ij}(m_i - m_i^2) m_j, \tag{2.28}$$

$$K^{ij}_{Xm} = -\delta_{ij} U_{\mathrm{se}} X_j, \quad K^{ij}_{XX} = \delta_{ij} \left(1 - \frac{1}{\tau}\right) - U_{\mathrm{se}} m_j, \tag{2.29}$$

where $1 \leq i, j \leq N$, and δ_{ij} is the Kronecker delta. If the Jacobian matrix has eigenvalues of 1 or less, the steady-state solution is stable.

2.4 Network with uniform connections

In a network with uniform connections,

$$J_{ij} = J_0/N. \tag{2.30}$$

2.4.1 Macroscopic steady-state equations

We derived macroscopic steady-state equations for a network with homogeneous connectivity by using the microscopic mean field equations (2.14) and (2.15). Given the symmetry of the synaptic weights in eq. (2.30), we can set the noise average of each neuron, m_i, to $m_i = \hat{m}_0$, where $\hat{m}_0 = \frac{1}{N}\sum_{i=1}^{N} m_i$. Substituting this condition into eq. (2.17), we obtain a macroscopic steady-state equation:

$$\hat{m}_0 = g_\beta \left[J_0 \left(\frac{2\hat{m}_0}{1+\gamma\hat{m}_0} - 1 \right) \right] \tag{2.31}$$

$$= \frac{1}{2}\left[1 + \tanh \beta J_0 \left(\frac{2\hat{m}_0}{1+\gamma\hat{m}_0} - 1 \right) \right]. \tag{2.32}$$

Equation. (2.32) gives the homogeneous steady-state solution.

2.4.2 Stability analysis

To examine the stability of the homogeneous steady-state solution obtained using eq. (2.32), namely, $m_i = \hat{m}_0$ and $X_i = \hat{X}_0$, we consider small deviations around a fixed point (Tsodyks et al. 1998, York and van Rossum 2009, Hansel and Sompolinsky 1998):

$$m_i(t) = \hat{m}_0 + \delta m_i(t), \quad X_i(t) = \hat{X}_0 + \delta X_i(t). \tag{2.33}$$

Substituting eqs. (2.30) and (2.33) into eqs. (2.19) and (2.26), we obtain

$$\delta m_i(t+1) = 4\beta J_0 \left(\hat{m}_0 - \hat{m}_0^2\right) \frac{1}{N} \sum_{j\neq i}^{N} \left[\hat{X}_0 \delta m_j(t) + \hat{m}_0 \delta X_j(t) \right]. \tag{2.34}$$

$$\delta X_i(t+1) = -U_{\mathrm{se}} \hat{X}_0 \delta m_i(t) + \left(1 - \frac{1}{\tau} - U_{\mathrm{se}} \hat{m}_0 \right) \delta X_i(t). \tag{2.35}$$

Since J_{ij} consists of the 0th Fourier component of J_0, discrete Fourier transform analysis can be used to diagonalize Jacobian matrix K [eq. (2.27)]. We therefore compute the

Fourier series for eqs. (2.34) and (2.35). The Fourier coefficients of $\delta m_i(t)$ and $\delta X_i(t)$ are given by

$$\delta\hat{m}_k(t) = \frac{1}{N}\sum_{i=1}^{N}\delta m_i(t)e^{\frac{-2\pi\mathrm{i}(ik)}{N}}, \quad \delta\hat{X}_k(t) = \frac{1}{N}\sum_{i=1}^{N}\delta X_i(t)e^{\frac{-2\pi\mathrm{i}(ik)}{N}}, \tag{2.36}$$

where i is the standard imaginary unit with the property $\mathrm{i}^2 = -1$. We then write $\delta m_i(t)$ and $\delta X_i(t)$ in Fourier series form:

$$\delta m_i(t) = \sum_{k=-\frac{N}{2}}^{\frac{N}{2}-1}\delta\hat{m}_k(t)e^{\frac{2\pi\mathrm{i}(ik)}{N}}, \quad \delta X_i(t) = \sum_{k=-\frac{N}{2}}^{\frac{N}{2}-1}\delta\hat{X}_k(t)e^{\frac{2\pi\mathrm{i}(ik)}{N}}. \tag{2.37}$$

Substituting eq. (2.37) for eqs. (2.34) and (2.35), we obtain

$$\sum_{k=-\frac{N}{2}}^{\frac{N}{2}-1}\delta\hat{m}_k(t+1)e^{\frac{2\pi\mathrm{i}(ik)}{N}} = 4\beta J_0\left(\hat{m}_0 - \hat{q}_0\right)\sum_{l=-\frac{N}{2}}^{\frac{N}{2}-1}\left[\hat{X}_0\delta\hat{m}_l(t) + \hat{m}_0\delta\hat{X}_l(t)\right]\frac{1}{N}\sum_{j\neq i}^{N}e^{\frac{2\pi\mathrm{i}(jl)}{N}}, \tag{2.38}$$

$$= 4\beta J_0\left(\hat{m}_0 - \hat{q}_0\right)\left[\hat{X}_0\delta\hat{m}_0(t) + \hat{m}_0\delta\hat{X}_0(t)\right], \tag{2.39}$$

$$\begin{aligned}\sum_{k=-\frac{N}{2}}^{\frac{N}{2}-1}\delta\hat{X}_k(t+1)e^{\frac{2\pi\mathrm{i}(ik)}{N}} &= \left(1-\frac{1}{\tau}\right)\sum_{l=-\frac{N}{2}}^{\frac{N}{2}-1}\delta\hat{X}_l(t)e^{\frac{2\pi\mathrm{i}(il)}{N}} \\ &\quad - U_{se}\sum_{l,l'=-\frac{N}{2}}^{\frac{N}{2}-1}\left[\delta\hat{m}_l(t)\hat{X}_{l'}(t) + \hat{m}_l(t)\delta\hat{X}_{l'}(t)\right]e^{\frac{2\pi\mathrm{i}\left[(l+l')i\right]}{N}},\end{aligned} \tag{2.40}$$

where $\hat{q}_k = \frac{1}{N}\sum_{i=1}^{N}(m_i)^2e^{\frac{-2\pi\mathrm{i}(ik)}{N}}$. We use the following equation in the limit of $N\to\infty$ to integrate the right side of eq. (2.38) with respect to j:

$$\frac{1}{N}\sum_{j\neq i}^{N}e^{\frac{2\pi\mathrm{i}(jl)}{N}} = \begin{cases}1 & (l=0)\\ 0 & (l\neq 0)\end{cases} \tag{2.41}$$

Since Fourier components are orthonormal, we can equate the coefficients of the Fourier components on the left and right sides. From the relations for the coefficients of eqs. (2.39) and (2.40), we obtain the Jacobian matrix for the system in Fourier space, H^{kk}:

$k = 0$

$$\begin{pmatrix} \delta m_0(t+1) \\ \delta X_0(t+1) \end{pmatrix} = H^{00} \begin{pmatrix} \delta \hat{m}_0(t) \\ \delta \hat{X}_0(t) \end{pmatrix} \tag{2.42}$$

$$= \begin{pmatrix} 4\beta J_0 \left(\hat{m}_0 - \hat{q}_0\right) \hat{X}_0 & 4\beta J_0 \left(\hat{m}_0 - \hat{q}_0\right) \hat{m}_0 \\ -U_{\rm se} \hat{X}_0 & 1 - \frac{1}{\tau} - U_{\rm se} \hat{m}_0 \end{pmatrix} \begin{pmatrix} \delta \hat{m}_0(t) \\ \delta \hat{X}_0(t) \end{pmatrix}, \tag{2.43}$$

$\mid k \mid \geq 1$

$$\begin{pmatrix} \delta \hat{m}_k(t+1) \\ \delta \hat{X}_k(t+1) \end{pmatrix} = H^{kk} \begin{pmatrix} \delta \hat{m}_k(t) \\ \delta \hat{X}_k(t) \end{pmatrix} \tag{2.44}$$

$$= \begin{pmatrix} 0 & 0 \\ -U_{\rm se} \hat{X}_0 & 1 - \frac{1}{\tau} - U_{\rm se} \hat{m}_0 \end{pmatrix} \begin{pmatrix} \delta \hat{m}_k(t) \\ \delta \hat{X}_k(t) \end{pmatrix}. \tag{2.45}$$

This form makes it easy to analyze the stability of a steady state since, for any k, the time evolution of each equation pair [$\delta \hat{m}_k(t)$ and $\delta \hat{X}_k(t)$] decouples from all other equation pairs. Eigenvalue λ_k of H^{kk} determines whether a steady-state solution is stable or not. The solution is stable if it is 1 or less. The values for the eigenvalues, $\lambda_k (\neq 0)$, are given by $\lambda_k = 0$ and $\left(1 - \frac{1}{\tau} - U_{\rm se} \hat{m}_0\right)$. Since $1 \leq \tau$, $0 \leq U_{\rm se} \leq 1$, $0 \leq \hat{m}_0 \leq 1$, $\mid \lambda_k \mid \leq 1$, and $\hat{m}_k$, $\hat{X}_k \to 0$ as $t \to \infty$. We consider the stability to homogeneous perturbations $\delta \hat{m}_0$ and $\delta \hat{X}_0$, and obtain eigenvalue λ_0 of H^{00}:

$$\lambda_0^{\pm} = \frac{1}{2} \left[4\beta J_0 \left(\hat{m}_0 - \hat{q}_0\right) + \left(1 - \frac{1}{\tau} - U_{\rm se} \hat{m}_0\right) \right]$$
$$\pm \frac{1}{2} \left\{ \left[4\beta J_0 \left(\hat{m}_0 - \hat{q}_0\right) + \left(1 - \frac{1}{\tau} - U_{\rm se} \hat{m}_0\right) \right]^2 - 16\beta J_0 \left(\hat{m}_0 - \hat{q}_0\right) \left(1 - \frac{1}{\tau}\right) \right\}^{\frac{1}{2}}. \tag{2.46}$$

We find that two types of linear instability of the stationary uniform state are possible (Roxin, Brunel and Hansel 2005). For $\mid \lambda_0^{\pm} \mid > 1$ and $\mathrm{Im}(\lambda_0^{\pm}) = 0$, homogeneous perturbations $\delta \hat{m}_0$ and $\delta \hat{X}_0$ cause firing-rate instability. If $\mid \lambda_0^{\pm} \mid$ is more than 1 and $\mathrm{Im}(\lambda_0^{\pm}) \neq 0$, homogeneous perturbations $\delta \hat{m}_0$ and $\delta \hat{X}_0$ yield a Hopf instability. This results in growing oscillations and instability. A small-amplitude limit-cycle periodic solution exists near the steady-state solution.

2.4.3 Results

To evaluate the effect of synaptic depression on a network with uniform connections, we investigated the steady-state solutions and their stability in the network. We obtained

the steady-state solutions to eq. (2.32) by solving

$$M = \hat{m}_0, \tag{2.47}$$

$$M = \frac{1}{2}\left(1 + \tanh \beta J_0 \left(\frac{2\hat{m}_0}{1+\gamma\hat{m}_0} - 1\right)\right). \tag{2.48}$$

Graphical solutions to eqs. (2.47) and (2.48) are shown in Fig. 2.2(a) for $T = 0.3$ (dot-dashed line) and $T = 0.8$ (dashed line) when $\gamma = \tau U_{\rm se} = 0.35$. Regardless of βJ_0, the line for eq. (2.47) passes through the point $(\frac{1}{2-\gamma}, 0.5)$ as shown in Fig. 2.2(a). When the level of noise was low ($T = 0.3$), eq. (2.32) had three fixed points. Since two of them were attracting and the other was repelling, we found that the network with uniform connections had a bistable region at low and high $\hat{m}_0$ values in the case of low noise. We defined a ferromagnetic (F) state as bistability in $\hat{m}_0$(Hamaguchi et al. 2008). When the level of noise was high ($T = 0.8$), the network with uniform connections had a monostable state for the $\hat{m}_0$ values. This state is called a "paramagnetic" (P) state(Hamaguchi et al. 2008). When $\gamma > 1$, $\frac{1}{2-\gamma} > 1$ and the network had only a P state.

The steady-state solutions obtained using eq. (2.32) and the results of stability analysis for $\tau = 2$ with a fixed degree of synaptic depression ($\gamma = 0.35$) are shown in Fig. 2.2(b). For $\gamma = 0.35$ and $\tau = 2$, the equilibrium point given by eq. (2.32) was stable. The solid lines in Fig. 2.2(b) denote stable solutions, and the dashed line denotes an unstable solution. A saddle node bifurcation occurred at $T_c = 0.36$ since $\mid \lambda_0^{\pm} \mid > 1$ and $\mathrm{Im}(\lambda_0^{\pm}) = 0$ (firing-rate instability). Hence, the F state was stable for a low noise level ($T < T_c$), while the P state was stable for a high noise level ($T > T_c$). Using eq. (2.46), we found that all solutions with $\hat{m}_0 \leq 0.5$ were stable. This means that synaptic depression stabilizes a low-firing-rate state in a network with uniform connections.

Hopf instability of homogeneous solution

We investigate the effect of the time constant τ on the stability of steady-state solutions. We set γ to 0.35 and τ to 2 and 100. The steady-state solutions obtained using eq. (2.32) and stability analysis are shown in Fig. 2.3(a) for $\tau = 2$ and in Fig. 2.3(b) for $\tau = 100$. The simulation results are represented by the squares. The number of neurons was 10^3, and the initial conditions for the firing-state variables and synaptic variables were $s_i(0) = 1$ and $x_i(0) = 1$ for all i and $s_i(0) = 0$ and $x_i(0) = 1$ for all i. Since $\gamma = 0.35$ in both cases, the steady-state solutions are the same. We found that, near the transition point between the P and F states, a fixed point ($\hat{m}_0 > 0.5$) was stable for $\tau = 2$ [Fig. 2.3(a)] but unstable for $\tau = 100$ [Fig. 2.3(b)]. Since $\mid \lambda_0^{\pm} \mid > 1$ and $\mathrm{Im}(\lambda_0^{\pm}) \neq 0$ at $\hat{m}_0 = 0.865$ and $T = 0.353$, as shown in Figs. 2.4(b) and 2.4(c), a Hopf

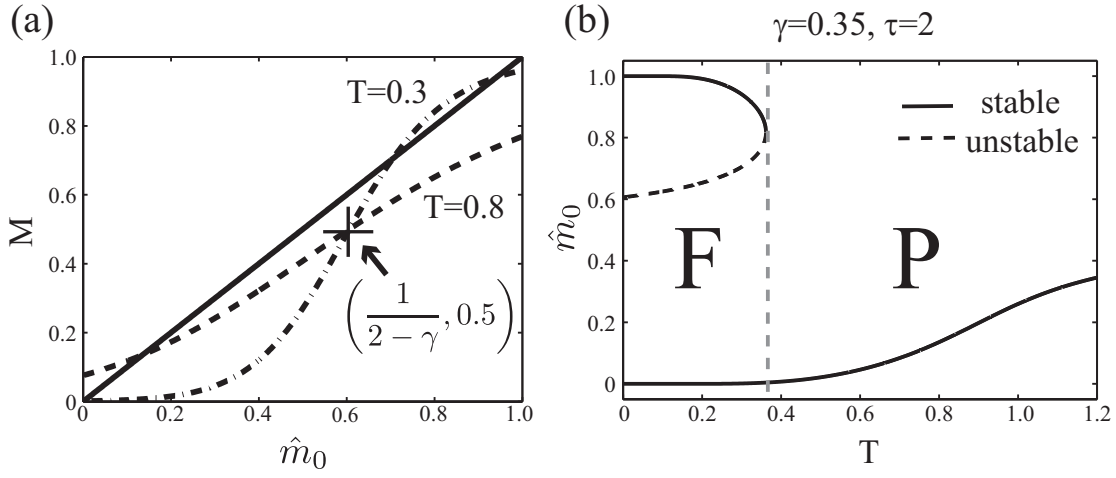

Fig. 2.2. (a) Graphical solutions to eq. (2.32). (b) Stable and unstable solutions to eq. (2.32) for $\gamma = 0.35$, $\tau = 2$.

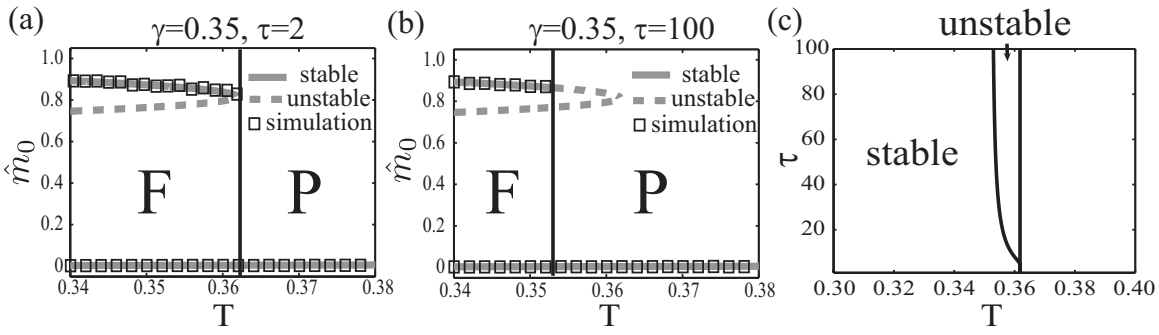

Fig. 2.3. Squares in figures (a) and (b) represent the firing rate $\hat{m}_0$ numerically obtained by simulation with $N = 10^3$. Solid lines denote stable solutions and dashed lines denote unstable solutions. (c) Phase diagram for stability of $\hat{m}_0 > 0.5$ state.

bifurcation occurred, and there was an OU state near $T = 0.353$. Figure. 2.5 shows $\hat{m}_0(t)[= \sum_i^N \hat{m}_i(t)]$ and $\hat{X}_0(t)[= \sum_i^N \hat{X}_i(t)]$ for the OU state, respectively given by eqs. (2.14) and (2.15) ($N = 10^3$). When T was more than 0.353, the OU state was unstable and the macroscopic property of the network changed to the P state. These results are consistent with the simulation. The phase diagram of the stability for $\hat{m}_0 > 0.5$ shown in Fig. 2.3(c) reveals that the state tended to be unstable when the time constant of the synaptic variable increased. The unstable region expanded until $\tau \approx 50$, and then it converged to an approximately constant region. These results show that the stability of the solution strongly depends on the time constant τ. Finally, we discuss the oscillatory instability in the neural network with uniform connections in the presence of synaptic depression. A neural network with synaptic depression can be considered as an activator-

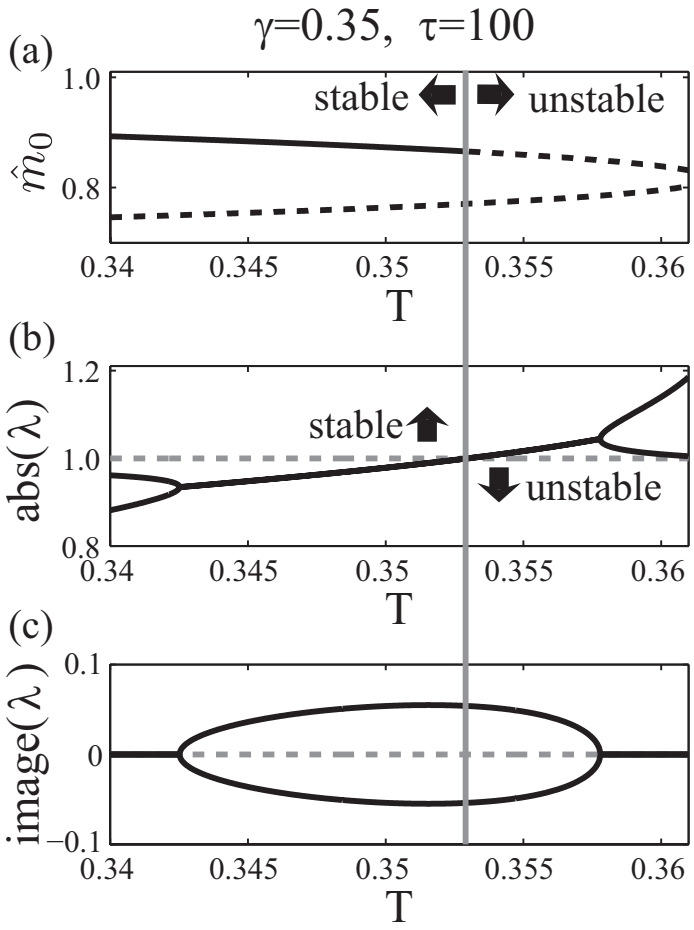

Fig. 2.4. Results of stability analysis for $\hat{m}_0 > 0.5$ and $0.34 \leq T \leq 0.362$. (a) Firing rate $\hat{m}_0$ state: solid line denotes stable solutions and the dashed lines denote unstable solutions. (b) Absolute value of $\lambda_0^{\pm}$. (c) Image part of $\lambda_0^{\pm}$.

inhibitor system in which firing rate m is an activator and synaptic variable X is an inhibitor. This is because inhibitor X is activated by m and inhibits activator production since the total synaptic input h decreases as X increases. In the activator-inhibitor system, an oscillatory instability (a Hopf instability) can exist(Kuramoto 2003). We found that the oscillatory uniform state remained for a sufficiently long time constant in a neural network with uniform connections in the presence of synaptic depression.

2.5 Ring attractor network with Mexican hat type connectivity

For a network with uniform connections, we found that the homogeneous steady state is unstable and that the oscillatory uniform state remains for a sufficiently long time constant.

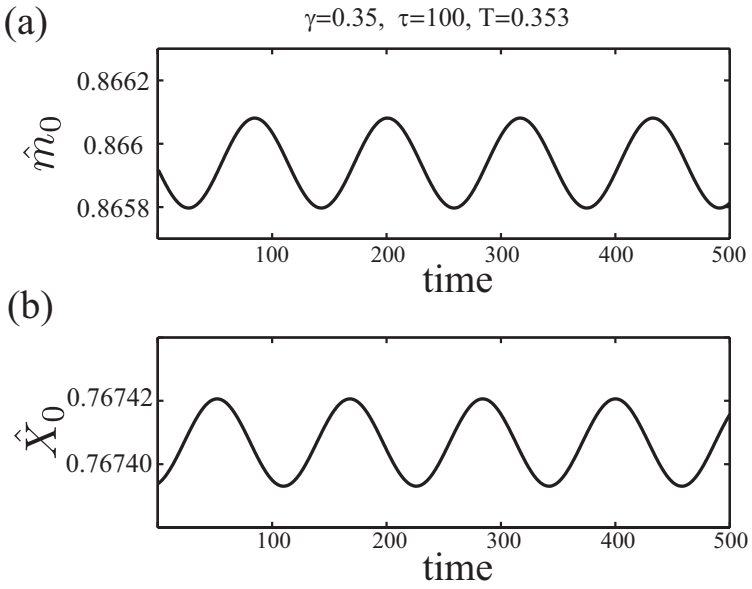

Fig. 2.5. (a) Firing rate $\hat{m}_0(t)$ and (b) average of synaptic efficacy $\hat{X}_0(t)$ corresponding to OU state.

Let us now turn to a ring attractor neural network with Mexican hat type connectivity. In this network, N neurons are located on a one-dimensional ring parameterized with $\theta \in [0, 2\pi)$. Neuron i is labeled using angle $\theta_i (= \frac{\pi i}{N} - \frac{\pi}{2})$. This does not imply the presence of such ring structures in neuroanatomy, merely that the neurons tuned to a periodic variable are functionally fully connected. This ring network model is thus not a one-dimensional lattice model and is often used as an appropriately approximated network model of the primary visual cortex or prefrontal cortex (Ben-Yishai et al. 1995, Compte et al. 2000, York and van Rossum 2009, Kilpatrick and Bressloff 2010). Following these previous studies, we used the conventional ring neural network model. The synaptic weight is

$$J_{ij} = \frac{J_0}{N} + \frac{J_1}{N} \cos 2(\theta_i - \theta_j), \tag{2.49}$$

where J_0 is a uniform interaction and J_1 is a lateral-inhibitory interaction (Ben-Yishai et al. 1995, Hamaguchi 2006, Hamaguchi et al. 2008).The model with $J_1 = 0$ reduces to a network with uniform connections. For $J_0 = 0$, the network is a balanced network with Mexican hat type connectivity, such as that studied by York and Rossum (York and van Rossum 2009).

2.5.1 Macroscopic steady-state equation

Using the microscopic mean field equations (2.14) and (2.15), we obtain macroscopic steady-state equations for the ring network with synaptic depression. Substituting eq. (2.49) into the microscopic steady-state equation (2.17), we obtain a microscopic equation:

$$m_i = g_\beta(h_i), \quad r_i = \frac{m_i}{1+\gamma m_i}, \tag{2.50}$$

$$h_i = J_0 r_0 + J_1 \left[\frac{(r_1 + r_{-1})}{2} \cos(2\theta_i) + \frac{(r_1 - r_{-1})}{2i} \sin(2\theta_i) \right], \tag{2.51}$$

where

$$r_0 = \frac{1}{N}\sum_{i=1}^{N} 2r_i - 1,\ r_1 = \frac{1}{N}\sum_{i=1}^{N}(2r_i-1)e^{-2\mathrm{i}\theta_i},\ r_{-1} = \frac{1}{N}\sum_{i=1}^{N}(2r_i-1)e^{2\mathrm{i}\theta_i}. \tag{2.52}$$

The renormalized output of the ith neuron due to the synaptic depression is $r_i = m_i/(1+\gamma m_i)$. We can obtain the following self-consistent equations for the macroscopic steady state in the limit $N \to \infty$,

$$r(\theta) = \frac{g_\beta\left[J_0 r_0 + J_1\left(r_1 e^{-2\mathrm{i}\theta} + r_{-1} e^{2\mathrm{i}\theta}\right)\right]}{1+\gamma g_\beta\left[J_0 r_0 + J_1\left(r_1 e^{-2\mathrm{i}\theta} + r_{-1} e^{2\mathrm{i}\theta}\right)\right]}, \tag{2.53}$$

$$r_0 = \frac{1}{\pi}\int_{-\frac{\pi}{2}}^{\frac{\pi}{2}} d\theta 2r(\theta) - 1,\ r_1 = \frac{1}{\pi}\int_{-\frac{\pi}{2}}^{\frac{\pi}{2}} d\theta 2r(\theta)e^{-2\mathrm{i}\theta},\ r_{-1} = \frac{1}{\pi}\int_{-\frac{\pi}{2}}^{\frac{\pi}{2}} d\theta 2r(\theta)e^{2\mathrm{i}\theta}. \tag{2.54}$$

The order parameters given by eq. (2.53) are used to calculate the 0th order Fourier component of $m(\theta)$ [$\hat{m}_0 = \frac{1}{\pi}\int_{-\frac{\pi}{2}}^{\frac{\pi}{2}} d\theta m(\theta)$], namely the firing rate, and the 1st order Fourier component of $m(\theta)$ [$\hat{m}_1 = \frac{1}{\pi}\int_{-\frac{\pi}{2}}^{\frac{\pi}{2}} d\theta m(\theta)e^{-2\mathrm{i}\theta}$]. The 1st order Fourier component, $\hat{m}_1$, indicates the degree of activity localization.

There are two types of solution to eq. (2.53). One is a homogeneous solution with $\hat{m}_1 = 0$, and the second one is a bump solution with $\hat{m}_1 \neq 0$, which is inhomogeneous.

2.5.2 Stability analysis

We investigated the stability of the steady-state solution given by eq. (2.53) for the ring network as done for a network with uniform connections (Tsodyks et al. 1998, York and van Rossum 2009, Hansel and Sompolinsky 1998). To examine the stability of the steady-state solution, m_i and X_i, obtained using eq. (2.53), we considered small

deviations around the steady state:

$$m_i(t) = m_i + \delta m_i(t), \quad X_i(t) = X_i + \delta X_i(t). \tag{2.55}$$

Since J_{ij} consists of the 0th Fourier component J_0 and the 1st Fourier component J_1 in the ring network, discrete Fourier transform analysis can be used to diagonalize Jacobian matrix K (eq. (2.27)) for the ring network as well as for a network with uniform connections. We hence write $\delta m_i(t)$ and $\delta X_i(t)$ in Fourier series form in a way similar to that used in §2.4.2. Substituting eqs. (2.37) and (2.49) and $\theta_i = \frac{\pi i}{N} - \frac{\pi}{2}$ into eqs. (2.21) and (2.26), we obtain

$$\sum_{k=-\frac{N}{2}}^{\frac{N}{2}-1} \delta\hat{m}_k(t+1)e^{2\mathrm{i}k\theta_i} = \frac{1}{N}\sum_{j\neq i}^{N}\left[4\beta J_0 + 4\beta J_1 \cos 2(\theta_i - \theta_j)\right] \times \sum_{k',l,l'=-\frac{N}{2}}^{\frac{N}{2}-1} (\hat{m}_{k'} - \hat{q}_{k'})\left[\hat{X}_{l'}\delta\hat{m}_l(t) + \hat{m}_{l'}\delta\hat{X}_l(t)\right] e^{2\mathrm{i}\left[k'\theta_i + (l+l')\theta_j\right]}, \tag{2.56}$$

$$= \sum_{k'=-\frac{N}{2}}^{\frac{N}{2}-1} (\hat{m}_{k'} - \hat{q}_{k'})\left[4\beta J_0 e^{2\mathrm{i}k'\theta_i}\sum_{l=-\frac{N}{2}}^{\frac{N}{2}-1}\hat{m}_l(t)\hat{X}_{-l}(t) + 2\beta J_1 e^{2\mathrm{i}(k'+1)\theta_i}\sum_{l=-\frac{N}{2}}^{\frac{N}{2}-1}\hat{m}_l(t)\hat{X}_{-(l-1)}(t) + 2\beta J_1 e^{-2\mathrm{i}(k'-1)\theta_i}\sum_{l=-\frac{N}{2}}^{\frac{N}{2}-1}\hat{m}_l(t)\hat{X}_{-(l+1)}(t)\right], \tag{2.57}$$

$$\sum_{k=-\frac{N}{2}}^{\frac{N}{2}-1} \delta\hat{X}_k(t+1)e^{2\mathrm{i}k\theta_i} = \left(1 - \frac{1}{\tau}\right)\sum_{l=-\frac{N}{2}}^{\frac{N}{2}-1}\delta\hat{X}_l(t)e^{2\mathrm{i}l\theta_i} - U_{se}\sum_{l,l'=-\frac{N}{2}}^{\frac{N}{2}-1}\left[\delta\hat{m}_l(t)\hat{X}_{l'}(t) + \hat{m}_l(t)\delta\hat{X}_{l'}(t)\right] e^{2\mathrm{i}(l+l')\theta_i}, \tag{2.58}$$

where we use the following equation in the limit of $N \to \infty$ to integrate the right side of eq. (2.56) with respect to θ_j,

$$\frac{1}{N}\sum_{j\neq i}^{N} e^{2\mathrm{i}(l\theta_j)} = \begin{cases} 1 & (l = 0) \\ 0 & (l \neq 0) \end{cases} \tag{2.59}$$

Since Fourier components are orthonormal, we can equate the coefficients of the Fourier components on the left and right sides. From the relations for the coefficients in eqs. (2.57)

and (2.58), we can obtain the Jacobian matrix for the system in Fourier space, H. The matrix has a size of $2N \times 2N$ with matrix elements

$$H^{kl} \equiv \begin{pmatrix} H^{kl}_{\hat{m}\hat{m}} & H^{kl}_{\hat{m}\hat{X}} \\ H^{kl}_{\hat{X}\hat{m}} & H^{kl}_{\hat{X}\hat{X}} \end{pmatrix}, \quad \begin{pmatrix} \delta\hat{m}_k(t+1) \\ \delta\hat{X}_k(t+1) \end{pmatrix} = H^{kl} \begin{pmatrix} \delta\hat{m}_l(t) \\ \delta\hat{X}_l(t) \end{pmatrix}, \tag{2.60}$$

$$\begin{aligned} H^{kl}_{\hat{m}\hat{m}} = {} & 4\beta J_0(\hat{m}_k - \hat{q}_k)\hat{X}_{-l} \\ & + 2\beta J_1(\hat{m}_{k-1} - \hat{q}_{k-1})\hat{X}_{-(l-1)} + 2\beta J_1(\hat{m}_{k+1} - \hat{q}_{k+1})\hat{X}_{-(l+1)}, \end{aligned} \tag{2.61}$$

$$\begin{aligned} H^{kl}_{\hat{m}\hat{X}} = {} & 4\beta J_0(\hat{m}_k - \hat{q}_k)\hat{m}_{-l} \\ & + 2\beta J_1(\hat{m}_{k-1} - \hat{q}_{k-1})\hat{m}_{-(l-1)} + 2\beta J_1(\hat{m}_{k+1} - \hat{q}_{k+1})\hat{m}_{-(l+1)}, \end{aligned} \tag{2.62}$$

$$H^{kl}_{\hat{X}\hat{m}} = -U_{\mathrm{se}}\hat{X}_{k-l}, \tag{2.63}$$

$$H^{kl}_{\hat{X}\hat{X}} = \delta_{kl}\left(1 - \frac{1}{\tau}\right) - U_{\mathrm{se}}\hat{m}_{k-l}, \tag{2.64}$$

where $-\frac{N}{2} \leq k, l \leq \frac{N}{2} - 1$, and δ_{kl} is the Kronecker delta. If the Jacobian matrix has eigenvalues of 1 or less, the steady-state solution is stable.

First, we consider the stability of the homogeneous steady state [$\hat{m}_k = 0$ and $\hat{X}_k = 0$ $(k \neq 0)$], which can be analytically considered as shown below (York and van Rossum 2009). If the network has a homogeneous steady-state solution, $\hat{X}_k = 0$ and $\hat{m}_k = 0$ $(k \neq 0)$, we have

$$H^{kl} = \begin{pmatrix} 0 & 0 \\ 0 & 0 \end{pmatrix} \quad (k \neq l). \tag{2.65}$$

This equation shows that the time evolution of each equation pair [$\delta\hat{m}_k(t)$ and $\delta\hat{X}_k(t)$] decouples from all other equation pairs. The Jacobian matrix for the ring network is therefore as easy to analyze as that for a network with uniform connections. The Jacobian matrix thus reduces to the following matrices:

$k = 0$

$$H^{00} = \begin{pmatrix} 4\beta J_0\left(\hat{m}_0 - \hat{q}_0\right)\hat{X}_0 & 4\beta J_0\left(\hat{m}_0 - \hat{q}_0\right)\hat{m}_0 \\ -U_{\mathrm{se}}\hat{X}_0 & 1 - \frac{1}{\tau} - U_{\mathrm{se}}\hat{m}_0 \end{pmatrix} \tag{2.66}$$

$k = \pm 1$

$$H^{11} = \begin{pmatrix} 2\beta J_1 \left(\hat{m}_0 - \hat{q}_0\right) \hat{X}_0 & 2\beta J_1 \left(\hat{m}_0 - \hat{q}_0\right) \hat{m}_0 \\ -U_{\mathrm{se}} \hat{X}_0 & 1 - \frac{1}{\tau} - U_{\mathrm{se}} \hat{m}_0 \end{pmatrix} \tag{2.67}$$

$$H^{-1-1} = H^{11} \tag{2.68}$$

$| k | > 1$

$$H^{kk} = \begin{pmatrix} 0 & 0 \\ -U_{\mathrm{se}} \hat{X}_0 & 1 - \frac{1}{\tau} - U_{\mathrm{se}} \hat{m}_0 \end{pmatrix}. \tag{2.69}$$

Since the eigenvalue λ_k of $H^{kk} (| k | > 1)$ is less than 1, $\delta \hat{m}_k$, $\delta \hat{X}_k \to 0$ as $t \to \infty$. We consider the stability under perturbations $\delta \hat{m}_0$, $\delta \hat{X}_0$, $\delta \hat{m}_1$, and $\delta \hat{X}_1$. The stability under perturbations $\delta \hat{m}_{-1}$ and $\delta \hat{X}_{-1}$ is identical to that under perturbations $\delta \hat{m}_1$ and $\delta \hat{X}_1$. The eigenvalue of H^{00} is given by eq. (2.46). Next, we obtain eigenvalue $\lambda_1^{\pm}$ of H^{11}:

$$\begin{aligned} \lambda_1^{\pm} = & \frac{1}{2} \left[2\beta J_1 \left(\hat{m}_0 - \hat{q}_0\right) + \left(1 - \frac{1}{\tau} - U_{\mathrm{se}} \hat{m}_0\right) \right] \\ & \pm \frac{1}{2} \left\{ \left[2\beta J_1 \left(\hat{m}_0 - \hat{q}_0\right) + \left(1 - \frac{1}{\tau} - U_{\mathrm{se}} \hat{m}_0\right) \right]^2 - 8\beta J_1 \left(\hat{m}_0 - \hat{q}_0\right) \left(1 - \frac{1}{\tau}\right) \right\}^{\frac{1}{2}}. \end{aligned} \tag{2.70}$$

The stability of the homogeneous steady-state solution is determined by eqs. (2.46) and (2.70). There are four types of linear instability of the homogeneous state: (1) firing-rate instability ($| \lambda_0^{\pm} | > 1, \mathrm{Im}(\lambda_0^{\pm}) = 0, | \lambda_1^{\pm} | < 1$), (2) Hopf instability ($| \lambda_0^{\pm} | > 1, \mathrm{Im}(\lambda_0^{\pm}) \neq 0, | \lambda_1^{\pm} | < 1$), (3) Turing instability ($| \lambda_0^{\pm} | < 1, | \lambda_1^{\pm} | > 1, \mathrm{Im}(\lambda_1^{\pm}) = 0$), and (4) Turing-Hopf instability ($| \lambda_0^{\pm} | < 1, | \lambda_1^{\pm} | > 1, \mathrm{Im}(\lambda_1^{\pm}) \neq 0$)(Roxin, Brunel and Hansel 2005). If there is a Turing-Hopf instability, a spatially homogeneous steady-state solution is unstable and spatial periodic patterns evolve.

In contrast to the homogeneous steady-state solutions, it is difficult to analyze the stability of inhomogeneous steady-state solutions since the time evolution of each equation pair [$\hat{m}_k(t)$ and $\hat{X}_k(t)$] is coupled with other equation pairs. We hence have to take into account stability under frequency perturbations $\delta \hat{m}_k$ and $\delta \hat{X}_k$ ($-N/2 \leq k, l \leq N/2 - 1$) since the highest Fourier component is $\hat{m}_{\pm N/2}$, $\hat{X}_{\pm N/2}$ in a network with N neurons according to the sampling theorem. Here we study how frequency perturbations $\delta \hat{m}_k$ and $\delta \hat{X}_k$ ($-N/2 \leq k, l \leq N/2 - 1$) affect the stability of the inhomogeneous steady-state solutions by considering the eigenvector of the Jacobian matrix [eq. (2.60)].

2.5.3 Results

Oscillatory states

In the section 2.4, using a simple network with uniform connections, we have shown that oscillatory instability is caused by synaptic depression because a neural network with synaptic depression can be considered as an activator-inhibitor system in which firing rate is an activator and synaptic variable is an inhibitor. Then what's the role of structured connections between neurons? We assume that the structured connectivity modulate neural dynamics and change the oscillation mode.

To test the hypothesis, we studied a parsimonious structured neural network, that is, a neural network with Mexican-hat type connections, and our investigation of the stability of the steady-state solution given by eq. (2.53) for the ring network revealed six states in the network. Three are homogeneous and were also found in a network with uniform connections: a ferromagnetic (F) state, a paramagnetic (P) state, and an oscillatory uniform (OU) state. The OU state appears in a way similar to that described in §2.4.3 (Fig. 2.4). The other three states are inhomogeneous: a bump (B) state, a rotating bump (RB) state (York and van Rossum 2009, Kilpatrick and Bressloff 2010), and an oscillatory bump (OB) state, as shown in Fig. 2.6. The B state can be obtained using a self-consistent equation, eq. (2.53), while the other two cannot because they are dynamic states resulting from the destabilization of steady states. We thus obtained them by using the dynamical mean field equations (2.14) and (2.15) with $N = 10^4$. The firing rate m_i, the average of the synaptic variable X_i, and the synaptic weight between the ith neuron with the preferred orientation $\theta_i = 0$ and the other neurons are shown in Fig. 2.6 for the three inhomogeneous states.

First, we discuss the behavior of the three inhomogeneous states in a ring network with synaptic depression. The B state is formed by a subset of the neurons firing in a self-reinforcing manner, causing localized activity [Fig. 2.6(a)], similar to the B state in the network without synaptic depression (Ben-Yishai et al. 1995, Hamaguchi 2006, York and van Rossum 2009). In the B state, the firing rates are high, while the averages of the synaptic variables are low [Figs. 2.6(a) and 2.6(b)]. Synaptic depression thus reduces the excitatory localized interaction and reduces the presynaptic inputs of the activated neuron, as shown in Fig. 2.6(c). In the RB state, a localized bump of activity propagates around the ring network, leaving a replenishing synaptic resource in its wake, as shown in Figs. 2.6(d) and 2.6(e) (York and van Rossum 2009). In this example, the profile is moving to the right. As a result, the synaptic weights dynamically changed in

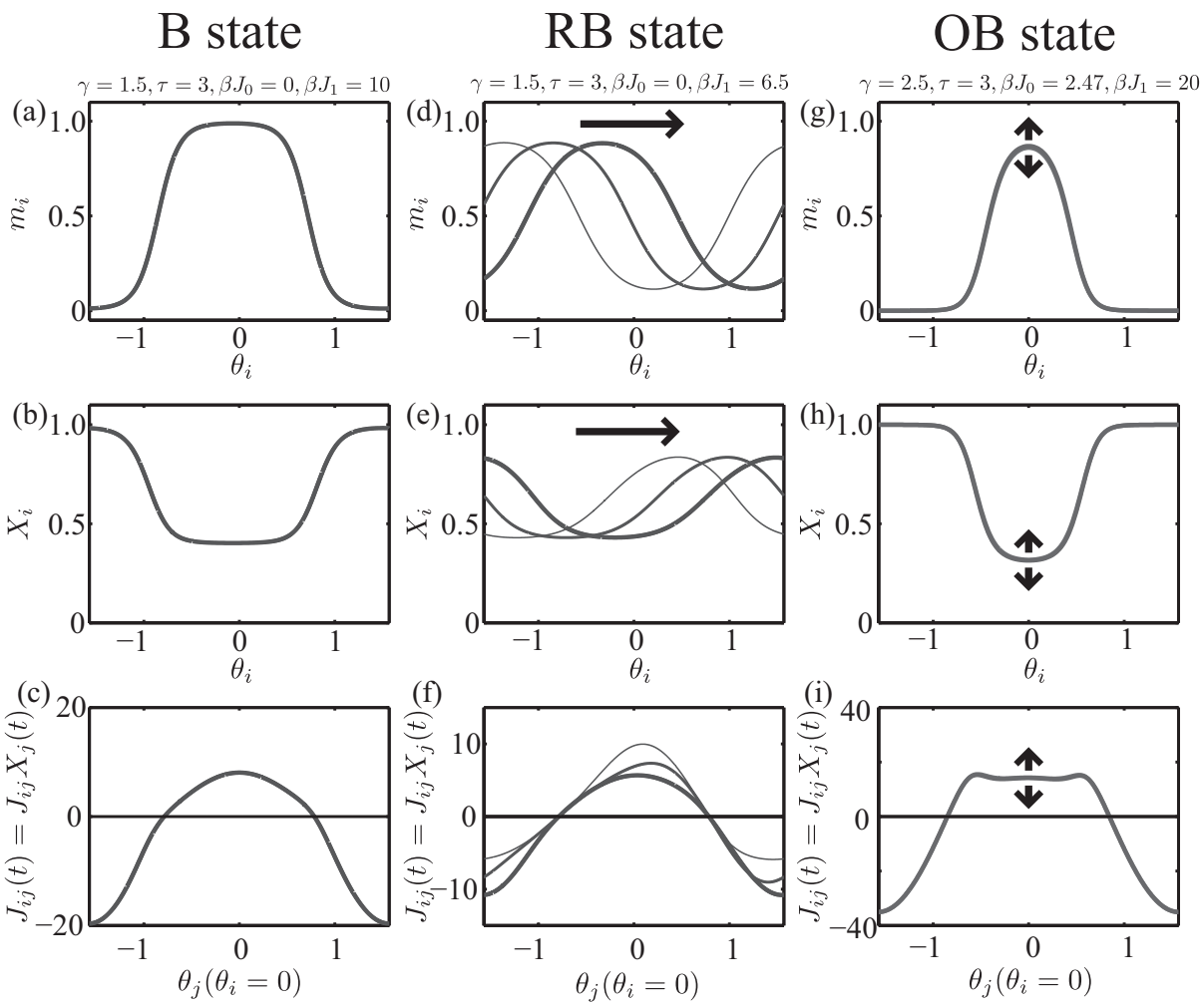

Fig. 2.6. Profiles for three inhomogeneous states (B, RB, OB). (a), (d), (g) Firing rate m_i. (b), (e), (h) Average of synaptic variable X_i. (c), (f), (i) Synaptic weight $J_{ij}(t) = J_{ij}X_j(t)$ between ith neuron with preferred orientation $\theta_i = 0$ and other neurons.

the RB state [Fig. 2.6(f)]. In the OB state, which is first reported here, the bump state activity moved up and down around the neurons with firing rates that were high, as shown in Figs. 2.6(g) and 2.6(h). Unlike in the RB state, the magnitude of notion is very small in the OB state [Figs. 2.6(g)-2.6(i)]. The occurrence of the two oscillatory states from the B state implies that there are two mechanisms destabilizing the B state.

Next, we provide evidence that the simulation results coincide with the dynamic solution obtained using eqs. (2.14) and (2.15) for the B state ($\beta J_0 = 0, \beta J_1 = 10$) and the RB state ($\beta J_0 = 0, \beta J_1 = 6.5$). Figures. 2.7(a) and 2.7(b) show raster plots of neuron activity obtained by numerical simulation with $N = 10^4$. The solid lines represent the dynamic solu-

tion obtained using eqs. (2.14) and (2.15). In the B state, the localized position fluctuated and moved around the ring network since the B state is stable anywhere in the ring [Fig. 2.7(a)](Hamaguchi 2006). In the RB state, the bumps propagated stably, i.e., there was a traveling wave [Fig. 2.7(b)] (York and van Rossum 2009, Kilpatrick and Bressloff 2010).

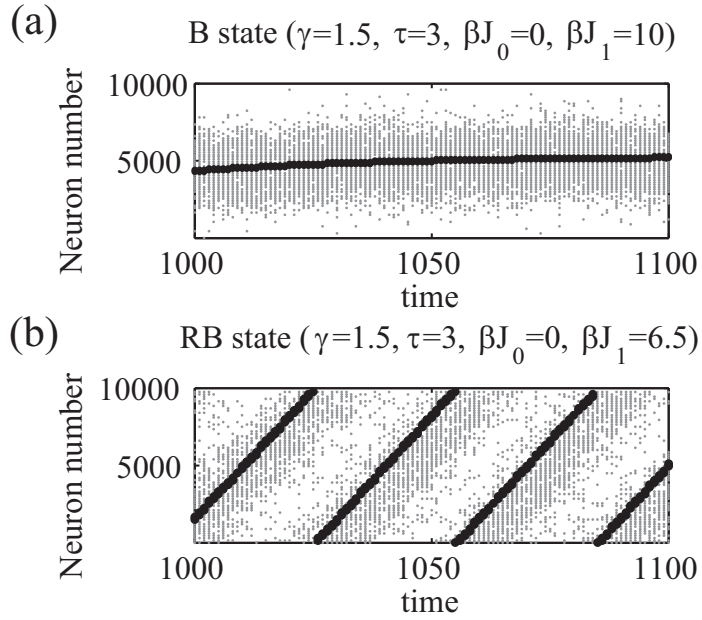

Fig. 2.7. Raster plots of neuron activity for numerical simulation ($N = 10^4$). Solid lines denote the temporal behaviors of bump position ϕ. (a) B state. (b) RB state.

In short, we found six states of activity in the ring network with synaptic depression: paramagnetic, ferromagnetic, bump, oscillatory uniform, rotating bump, and oscillatory bump states.

Hopf and Turing instabilities of inhomogeneous solution

We considered the stability of the inhomogeneous steady-state solution (the B state) in order to identify the destabilization mechanisms leading to the two inhomogeneous oscillatory states, the RB and OB states. To analyze the stability of a network with $N = 10^3$, we computed the eigenvalues of the Jacobian matrix H [eq. (2.60), 2000×2000] for frequency perturbations $\delta\hat{m}_k$ and $\delta\hat{X}_k$ ($-5 \times 10^2 \leq k \leq 5 \times 10^2 - 1$). Note that the highest Fourier components are $\hat{m}_{\pm 5\times 10^2}$ and $\hat{X}_{\pm 5\times 10^2}$ in a network with $N = 10^3$, as determined by the sampling theorem.

To begin our analysis, we consider a network with a fixed degree of synaptic depression ($\gamma = 1.5$) and a time constant ($\tau = 3$), in which the RB state occurs near the transition point between the P and B states. Figure . 2.8(a) shows how the amplitude of localized

activity, $\hat{m}_1$, depends on βJ_1 for $\beta J_0 = 0$. The solid and dashed lines respectively represent stable and unstable solutions to eq. (2.53). Figure. 2.8(b) shows the distribution of eigenvalues for Jacobian matrix H. There are two mechanisms of destabilization that lead to the RB state. First, as βJ_0 crosses 4.5 from below, the P state becomes unstable and a Turing-Hopf instability leads to the RB state because $\mid \lambda_0^{\pm} \mid < 1$, $\mid \lambda_1^{\pm} \mid > 1$, and $\mathrm{Im}(\lambda_1^{\pm}) \neq 0$.

Next, we show that as βJ_1 crosses 8 from above, the B state becomes unstable and a Turing instability leads to the RB state. Figure. 2.8(b) shows that there are eigenvalues continuously distributed between $\lambda = 0.15$ and 0.65 that do not contribute to destabilization and that there are a few eigenvalues greater than 1 that do contribute. Figures. 2.8(c) and 2.8(d) show the eigenvector of the largest eigenvalue for $\beta J_0 = 0$ and $\beta J_1 = 6.5$, which is indicated by the $\times$ mark in Fig. 2.8(b). We see from Figs. 2.8(c) and 2.8(d) that their eigenvectors mainly consist of $\delta\hat{m}_1$, $\delta\hat{X}_1$, $\delta\hat{m}_{-1}$, and $\delta\hat{X}_{-1}$ and not $\delta\hat{m}_0$ or $\delta\hat{X}_0$. In addition, they do not have an imaginary part. We hence found that the B state was unstable and that the RB state appeared owing to a Turing instability.

Next, we consider a ring network with $\gamma = 2.5$ and $\tau = 3$, in which the B state is unstable and the OB state occurs at the transition point ($\beta J_0 = 2.47$) between the B and P states. As βJ_0 crosses 2.47 from below, the OB state becomes unstable and the P state appears. Figure. 2.9(a) shows how the amplitude of localized activity $\hat{m}_1$ depends on βJ_0 for $\beta J_1 = 20$. Figure. 2.9(b) shows the distribution of eigenvalues for Jacobian matrix H. Only a few eigenvalues are greater than 1, as in Fig. 2.8(b). Figures. 2.9(c) and 2.9(d) show the eigenvector of the largest eigenvalue for $\beta J_0 = 2.47$ and $\beta J_1 = 20$ indicated by the $\times$ mark in Fig. 2.9(b), which indicates that the eigenvectors mainly consisted of $\delta\hat{m}_0$ and $\delta\hat{X}_0$. Furthermore, they had an imaginary part. The B state was thus unstable, and a Hopf bifurcation led to the OB state for $\beta J_0 = 2.47$.

These results clearly show that there were two mechanisms destabilizing the B state, i.e., a Turing instability and a Hopf instability, which led to the RB and OB states, respectively. Moreover, we found that there were few eigenvalues that were larger than 1, which affect the stability of the system, as shown in Figs. 2.8 and 2.9, and that their eigenvectors consisted of only low-frequency Fourier components.

Phase diagram

We investigated how neuron interactions affect the macroscopic states of networks by changing the strength of the uniform connections (J_0) and the lateral-inhibitory connections (J_1). Figure. 2.10 shows the phase diagrams in the (βJ_0, βJ_1) plane with a fixed

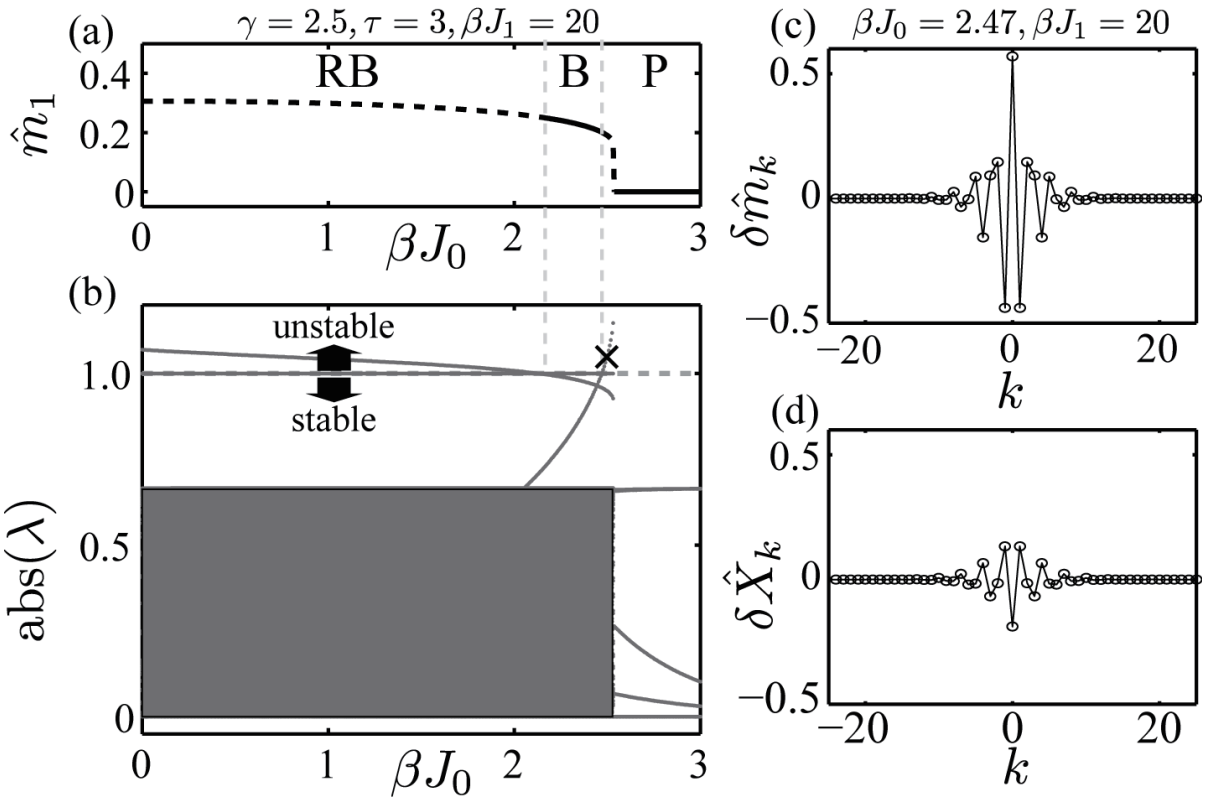

Fig. 2.8. (a) Stable (solid lines) and unstable (dashed line) solutions to amplitude of localized activity $\hat{m}_1$. (b) Distribution of eigenvalues for Jacobian matrix $H(2.60)$ with size of 2000×2000. (c), (d) Eigenvector with largest eigenvalue, 1.1, for $\beta J_0 = 0$ and $\beta J_1 = 6.5$, as shown by $\times$ mark in (b).

degree of synaptic depression ($\gamma = \{0, 0.4, 1.5, 2.5\}$). To analyze the stability of the steady-state solutions in a network with $N = 10^3$, we computed the eigenvalues of Jacobian matrix H for only low-frequency perturbations, namely, $\delta\hat{m}_k$ and $\delta\hat{X}_k$ ($-5 \times 10 \leq k \leq 5 \times 10 - 1$), since high-frequency perturbations do not affect the stability of the system when there is a weak lateral-inhibition (J_1) (see Appendix). The instability of an oscillatory state was numerically investigated using eqs. (2.14) and (2.15) with $N = 10^3$.

To begin with, we describe the behavior of a network with nondepressed synapses ($\gamma = 0$). Figure. 2.10(a) shows the phase diagram for $\gamma = 0$(Hamaguchi 2006). The relative strengths of βJ_0 and βJ_1 determine the network state. The F or B states become stable once βJ_0 and βJ_1 exceed certain thresholds. Between these two states, there are bistable regions where both F and B states are locally stable (F+B). If both βJ_0 and βJ_1 are small, a stable P state exists.

In the presence of weak synaptic depression ($\gamma = 0.4$, $\tau = 3$) [Fig. 2.10(b)], the P region

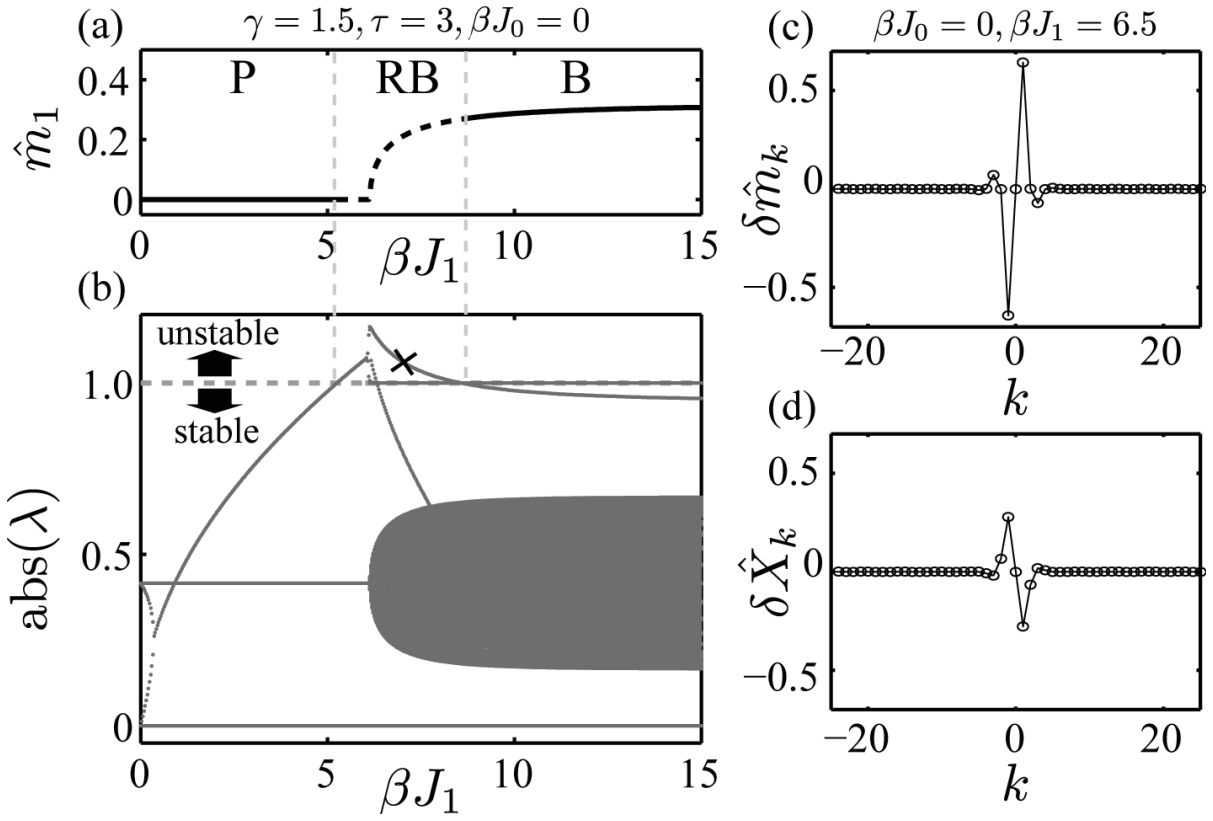

Fig. 2.9. (a) Stable (solid lines) and unstable (dashed lines) solutions to amplitude of localized activity $\hat{m}_1$. (b) Distribution of eigenvalues for Jacobian matrix $H(2.60)$ with size of 2000×2000. (c), (d) Eigenvector with largest eigenvalue, 1.04, for $\beta J_0 = 2.47$ and $\beta J_1 = 20$, as shown by $\times$ mark in (b).

expanded and the bistable regions shrank since the synaptic depression effectively reduced the lateral-inhibitory connection (J_1). Bistable regions, where both P and B states were locally stable (P+B), developed. As the degree of synaptic depression increased ($\gamma = 1.5$, $\tau = 3$), the RB state became stable near the transition point between the P and B states, as shown in Fig. 2.10(c). Since $\gamma > 1$, the F state was unstable.

In the presence of strong synaptic depression ($\gamma = 2.5$, $\tau = 3$) [Fig. 2.10(d)], the RB region expanded and the P+B region shrank. Bistable regions, where both the P and RB states are locally stable (P+RB), developed. The B state was unstable, and an OB region developed at the transition between the B+P and P states [Fig. 2.6(g)-2.6(i)]. Otherwise, the OB state was unstable, and the P state was stable.

We have shown that for a sufficiently strong degree of synaptic depression, the B state is unstable and the oscillatory states (RB and OB) appear near the transition between the B and P states. A sufficiently strong lateral-inhibition (J_1) leads to a Turing instability

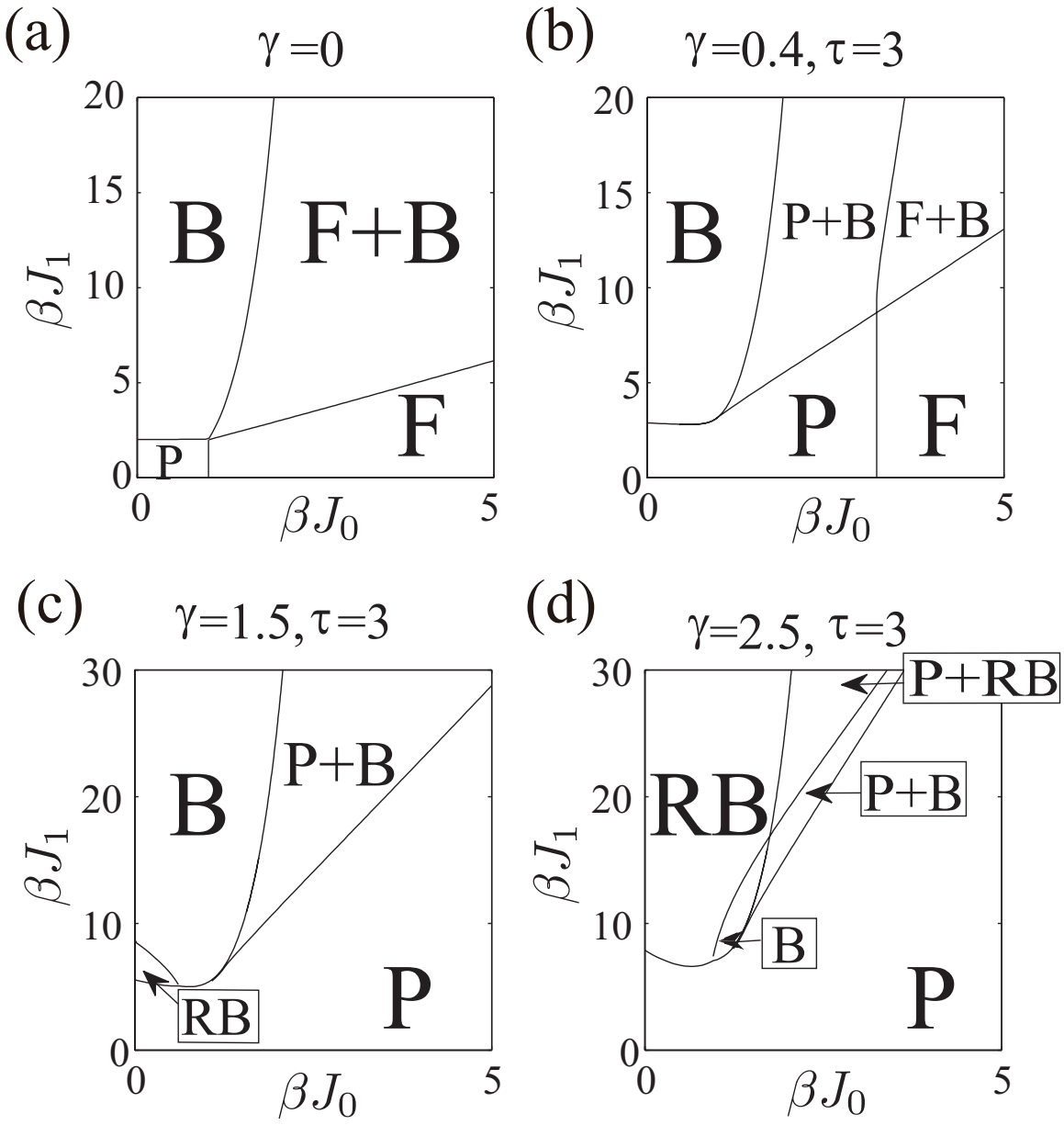

Fig. 2.10. Phase diagrams in interaction of $(\beta J_0, \beta J_1)$ plane for $\gamma = \{0, 0.4, 1.5, 2.5\}$. For (b) to (d), $\tau = 3$. P: the monostability in $\hat{m}_0$, and $\hat{m}_1 = 0$. F: bistability in $\hat{m}_0$, and $\hat{m}_1 = 0$. B: $\hat{m}_1 \neq 0$. RB: $\hat{m}_1 \neq 0$. The OB state occurs on the transition line between the P+B state and the P state with $\gamma = 2.5$ and $\tau = 3$ in (d).

and the RB state appears. A sufficiently strong uniform connection (J_0) leads to a Hopf instability, leading to the OB state.

2.5.4 Discussion

In the ring attractor network with synaptic depression, there are homogeneous steady states (F, P) and an inhomogeneous steady state (B). We have shown that, depending on the strength of the interneuron connections, instability in these states leads to three oscillatory states: oscillatory uniform (OU), rotating bump (RB), and oscillatory bump (OB) states.

Using two neural networks with uniform connections and with parsimonious structured connections, we shown that oscillatory instability is caused by synaptic depression because a neural network with synaptic depression can be considered as an activator-inhibitor system in which firing rate is an activator and synaptic variable is an inhibitor and that the role of structured connections between neurons is to modulate the neural dynamics and oscillation mode. We then summarize how the interactions between neurons affect the stabilities of the steady-state solutions by changing the strengths of the uniform connections (J_0) and the lateral-inhibitory connections (J_1). Figure. 2.11 shows a schematic view of the stability analysis for a ring network with synaptic depression. First, for sufficiently weak uniform connections and a sufficiently long time constant (τ), the homogeneous steady-state solution, which has a high firing rate, was unstable near the transition point between the P and F states. An OU state then developed owing to a Hopf bifurcation, as explained in §2.5.3 [Fig. 2.11(a)→(i)]. Note that the OU state developed in the presence of lateral-inhibitory connections (J_1) as well as in their absence. Next, as the strength of the uniform connections increased, the inhomogeneous steady-state solution became unstable near the transition point between the B and P states (Fig. 2.9). The OB state then developed because of a Hopf instability, as explained in §2.5.3 [Fig. 2.11(b)→(iii)]. In the OB state, bump state activity moved up and down around the most activated neuron [Figs. 2.6(g)-2.6(i)]. Finally, the homogeneous state (P) and inhomogeneous state (B) became unstable near the transition point between them [Fig. 2.8(a)], and the RB state developed, as explained in §2.5.3 [Figs. 2.6(d)-2.6(f)]. As the strength of the lateral-inhibitory connections (J_1) increased, the homogeneous steady-state solution became unstable, and an RB state developed because of a Turing-Hopf instability [Fig. 2.11(a)→(ii)]. As the strength of the lateral-inhibitory connections (J_1) decreased, the inhomogeneous steady-state solution became unstable and an RB state developed owing to a Turing instability [Fig. 2.11(b)→(ii)].

These results show that medium-strength uniform connections cause a Hopf instability near the transition point and up-and-down movement of the firing rates and the average

synaptic variables, and that medium-strength lateral connections cause a Turing instability near the transition point and propagation of a localized bump of activity around the ring network. To summarize, various oscillatory states appear depending on the strength of the interneuron connections in a ring network with synaptic depression.

Large-scale neuronal networks can exhibit a number of spatially structured activity states in vivo, which may be observed experimentally using multi electrode arrays or voltage-sensitive dye imaging (Kenet et al. 2003, Buzsaki 2006, Xu et al. 2007, Benucci et al. 2007, Han et al. 2008). Here we compare experimental evidence obtained by these methods with the various states we found in the ring network with synaptic depression. We showed that a bump state (B), which is an inhomogeneous steady state, occurs in the network, similar to the B state in the network without synaptic depression (Ben-Yishai et al. 1995, Hamaguchi 2006, York and van Rossum 2009). The B state has been observed during working-memory tasks (Compte et al. 2000) in the prefrontal cortex and in the context of the tuning of neuronal responses in the primary visual cortex to the orientation of a visual stimulus (Ben-Yishai et al. 1995). Next, we discuss two oscillatory states, the OB state and the OU state. If the two oscillatory states can appear in the primary visual cortex or prefrontal cortex, an oscillatory synchronous firing can be observed experimentally. However such activity has seldom been reported, which is consistent with our results that these states only appear in a rather narrow parametric region. Finally, we consider the functional aspects of the RB state, which appeared in a relatively broad region. Some researchers have reported that a traveling wave in the absence of an input has been found in the primary visual cortex in a cat (Kenet et al. 2003). Interestingly, a small visual stimulus can evoke the traveling wave (Kenet et al. 2003, Xu et al. 2007, Benucci et al. 2007, Han et al. 2008). Han *et al.* found that repeated visual stimulation causes a significant increase in the percentage of spontaneous waves that are similar to the cortical response evoked in a rat by a training stimulus (Han et al. 2008). Such dynamics provide a potential mechanism for learning effects such as short-term visual memory(Philips 1974) and visual priming (Tulving and Schacter 1990). Our results indicate that recurrent, depressing, synaptic connectivity can naturally lead to the emergence of such dynamic patterns. Further investigation is needed to search for determining the relationship between an external visual stimulus and the speed and pattern of propagating waves in a network with synaptic depression.

According to our results, we predict the following new experimental phenomena. In a ring network with Mexican hat type connections, which has been used as a model of the

prefrontal cortex, a stable B state exists. The B state corresponds to selective persistent activity in the absence of inputs, underlying spatial working memory(Compte et al. 2000). In a ring network with synaptic depression, we show that while a B state appeared in the case of $\tau = 3$ [Fig. 2.10(b)], the B state became unstable and an RB state appeared with $\tau = 10$ and a fixed $U_{\rm se}$. It was reported that the Ca^{2+} chelator EGTA prevents rapid recovery from depression and increases the time constant τ(Zucker and Regehr 2002). On the basis of these findings, we predict the following experimental phenomena. Let us consider a situation that a monkey performs spatial working memory tasks. If the Ca^{2+} chelator EGTA is introduced into the prefrontal cortex when a persistent activity occurs, the B state becomes unstable.

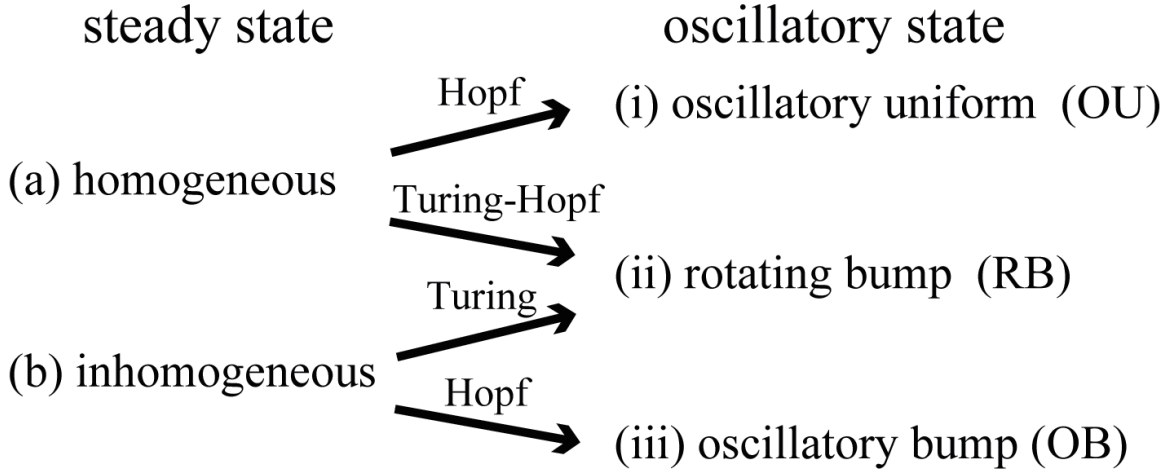

Fig. 2.11. Schematic view of stability analysis for ring network with synaptic depression.

2.6 Summary

We have explored the macroscopic properties of two types of stochastic binary neural networks with synaptic depression: a network with homogeneous connectivity and a ring attractor network with Mexican hat type connectivity. Although a stochastic binary neural network model with synaptic depression cannot be analyzed owing to the asymmetry of connections by the conventional equilibrium statistical-mechanical approach, we derive the microscopic dynamical mean field equations for the network model. Because in the equations the averaged product of the two stochastic variables is decoupled as the product of their averages, they must be independent. We proved the independence and derived the microscopic equations in this paper, assuming that the synaptic weight J_{ij} is of the order of $1/N$ with respect to the number of neurons N. Using the microscopic mean field equa-

tions, we derived macroscopic steady-state equations for these networks and investigated the stability of the steady-state solutions obtained. The results coincided with those of a simulation. We conclude that the presence of synaptic depression leads to oscillatory instability and that various oscillatory states appear depending on the strength of the interneuron connections. Synaptic depression thus causes the diversity of dynamic states in large networks of spiking neurons.

We focused only on non frustrated systems, in which $J_{ij} \sim O(1/N)$. A extension of this study will be to extend the microscopic dynamical mean field theory to frustrated systems such as the Sherrington and Kirkpatrick model(Sherrington and Kirkpatrick 1975).

Chapter 3

Theory of correlations in stochastic neural network models with synaptic depression

3.1 Background

A marked feature of synaptic transmission between neocortical neurons is the pronounced frequency dependence of synaptic responses on presynaptic spike trains (Thomson and Deuchars 1994). High-frequency input reduces the efficacy of signal transmission due to the depletion of neurotransmitters. Short-term synaptic depression, which has been described in detail by using a phenomenological model (Abbott et al. 1997, Tsodyks et al. 1998), occurs over milliseconds to minutopdses in various regions such as the primary visual cortex and the hippocampus (Zucker and Regehr 2002, Varela et al., 1997, Dobrunz and Stevens 1999). Because of its rapid effects, short-term synaptic depression enables synapses to perform critical computational functions in neural circuits such as belief adaptation to external stimuli and short-term memory (Abbott and Regehr 2004, Tsodyks and Gilbert 2004, Kohn 2007).

To evaluate how synaptic depression affects the amount of information on stimuli that can be extracted from noisy neural activities, we need to investigate the effects of synaptic depression not only on the firing rates but also on neural correlations. Even small correlations between neurons can greatly change the amount of information conveyed by the activities of the neural population and consequently affect the accuracy of sensory discriminations (Zohary et al 1994, Abbott and Dayan 1999,

Sompolinsky et al. 2001, Series et al. 2004, Averbeck, Latham and Pouget 2006, Gutnisky and Dragoi 2008, Cohen and Maunsell 2009, Cortes et al. 2010). Similar to the derivation of the linear-response function for an Ising system with transition rates (Glauber 1963, Suzuki and Kubo 1968), some researchers have gone beyond mean-field theory and developed such a theory of correlation in a spiking neuron model including a time course for postsynaptic potential and refractory properties (Ginzburg and Sompolinsky 1994, Meyer and van Vreeswijk 2002, Toyoizumi et al. 2008, Oizumi et al. 2010). However, short-term synaptic depression, which rapidly changes the interaction between neurons, has not been taken into account and the effect of the interaction change on neural correlation remains unknown. Here, we expanded the previous theoretical framework to spiking neuron models with short-term synaptic depression.

We investigated the effects of synaptic depression on the macroscopic behavior of stochastic neural networks in previous studies, viz., the firing rates (Igarashi et al. 2009, Igarashi et al. 2010). Dynamical mean field equations were derived for these networks by taking the average of two stochastic variables: a firing-state variable and a synaptic variable. Because synaptic depression is activity-dependent and leads to the independence of the two stochastic variables, the average product of these variables is decoupled as the product of their averages and we can then calculate the firing rates. We used the independence in this study to calculate the neural correlations and constructed a theoretical framework for analytically calculating correlations of neural activities in a neural network with synaptic depression.

We studied how short-term synaptic depression affects neural correlations for a ring attractor network with Mexican-hat-type connectivity using this theory as an example, which is known as a neural network model of the primary visual cortex (Ben-Yishai et al. 1995, Series et al. 2004, Hamaguchi 2006, Cortes et al. 2010). We analytically calculated the neural correlations and investigated not only the effects of synaptic depression at the single cell level (Goldman et al. 2002) but also what influence changes in single neurons have on network activity as a whole. We found that synaptic depression substantially reduces neural correlations. We also demonstrated that this reduction in neural correlations due to synaptic depression can improve the accuracy of population coding, even though the signal strength, viz., the mean firing rates, is reduced by synaptic depression.

3.2 Model

We used a discrete time version of a spike response model with threshold noise (Gerstner and Hemmen 1992, Oizumi et al. 2010). The network consists of N neurons, which take either a resting-state, $S = 0$, or a firing-state, $S = 1$. The state of every neuron S_i is stochastically updated in parallel. The probability that S_i takes the 0 or 1 state depends on the membrane potential, u_i:

$$\begin{aligned} &P[S_i(t) = 1] \equiv g[u_i(t)], \\ &P[S_i(t) = 0] = 1 - P[S_i(t) = 1], \end{aligned} \tag{3.1}$$

where g is the "escape function" (Gerstner and Kistler 2002), which monotonically increases and is a differentiable function that takes values between 0 and 1. The membrane potential, u_i , is determined by the past spike histories of N neurons, as

$$\begin{aligned} u_i(t) = &\sum_{\tau=1}^{\infty} \sum_{j \neq i} J_{ij} \epsilon_{ij}(\tau)(2x_j(t-\tau)S_j(t-\tau) - 1) \\ &+ h_i + u_r, \end{aligned} \tag{3.2}$$

where $\epsilon_{ij}(\tau)$ describes the time course of a postsynaptic potential evoked by the firing of presynaptic neurons, h_i is an input potential, and u_r is a resting potential. We have not taken into account the effect of refractoriness to simplify the network model and investigate the effect of synaptic plasticity on the correlation between neural activities. The synaptic connection, $J_{ij}(t)(= J_{ij}x_j(t))$, in this model dynamically changes with the efficacy of signal transmission at the jth neuron, $x_j(t)$. $x_j(t)$ dynamically changes with synaptic depression and is determined by both itself and the corresponding neuron state at the preceding time, $t - 1$:

$$x_i(t+1) = x_i(t) + \frac{1 - x_i(t)}{\tau_D} - U x_i(t) S_i(t). \tag{3.3}$$

The phenomenological model of synaptic depression described by Eq. (3.3) has previously been proposed by several researchers (Abbott et al. 1997, Tsodyks et al. 1998). The jth neuron, which is called a presynaptic neuron, exhausts neurotransmitters when it transmits signals. The efficacy of signal transmission at presynaptic neuron j at time t decreases by a certain fraction, $Ux_j(t-1)(0 < U \leq 1)$, after the presynaptic neuron, $S_j(t-1) = 1$, is fired and it recovers with time constant $\tau_D(\tau_D \geq 1)$, as shown in Eq. (3.3).

3.3 Theory of correlations

3.3.1 Instantaneous firing rate and synaptic efficacy

First, we consider the noise average of neuronal states and synaptic variables, which are denoted by $\langle S_i(t)\rangle$ for the former and $\langle x_i(t)\rangle$ for the latter. We call these values the instantaneous firing rate and synaptic efficacy at time t. We derive dynamical mean field equations in this section for a network with synaptic depression by taking the average of two stochastic variables: a firing-state variable, $S(t)$, and a synaptic variable, $x(t)$. The average product of the variables in these equations is decoupled as the product of their averages because the stochastic variables are independent in the limit of $N \to \infty$ (Igarashi et al. 2010). We derived the instantaneous firing rate and synaptic efficacy at a steady state by using these equations.

The noise average of a function, $\langle f\rangle$, is defined as

$$\begin{aligned}\langle f(\mathbf{S}^t, \mathbf{S}^{t-1}, \ldots, \mathbf{S}^0)\rangle \equiv \sum_{\mathbf{S}^t}\sum_{\mathbf{S}^{t-1}}\cdots\sum_{\mathbf{S}^0} f(\mathbf{S}^t, \mathbf{S}^{t-1}, \ldots, \mathbf{S}^0) \\ \times P(\mathbf{S}^t, \mathbf{S}^{t-1}, \ldots, \mathbf{S}^0),\end{aligned} \tag{3.4}$$

where $\mathbf{S}^t$ represents the spike pattern of N neurons at time t and $\sum_{\mathbf{S}^t}$ represents the summation over all possible configurations $\mathbf{S}^t$. $P(\mathbf{S}^t, \mathbf{S}^{t-1}, \ldots, \mathbf{S}^0)$ is the probability of finding a system in a state, $\{\mathbf{S}^t, \mathbf{S}^{t-1}, \ldots, \mathbf{S}^0\}$. $P(\mathbf{S}^t, \mathbf{S}^{t-1}, \ldots, \mathbf{S}^0)$ is described by the following master equation:

$$\begin{aligned}P(\mathbf{S}^t, \mathbf{S}^{t-1}, \ldots, \mathbf{S}^0) = W(\mathbf{S}^t|\mathbf{S}^{t-1}, \mathbf{S}^{t-2}, \ldots, \mathbf{S}^0) \\ \times P(\mathbf{S}^{t-1}, \mathbf{S}^{t-2}, \ldots, \mathbf{S}^0),\end{aligned} \tag{3.5}$$

where $W(\mathbf{S}^t|\mathbf{S}^{t-1}, \mathbf{S}^{t-2}, \ldots, \mathbf{S}^0)$ is the transition probability, which is determined by the update rule [Eq.3.1]

$$\begin{aligned}&W(\mathbf{S}^t|\mathbf{S}^{t-1}, \mathbf{S}^{t-2}, \ldots, \mathbf{S}^0) \\ &= \prod_{i=1}^{N} \frac{1 + [2S_i(t) - 1]\{2g[u_i(t)] - 1\}}{2}.\end{aligned} \tag{3.6}$$

To simplify the equation, $\{\mathbf{S}^{t-1}, \mathbf{S}^{t-2}, \ldots, \mathbf{S}^0\}$ are denoted by Y^{t-1}.

By using Eq.(3.5), the instantaneous firing rate at time t, $\langle S_i(t)\rangle$, can be computed as

$$\langle S_i(t)\rangle = \sum_{Y^{t-1}} P(Y^{t-1}) \sum_{\mathbf{S}^t} S_i(t) W(\mathbf{S}^t|Y^{t-1}), \tag{3.7}$$

$$= \langle g[u_i(t)]\rangle, \tag{3.8}$$

where $\sum_{Y^{t-1}}$ represents the summation over all possible configurations of the past spike histories, Y^{t-1}.

We derived microscopic dynamical mean field equations by first taking the noise average of the firing-state variable at time t [Eq.(3.8)]. Taylor expansion provides us with

$$\langle S_i(t)\rangle = \left\langle g[\langle u_i(t)\rangle] + g'[\langle u_i(t)\rangle]\delta u_i(t) + \frac{1}{2}g''[\langle u_i(t)\rangle](\delta u_i(t))^2 + \dots \right\rangle,$$

$$= g[\langle u_i(t)\rangle] + \left\langle \frac{1}{2}g''[\langle u_i(t)\rangle](\delta u_i(t))^2 \right\rangle + \dots, \tag{3.9}$$

where we define $\delta u_i(t) = u_i(t) - \langle u_i(t)\rangle$, $g'(u) = dg(u)/dt$, and $g''(u) = d^2g(u)/dt^2$. When each neuron is connected to a number of neurons of order N and connections J_{ij} are all of order $1/N$, $\langle \delta u_i(t))^2\rangle$ are of order $1/N$ (See Appendix B). The second order and the higher-order terms of Eq. (3.9) in such a situation are no more than order $1/N$. Hence, considering the limit of $N \to \infty$, one obtains leading order

$$\langle S_i(t)\rangle = g\left\{ \sum_{\tau=1}^{\infty} \sum_{j\neq i} J_{ij}\epsilon_{ij}(\tau)(2\langle x_j(t-\tau)S_j(t-\tau)\rangle - 1) + h_i + u_r \right\}. \tag{3.10}$$

We take advantage of the independence of $x_j(t)$ and $S_j(t)$ in the limit of large networks, $N \to \infty$ (Igarashi et al. 2010), and thereby obtain the dynamical mean field equations for $\langle S_i(t)\rangle$:

$$\langle S_i(t)\rangle = g\left\{ \sum_{\tau=1}^{\infty} \sum_{j\neq i} J_{ij}\epsilon_{ij}(\tau)(2\langle x_j(t-\tau)\rangle\langle S_j(t-\tau)\rangle - 1) + h_i + u_r \right\}. \tag{3.11}$$

Similarly, we consider the noise average of Eq. (3.3) for the synaptic variable:

$$\langle x_i(t+1)\rangle = \langle x_i(t)\rangle + \frac{1 - \langle x_i(t)\rangle}{\tau_D} - U\langle x_i(t)\rangle\langle S_i(t)\rangle. \tag{3.12}$$

Eqs. (3.11) and (3.12) for the stochastic neural network model coincide with equations for an analog neural network with synaptic depression (Tsodyks et al. 1998, York and van Rossum 2009, Kilpatrick and Bressloff 2010). We then obtain the micro-

scopic steady-state equation for $\langle S_i \rangle$ and $\langle x_i \rangle$.

$$\langle S_i \rangle = g\left\{ \sum_{\tau=1}^{\infty} \sum_{j \neq i} J_{ij} \epsilon_{ij}(\tau)(2\langle x_j \rangle \langle S_j \rangle - 1) + h_i + u_r \right\}, \tag{3.13}$$

$$\langle x_i \rangle = \langle x_i \rangle + \frac{1 - \langle x_i \rangle}{\tau_D} - U\langle x_i \rangle \langle S_i \rangle, \tag{3.14}$$

where $\langle S_i \rangle = \lim_{t\to\infty} \langle S_i(t) \rangle$ and $\langle x_i \rangle = \lim_{t\to\infty} \langle x_i(t) \rangle$. The steady-state equation for noise average $\langle x_i \rangle$ is

$$\langle x_i \rangle = \frac{1}{1 + \gamma \langle S_i \rangle}, \quad \gamma = \tau_D U. \tag{3.15}$$

Finally, we obtain the microscopic steady-state equation for $\langle S_i \rangle$ in a network with synaptic depression

$$\langle S_i \rangle = g\left\{ \sum_{\tau=1}^{\infty} \sum_{j \neq i} J_{ij} \epsilon_{ij}(\tau) \left(2\frac{\langle S_j \rangle}{1 + \gamma \langle S_j \rangle} - 1 \right) + h_i + u_r \right\}. \tag{3.16}$$

According to Eq. (3.16), the steady state depends on γ ($= \tau_D U$), which ranges from 0 to U because of $0 < U \leq 1$ and $\tau_D \geq 1$ (Tsodyks et al. 1998, Igarashi et al. 2010). Therefore, we can easily figure out the effect of synaptic depression by varying γ. If we solve the self-consistent equation (3.16), we can obtain instantaneous firing rates $\langle S_i \rangle$ and synaptic efficacies at equilibrium $\langle x_i \rangle$.

We derive auto-correlation functions and cross-correlation functions in this section and the one that follows it to calculate correlations between neural activities at equilibrium. As a synaptic variable, x, dynamically changes in this network model, we need to discuss not only correlations between the activities of cortical neurons but also those between neural activities and synaptic variables. We then have to derive and solve 15 types of equations to calculate neural correlations at equilibrium. We define neural correlation in this section and the next and briefly explain how the equations are derived. We present the technical details on the calculations in Appendix B.1.

Auto-correlation functions are defined as

$$\begin{aligned} A_i^s(t, t+\tau) &\equiv \langle \delta S_i(t) \delta S_i(t+\tau) \rangle, \\ A_i^{sx}(t, t+\tau) &\equiv \langle \delta S_i(t) \delta x_i(t+\tau) \rangle, \\ A_i^{xs}(t, t+\tau) &\equiv \langle \delta x_i(t) \delta S_i(t+\tau) \rangle, \\ A_i^x(t, t+\tau) &\equiv \langle \delta x_i(t) \delta x_i(t+\tau) \rangle. \end{aligned} \tag{3.17}$$

We also define cross-correlation functions as

$$\begin{aligned} C_{ij}^{s}(t,t+\tau) &\equiv \langle \delta S_i(t)\delta S_j(t+\tau)\rangle, \\ C_{ij}^{sx}(t,t+\tau) &\equiv \langle \delta S_i(t)\delta x_j(t+\tau)\rangle, \\ C_{ij}^{xs}(t,t+\tau) &\equiv \langle \delta x_i(t)\delta S_j(t+\tau)\rangle, \\ C_{ij}^{x}(t,t+\tau) &\equiv \langle \delta x_i(t)\delta x_j(t+\tau)\rangle, \end{aligned} \tag{3.18}$$

where $i \neq j$. We denote the auto-correlation functions and cross-correlation functions at equilibrium as

$$\begin{aligned} A_{i}^{s}(\tau) &\equiv \lim_{t\to\infty} \langle \delta S_i(t)\delta S_i(t+\tau)\rangle, \\ A_{i}^{sx}(\tau) &\equiv \lim_{t\to\infty} \langle \delta S_i(t)\delta x_i(t+\tau)\rangle, \\ A_{i}^{xs}(\tau) &\equiv \lim_{t\to\infty} \langle \delta x_i(t)\delta S_i(t+\tau)\rangle, \\ A_{i}^{x}(\tau) &\equiv \lim_{t\to\infty} \langle \delta x_i(t)\delta x_i(t+\tau)\rangle, \end{aligned} \tag{3.19}$$

$$\begin{aligned} C_{ij}^{s}(\tau) &\equiv \lim_{t\to\infty} \langle \delta S_i(t)\delta S_j(t+\tau)\rangle, \\ C_{ij}^{sx}(\tau) &\equiv \lim_{t\to\infty} \langle \delta S_i(t)\delta x_j(t+\tau)\rangle, \\ C_{ij}^{xs}(\tau) &\equiv \lim_{t\to\infty} \langle \delta x_i(t)\delta S_j(t+\tau)\rangle, \\ C_{ij}^{x}(\tau) &\equiv \lim_{t\to\infty} \langle \delta x_i(t)\delta x_j(t+\tau)\rangle. \end{aligned} \tag{3.20}$$

We use instantaneous firing rate $\langle S_i\rangle$ and synaptic efficacy $\langle x_i\rangle$ in a steady state to calculate the equilibrium values of auto-correlation functions and cross-correlation functions in this and the following section.

We derive the equal-time auto-correlation functions, $A_i^s(0)$, $A_i^{sx}(0)$, $A_i^{xs}(0)$, $A_i^x(0)$, and the equal-time cross-correlation functions, $C_{ij}^s(0)$, $C_{ij}^{sx}(0)$, $C_{ij}^{xs}(0)$, $C_{ij}^x(0)$ in this section.

First, we calculate $A_i^s(0)$ at equilibrium. Since the neural network consists of binary neurons, $S_i = 0, 1$, we can derive $S_i^2 = S_i$. Using this equation yields

$$A_i^s(0) = \langle S_i\rangle(1 - \langle S_i\rangle). \tag{3.21}$$

The equal-time cross-correlation functions between $S_i(t)$ and $S_j(t)(j \neq i)$, i.e., $C_{ij}^s(0)$, can be written as

$$\begin{aligned} C_{ij}^{s}(t,t) &= \langle S_i(t)S_j(t)\rangle - \langle S_i(t)\rangle\langle S_j(t)\rangle, && (3.22)\\ &= \sum_{Y^{t-1}} \Big\{ \mathbf{P}(Y^{t-1}) \sum_{\mathbf{S}^t} S_i(t)S_j(t)\mathbf{W}(\mathbf{S}^t|Y^{t-1}) \\ &\quad - \langle S_i(t)\rangle\langle S_j(t)\rangle \Big\}, && (3.23)\\ &= \langle g[u_i(t)]g[u_j(t)]\rangle - \langle g[u_i(t)]\rangle\langle g[u_j(t)]\rangle. && (3.24) \end{aligned}$$

By expanding $g[u_i(t)]$ around the noise average of $\hat{u}_i$ and taking limit $t \to \infty$, we obtain (see Appendix B.1 for details)

$$C_{ij}^{s}(0) = \sum_{\tau,\tau'}^{\infty} \sum_{k\neq i} \sum_{l\neq j,k} \tilde{J}_{ik}(\tau)\tilde{J}_{jl}(\tau')Z_{kl}(\tau-\tau') + \sum_{\tau,\tau'}^{\infty} \sum_{k\neq i} \tilde{J}_{ik}(\tau)\tilde{J}_{jk}(\tau')Z_{k}(\tau-\tau'), \tag{3.25}$$

where we denote $\tilde{J}_{ik}(\tau) = 2g'(\langle u_i \rangle)J_{ik}\epsilon_{ik}(\tau)$ and

$$\begin{aligned} Z_{kl}(t,t+\tau) &\equiv \langle \delta(x_k(t)S_k(t))\delta(x_l(t+\tau)S_l(t+\tau))\rangle, \\ Z_{kl}(\tau) &\equiv \lim_{t\to\infty} Z_{kl}(t,t+\tau), \qquad (3.26) \\ Z_{k}(t,t+\tau) &\equiv \langle \delta(x_k(t)S_k(t))\delta(x_k(t+\tau)S_k(t+\tau))\rangle. \\ Z_{k}(\tau) &\equiv \lim_{t\to\infty} Z_{k}(t,t+\tau). \qquad (3.27) \end{aligned}$$

We evaluate $Z_{kl}(\tau)$ and $Z_k(\tau)$ at equilibrium and derive (see Appendix B.1 for details)

$$\begin{aligned} Z_{kl}(\tau) = C_{kl}^{s}(\tau)\langle x_k\rangle\langle x_l\rangle + C_{kl}^{sx}(\tau)\langle x_k\rangle\langle S_l\rangle \\ + C_{kl}^{xs}(\tau)\langle S_k\rangle\langle x_l\rangle + C_{kl}^{x}(\tau)\langle S_k\rangle\langle S_l\rangle. \end{aligned} \tag{3.28}$$

For $k = l$, we obtain

$$\begin{aligned} Z_{k}(\tau) = A_{k}^{s}(\tau)\langle x_k\rangle\langle x_k\rangle + A_{k}^{sx}(\tau)\langle x_k\rangle\langle S_k\rangle \\ + A_{k}^{xs}(\tau)\langle S_k\rangle\langle x_k\rangle + A_{k}^{x}(\tau)\langle S_k\rangle\langle S_k\rangle. \end{aligned} \tag{3.29}$$

Equations such as (3.25), (3.28), and (3.29) for the equal-time cross-correlations, $C_{ij}^{s}(0)$, include correlation functions between neural activities and synaptic variables, such as C_{ij}^{sx}, C_{ij}^{xs}, C_{ij}^{x}, A_{i}^{sx}, A_{i}^{xs}, and A_{i}^{x}. We thus need the equations for these correlation functions between neural activities and synaptic variables to solve these equations.

Next, let us consider equal-time correlation functions, $C_{ij}^{sx}(0)$, $C_{ij}^{xs}(0)$, $C_{ij}^{x}(0)$, $A_{i}^{sx}(0)$, $A_{i}^{xs}(0)$, and $A_{i}^{x}(0)$. Similar to the approach we took in calculating $C_{ij}^{s}(0)$, we obtain (see Appendix B.1 for details)

$$\begin{aligned} C_{ij}^{sx}(0) = \sum_{\tau=1}^{\infty} \sum_{k\neq i,j} \tilde{J}_{ik}(\tau)\Big\{ \left(1-\frac{1}{\tau_d}\right)[C_{kj}^{x}(\tau-1)\langle S_k\rangle + C_{kj}^{sx}(\tau-1)\langle x_k\rangle] - UZ_{kj}(\tau-1)\Big\} \\ + \sum_{\tau=1}^{\infty} \tilde{J}_{ij}(\tau)\Big\{ \left(1-\frac{1}{\tau_d}\right)[A_{j}^{x}(\tau-1)\langle S_j\rangle + A_{j}^{sx}(\tau-1)\langle x_j\rangle] - UZ_{j}(\tau-1)\Big\}, \end{aligned} \tag{3.30}$$

$$C_{ij}^{x}(0) = \left(1 - \frac{1}{\tau_d}\right)^2 C_{ij}^{x}(0) + U^2 Z_{ij}(0) - U\left(1 - \frac{1}{\tau_d}\right) \times [C_{ij}^{x}(0)(\langle S_i\rangle + \langle S_j\rangle) + C_{ij}^{sx}(0)\langle x_i\rangle + C_{ij}^{xs}(0)\langle x_j\rangle]. \quad (3.31)$$

Since $C_{ij}^{xs}(t,t) = C_{ji}^{sx}(t,t)$, we can also obtain $C_{ji}^{sx}(0)$ from Eq. (3.30). If we set $j = i$ in Eq. (3.30), we derive the equations for equal-time auto-correlations $A_i^{sx}(0)$,

$$A_i^{sx}(0) = \sum_{\tau=1}^{\infty}\sum_{k\neq i}\tilde{J}_{ik}(\tau)\Bigg[\left(1 - \frac{1}{\tau_d}\right) \times (\langle x_k\rangle C_{ki}^{sx}(\tau-1) + \langle S_k\rangle C_{ki}^{x}(\tau-1)) - U Z_{ki}(\tau-1)\Bigg]. \quad (3.32)$$

Since $A_i^{xs}(0) = A_i^{sx}(0)$, we simultaneously obtain $A_i^{xs}(0)$. Similarly, we set $i = j$ in Eq.(3.31) to obtain equal-time auto correlation, $A_i^{x}(0)$, as

$$A_i^{x}(0) = \left(1 - \frac{1}{\tau_d}\right)^2 A_i^{x}(0) + U^2 Z_i(0) - U\left(1 - \frac{1}{\tau_d}\right) 2[A_i^{x}(0)\langle S_i\rangle + A_i^{sx}(0)\langle x_i\rangle]. \quad (3.33)$$

Because $A_i^{x}(0)$ and $A_i^{sx}(0)$ are 1 and $1/N$ orders, respectively, we ignore $A_i^{sx}(0)$ and derive

$$A_i^{x}(0) = \frac{U^2 A_i^{s}(0)\langle x_i\rangle^2}{1 - (1-1/\tau_d)^2 - U^2\langle S_i\rangle^2 + -2U(1-1/\tau_d)\langle S_i\rangle}. \quad (3.34)$$

These equations for equal-time cross-correlations $C_{ij}^{s}(0)$ and $C_{ij}^{sx}(0)$ and equal-time auto-correlations $A_i^{sx}(0)$ include time-delayed cross-correlations, such as $C_{ij}^{s}(\tau)$, $C_{ij}^{sx}(\tau)$, $C_{ij}^{xs}(\tau)$, and $C_{ij}^{x}(\tau)$, and time-delayed auto-correlations such as $A_i^{s}(\tau)$, $A_i^{sx}(\tau)$, $A_i^{xs}(\tau)$, and $A_i^{x}(\tau)$. We thus need the equations for these time-delayed correlation functions to solve these equations.

3.3.2 Time-delayed correlation functions

We derive the equations for the time-delayed correlation functions in this section Let us consider time-delayed cross-correlation functions between neural activities, $C_{ij}^{s}(t, t+\tau)$.

The time-delayed cross-correlation functions can be written as

$$\begin{aligned} C_{ij}^{s}(t,t+\tau) &= \langle S_i(t)S_j(t+\tau)\rangle - \langle S_i(t)\rangle\langle S_j(t+\tau)\rangle, \\ &= \sum_{Y^{t+\tau-1}} P(Y^{t+\tau-1})S_i(t)\sum_{\mathbf{S}^{t+\tau}}\Big\{S_j(t+\tau) \\ &\times W(\mathbf{S}^{t+\tau}|Y^{t+\tau-1}) - \langle S_i(t)\rangle\langle S_j(t+\tau)\rangle\Big\}, \\ &= \langle S_i(t)g(u_j(t+\tau))\rangle - \langle S_i(t)\rangle\langle S_j(t+\tau)\rangle, \\ &= \langle \delta S_i(t)g(u_j(t+\tau))\rangle. \end{aligned} \tag{3.35}$$

By expanding $g(u_j(t+\tau))$ around the noise average of u_j and taking in limit $t\to\infty$, we derive the time-delayed cross-correlation functions as

$$\begin{aligned} C_{ij}^{s}(\tau) = \sum_{\tau'=1}^{\infty}\sum_{k\neq j,i}\tilde{J}_{jk}(\tau')[C_{ik}^{sx}(\tau-\tau')\langle S_k\rangle + C_{ik}^{s}(\tau-\tau')\langle x_k\rangle] \\ + \sum_{\tau'=1}^{\infty}\tilde{J}_{ji}(\tau')[A_{i}^{sx}(\tau-\tau')\langle S_i\rangle + A_{i}^{s}(\tau-\tau')\langle x_i\rangle]. \end{aligned} \tag{3.36}$$

If we set $j=i$ in Eq. (3.36), we obtain time-delayed auto-correlation functions between neural states, $A_i^s(\tau)$, at equilibrium:,

$$A_{i}^{s}(\tau) = \sum_{\tau'=1}^{\infty}\sum_{k\neq i}\tilde{J}_{ik}(\tau')[C_{ik}^{sx}(\tau-\tau')\langle S_k\rangle + C_{ik}^{s}(\tau-\tau')\langle x_k\rangle]. \tag{3.37}$$

Next, we consider time-delayed cross-correlation functions between S_i and x_j, i.e., $C_{ij}^{sx}(\tau)$. Substituting Eq. (3.3) into Eq. (3.18) and taking limit $t\to\infty$ gives

$$\begin{aligned} C_{ij}^{sx}(\tau) = \lim_{t\to\infty}\Bigg\langle \delta S_i(t)\Bigg(\left(1-\frac{1}{\tau_d}\right)\delta x_j(t+\tau-1) \\ - U\delta(x_j(t+\tau-1)S_j(t+\tau-1))\Bigg)\Bigg\rangle, \\ = \left(1-\frac{1}{\tau_d}-U\langle S_j\rangle\right)C_{ij}^{sx}(\tau-1) - U\langle x_j\rangle C_{ij}^{s}(\tau-1). \end{aligned} \tag{3.38}$$

If we set $j=i$ in Eq. (3.38), we derive the time-delayed auto-correlation functions between S_i and x_i, $A_i^{sx}(\tau)$, as

$$A_{i}^{sx}(\tau) = \left(1-\frac{1}{\tau_d}-U\langle S_i\rangle\right)A_{i}^{sx}(\tau-1) - U\langle x_i\rangle A_{i}^{s}(\tau-1). \tag{3.39}$$

Taking into account the order of $A_i^{sx}(\tau)$ and $A_i^s(\tau)$, we can simplify Eq. (3.39). $A_i^{sx}(0)$ and $A_i^{sx}(\tau)(1\leq\tau)$ are each on the order of $1/N$ and 1, while $A_i^s(0)$ and $A_i^s(\tau)(1\leq\tau)$ are on the order of 1 and $1/N$, respectively. Ignoring $A_i^{sx}(0)$ and $A_i^s(\tau)(1\leq\tau)$, we obtain

1, $\tau = 1$

$$A_i^{sx}(1) = -U\langle x_i\rangle A_i^s(0), \tag{3.40}$$

2, $\tau > 1$

$$A_i^{sx}(\tau) = \left(1 - \frac{1}{\tau_d} - U\langle S_i\rangle\right) A_i^{sx}(\tau - 1). \tag{3.41}$$

Similar to the approach we took in the previous section, time-delayed cross-correlation functions between x_i and S_j, $C_{ij}^{xs}(t, t+\tau)$ can be written as $C_{ij}^{xs}(t, t+\tau) = \langle \delta x_i(t) g(u_j(t+\tau))\rangle$. By expanding $g(u_j(t+\tau))$ around the noise average of u_j and taking in limit $t \to \infty$, we obtain

$$\begin{aligned} &C_{ij}^{xs}(\tau) \\ &\quad = \sum_{\tau'=1}^{\infty} \sum_{k\neq j,i} \tilde{J}_{jk}(\tau')[C_{ik}^{x}(\tau - \tau')\langle S_k\rangle + C_{ik}^{xs}(\tau - \tau')\langle x_k\rangle] \\ &\qquad + \sum_{\tau'=1}^{\infty} \tilde{J}_{ji}(\tau')[A_i^{x}(\tau - \tau')\langle S_i\rangle + A_i^{xs}(\tau - \tau')\langle x_i\rangle]. \end{aligned} \tag{3.42}$$

If we set $j = i$ in Eq. (3.42), we obtain time-delayed auto-correlation functions between x_i and S_i, $A_i^{xs}(\tau)$, as

$$A_i^{xs}(\tau) = \sum_{\tau'=1}^{\infty} \sum_{k\neq i} \tilde{J}_{ik}(\tau')[C_{ik}^{x}(\tau - \tau')\langle S_k\rangle + C_{ik}^{xs}(\tau - \tau')\langle x_k\rangle]. \tag{3.43}$$

Finally, we derive time-delayed cross-correlation functions between x_i and x_j, i.e., $C_{ij}^{x}(\tau)$. Substituting Eq. (3.3) into Eq. (3.18) and taking limit $t \to \infty$ gives

$$\begin{aligned} C_{ij}^{x}(\tau) &= \lim_{t\to\infty} \Bigg\langle \delta x_i(t) \Bigg(\left(1 - \frac{1}{\tau_d}\right) \delta x_j(t + \tau - 1) \\ &\qquad - U\delta(x_j(t + \tau - 1) S_j(t + \tau - 1)) \Bigg) \Bigg\rangle, \\ &= \left(1 - \frac{1}{\tau_d} - U\langle S_j\rangle\right) C_{ij}^{x}(\tau - 1) - U\langle x_j\rangle C_{ij}^{xs}(\tau - 1). \end{aligned} \tag{3.44}$$

If we set $j = i$ in Eq. (3.44), we obtain time-delayed auto-correlation functions between synaptic variables at equilibrium:,

$$A_i^{x}(\tau) = \left(1 - \frac{1}{\tau_d} - U\langle S_i\rangle\right) A_i^{x}(\tau - 1), \tag{3.45}$$

where we ignore $A_i^{xs}(\tau-1)$, because $A_i^x(\tau)$ and $A_i^{xs}(\tau-1)$ are on the order of 1 and $1/N$, respectively. By solving Eqs. (3.21), (3.25), (3.30), (3.32), (3.31), (3.34), (3.37), (3.36), (3.38), (3.40), (3.41), (3.42), (3.43), (3.44), and (3.45), we eventually obtain the equilibrium value for correlations between the activities of cortical neurons and those between neural activities and synaptic variables.

3.3.3 Correlations of mean firing rate

We calculated the correlations of spikes, $\langle \delta S_i \delta S_j \rangle$, in the previous section. Here, we compute the correlation functions of the mean firing rate within time window T, $Q_{ij} = \langle \delta r_i \delta r_j \rangle$, where $\delta r_i \equiv r_i - \langle r_i \rangle$, and we call the value, r_i, the mean firing rate. We calculate the rate correlations to evaluate the effect of synaptic depression on the correlations between neural activities within the long term, T. Firing rate r_i and synaptic efficacy q_i within T is defined as

$$r_i = \frac{1}{T}\sum_{\tau=1}^{T} S_i(\tau),\ q_i = \frac{1}{T}\sum_{\tau=1}^{T} x_i(\tau). \tag{3.46}$$

Mean firing rate f_i and mean synaptic efficacy X_i at equilibrium are the same as instantaneous firing rate $\langle S_i \rangle$ and instantaneous synaptic efficacy $\langle x_i \rangle$, respectively:

$$\begin{aligned} f_i \equiv \langle r_i \rangle &= \frac{1}{T}\sum_{\tau=1}^{T} \langle S_i(\tau) \rangle \\ &= \langle S_i \rangle, \\ X_i \equiv \langle q_i \rangle &= \frac{1}{T}\sum_{\tau=1}^{T} \langle x_i(\tau) \rangle \\ &= \langle x_i \rangle. \end{aligned} \tag{3.47}$$

The correlation for the mean firing rate can be calculated as in (Macke et al. 2009, Oizumi et al. 2010).

$$\begin{aligned}
Q_{ij} &= \langle \delta r_i \delta r_j \rangle, \\
&= \langle (r_i - f_i)(r_j - f_j), \\
&= \left\langle \left(\frac{1}{T} \sum_{\tau=1}^{T} S_i(\tau) - f_i \right) \left(\frac{1}{T} \sum_{\tau'=1}^{T} S_j(\tau') - f_j \right) \right\rangle, \\
&= \frac{1}{T^2} \sum_{\tau=1}^{T} \sum_{\tau'=1}^{T} \langle S_i(\tau) S_j(\tau') \rangle - f_i f_j, \\
&= \frac{1}{T^2} \sum_{\tau=1}^{T} \sum_{\tau'=1}^{T} [\langle \delta S_i(\tau) \delta S_j(\tau') \rangle + \langle S_i(\tau) \rangle \langle S_j(\tau') \rangle] \\
&- f_i f_j, \\
&= \frac{1}{T^2} \sum_{\tau=1}^{T} \sum_{\tau'=1}^{T} C_{ij}^{s}(\tau' - \tau).
\end{aligned} \tag{3.48}$$

Using mean firing rate correlations Q_{ij}, which can be computed though Eq. (3.48), we can evaluate the effect of synaptic depression on neural correlations over the long-term.

3.3.4 Fisher information

Let us consider the problem of how accurately stimulus θ, which is a single variable, can be estimated from the mean firing rates of neuronal population $\mathbf{r} = \{r_1, r_2, \ldots, r_N\}$. Through the Cramer-Rao bound, the average squared decoding error for an unbiased estimation of stimulus $\hat{\theta}$ is greater than or equal to $1/I(\theta)$,

$$\langle (\theta - \hat{\theta})^2 \rangle \geq \frac{1}{I(\theta)}, \tag{3.49}$$

when $I(\theta)$ is Fisher information. Fisher information is given by

$$I(\theta) = \int d\mathbf{r} P[\mathbf{r}|\theta] \left(-\frac{\partial^2 \ln P[\mathbf{r}|\theta]}{\partial \theta^2} \right), \tag{3.50}$$

where $P[\mathbf{r}|\theta]$ is the conditional probability distribution, which is the probability that neural response $\mathbf{r}$ will be evoked by the presentation of a multivariate Gaussian probability distribution with covariance matrix $Q(\theta)$,

$$\begin{aligned}
P[\mathbf{r}|\theta] &= \frac{1}{\sqrt{(2\pi)^N \det \mathbf{Q}(\theta)}} \\
&\times \exp \left[-\frac{1}{2} [\mathbf{r} - \mathbf{f}(\theta)]^T \mathbf{Q}^{-1}(\theta) [\mathbf{r} - \mathbf{f}(\theta)], \right],
\end{aligned} \tag{3.51}$$

where $\mathbf{f}$ is the mean value of $\mathbf{r}$. Note that the (i,j)th element of covariance matrix Q_{ij} represents mean firing rate correlation $\langle \delta r_i \delta r_j \rangle$. Under this assumption, Fisher information can be written as in (Kay 1993):

$$I(\theta) = I_{\mathrm{mean}}(\theta) + I_{\mathrm{cov}}(\theta), \tag{3.52}$$

$$I_{\mathrm{mean}}(\theta) = \mathbf{f}'(\theta)^T \mathbf{Q}^{-1}(\theta)\mathbf{f}'(\theta), \tag{3.53}$$

$$I_{\mathrm{cov}}(\theta) = \mathrm{Tr}[\mathbf{Q}'(\theta)\mathbf{Q}^{-1}(\theta)\mathbf{Q}{-}1(\theta)]/2, \tag{3.54}$$

where Tr stands for the trace operation, $f'(\theta) = df(\theta)/d\theta$, and $\mathbf{Q}'(\theta) = d\mathbf{Q}/d\theta$. Because mean firing rates r and mean firing rate correlations Q_{ij} can be analytically calculated in the spike response model as discussed earlier in Section 3.3.3, Fisher information can also be analytically calculated from Eq. (3.52).

3.4 Ring attractor network with Mexican hat type connectivity

3.4.1 Model

Let us now consider a ring attractor neural network with Mexican hat type connectivity (Ben-Yishai et al. 1995, Hamaguchi 2006). We do not this to imply the presence of such ring structures in neuroanatomy, but merely to illustrate that neurons tuned to a periodic variable are functionally fully connected. This ring network model is thus not a one-dimensional lattice model but has often been used as an appropriately approximated network model of the primary visual cortex (Ben-Yishai et al. 1995). Following these previous studies, we used the conventional ring neural network model and investigated what effect synaptic depression had on neural correlations.

In this network, $N = 1000$ neurons are divided into a $K = 10$ subpopulation. The choice of the number of subpopulations does not qualitatively affect the results. The number of neurons in each population is $G = 100$. All neurons in each population have the same preferred orientation and neuron i in the kth population is labeled using angle θ_k. We assume that the preferred orientations of $K = 10$ subpopulations are evenly distributed from $-\pi/2$ to $\pi/2$, and divide 2π in $K = 10$, i.e., $\theta_k = -\pi/2 + k\pi/K$. The strength of connections J_{kl} between a neuron in the kth population and a neuron in the lth population is calculated as

$$J_{kl} = J_0/N + J_1 \cos 2(\theta_k - \theta_l)/N, \tag{3.55}$$

where J_0 is a uniform interaction and J_1 is a lateral-inhibitory interaction. The model

with $J_1 = 0$ is reduced to a network with uniform connections. We set uniform interaction $J_0 = 0.5$ and lateral-inhibitory interaction $J_1 = 3$ to stabilize the steady states (York and van Rossum 2009, Igarashi et al. 2010). Neurons in simulations are evolved at maximum 10^3 time steps with initial state $S_i(0) = 0$ and $x_i(0) = 1$ $\forall i$, until they reach a stable equilibrium point. Instantaneous firing rates and correlation functions are estimated from simulations over $5 \cdot 10^6$ time steps in equilibrium.

3.4.2 Correlation functions

To investigate the effect of synaptic depression on neural correlations, we adjust the external inputs to neurons, h_i, and maintain the firing rate, $\langle S_i(t) \rangle$, regardless of the strength of synaptic depression, γ (See Appendix B.2). We set h_i as follows.

$$h_i = h_i^0 + \sum_{\tau}^{\infty} \sum_{j \neq i}^{N} J_{ij} \epsilon_{ij}(\tau) \frac{2\gamma \langle S_i^0 \rangle^2}{1 + \gamma \langle S_i^0 \rangle}, \tag{3.56}$$

where we define h_i^0 and $\langle S_i^0 \rangle$ as the respective input and instantaneous firing rate in the absence of synaptic depression, i.e., $\gamma = 0$. We set $h_i^0 = f_0 \cos(2(\theta_i - \phi))$, $f_0 = 0.05$, and the orientation of stimuli $\phi = 0$. Using self-consistent Eq. (3.16), we can derive $\langle S_i^0 \rangle$. We then adjust external inputs h_i and obtained constant firing rates regardless of synaptic depression, as can be seen in Figs. 3.1(a) and (b). In addition, each neuron follows a probabilistic dynamic depending on the firing probability, $g[u_i(t)] = \frac{1}{2}\{1 + \tanh[\beta u_i(t)]\}$, where $1/\beta (= T)$ is the level of noise due to stochastic synaptic activity and we set $\beta = 1$ (Oizumi et al. 2010, Hamaguchi 2006). The response kernels of the discrete spike model are given by $\epsilon_{ij}(\tau) = [1 - \exp(-1/\tau_s)] \exp(-\tau/\tau_s)$, where $\tau_s = 2$.

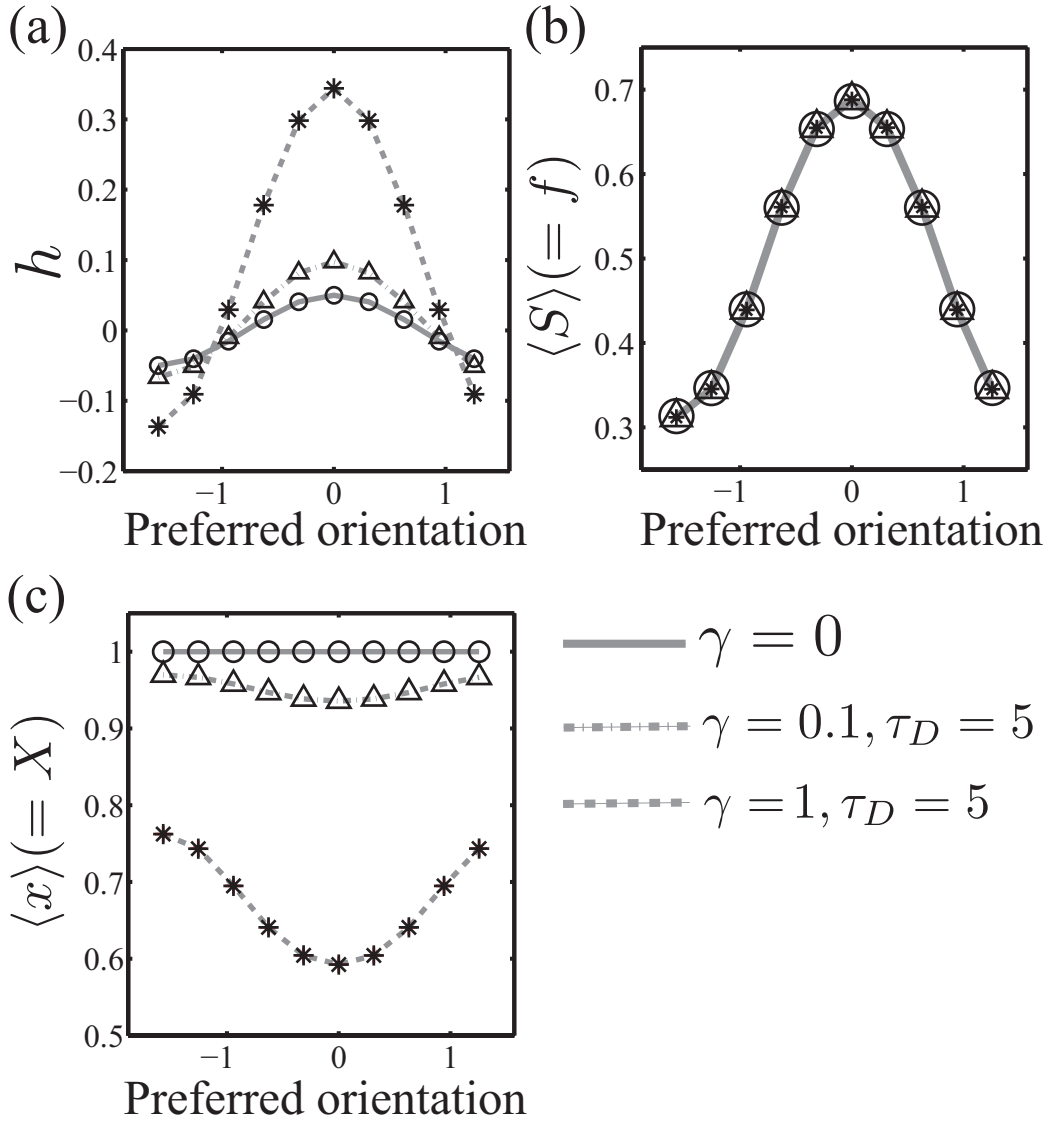

Fig. 3.1. (a) Inputs, (b) instantaneous firing rates $\langle S \rangle$, and (c) synaptic efficacy $\langle x \rangle$ obtained from simulations (open circles, triangles, and asterisks) compared with theory (solid lines) in absence and presence of synaptic depression, $\gamma = 0$, 0.1, and 1, respectively, with $\tau_D = 5$. Parameters of connections are $J_0 = 0.5$ and $J_1 = 3$.

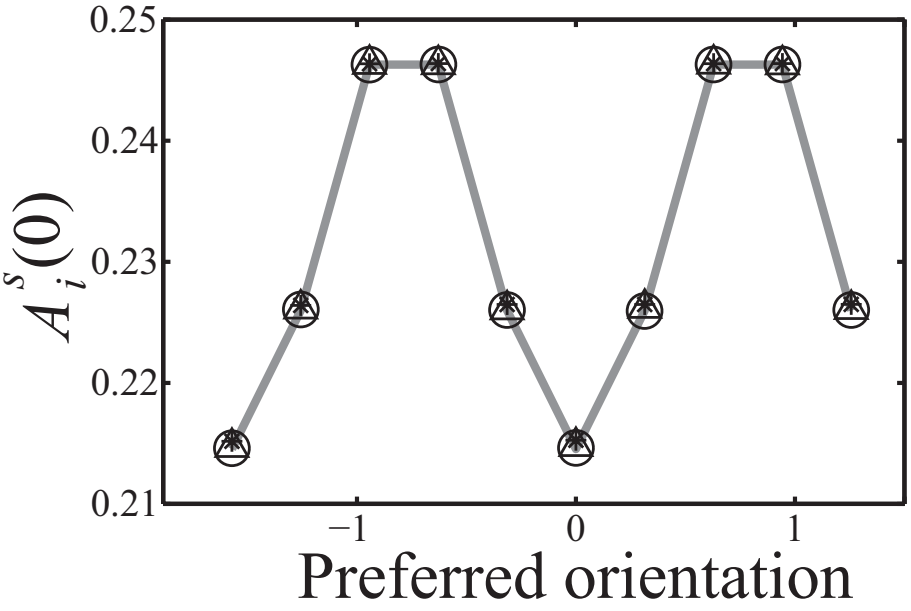

Fig. 3.2. Equal-time auto-correlation functions $A_i^s(0)$ obtained from simulations (open circles, triangles, and asterisks) compared with theory (solid, chain, and dotted lines) in absence and presence of synaptic depression, $\gamma = 0$, 0.1, and 1, respectively, with $\tau_D = 5$. Because of firing rates in presence of synaptic depression as well as those in its absence (Fig. 3.1(b)), $A_i^s(0)$ agree completely with each other.

We found that the firing correlations obtained under these conditions by using our theory coincided with the results from simulations, as seen in Figs. 3.2 and 3.3. Figure 3.2 shows equal-time auto-correlation functions $A_i^s(\tau)$ of a neuron with preferred orientations from $-\pi/2$ to $2\pi/5$. Equal-time auto-correlation functions $A_i^s(0)$ in absence of synaptic depression coincide with those in presence of synaptic depression (as indicated in Fig. 3.2) because the auto-correlation functions of neural activity depend on instantaneous firing rates (Eq. (3.21)) and the instantaneous firing rates for in the case of $\gamma = 0$ are the same as those for $\gamma = 0.1$ and 1 (Fig. 3.1(b)). Let us then consider the results for time-delayed auto correlations $A_i^s(\tau)$ where $\tau > 1$. Figure 3.3(a) plots the auto-correlation functions of a neuron with preferred orientation 0 rad. We found that the strength of synaptic depression, γ, increases and sequences of spikes are less correlated. The simulation results are in agreement with both those from the theoretical solution and a previous study (Goldman et al. 2002).

Next, let us consider what effects synaptic depression has on neural cross-correlations between neurons. Figure 3.3(b) plots the cross-correlation functions between a neuron with preferred orientation 0 rad and a neuron with preferred orientation $\pi/10$ rad where

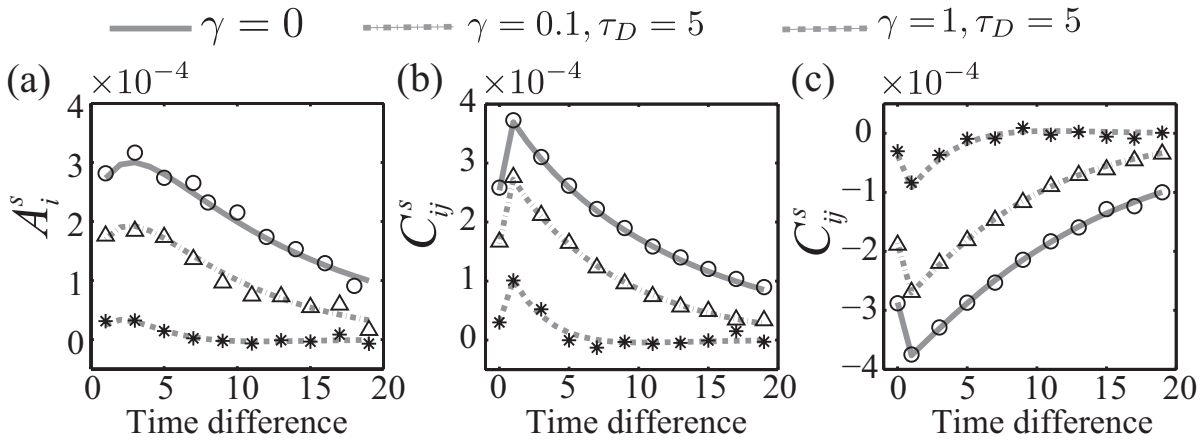

Fig. 3.3. Auto-correlation and cross-correlation functions from simulations (open circles, triangles, and asterisks) compared with theory (solid, chain, and dotted lines) in absence and presence of synaptic depression, $\gamma = 0$, 0.1, and 1, respectively, with $\tau_D = 5$. (a) Auto-correlation functions of neuron with preferred orientation 0 rad, $A_i^s(\tau)$, where $\tau > 1$. (b) Cross-correlation functions between neuron i with preferred orientation 0 rad and neuron j with preferred orientation $\pi/10$ rad, $C_{ij}^s(\tau)$, where $J_{ij} > 0$. (c) Cross-correlation functions between neuron i with preferred orientation 0 rad and neuron j with preferred orientation $\pi/2$ rad, $C_{ij}^s(\tau)$, where $J_{ij} < 0$.

$J_{ik} > 0$. For $J_{ik} > 0$, $C_{ij}^s(\tau) > 0$ because the synaptic strength between the neurons is positive regardless of synaptic depression. We found that synaptic depression reduces $C_{ij}^s(\tau)$. Next, we will discuss how depressing synapses affect $C_{ij}^s(\tau)$ where $J_{ik} < 0$. Figure 3.3(c) plots the cross-correlation functions between a neuron with preferred orientation 0 rad and a neuron with preferred orientation $\pi/2$ rad where synaptic connection $J_{ik} < 0$. Since the synaptic strength between the neurons is negative, $C_{ij}^s(\tau) < 0$ regardless of synaptic depression. We found that synaptic depression increases cross-correlation $C_{ij}^s(\tau)$.

Using correlation theory to solve self-consistent equations in a network with synaptic depression enables us to understand how synaptic depression quantitatively affects neural correlation. As shown in Fig. 3.3, neural activities gradually decorrelate depending on the strength of synaptic depression, γ, and the reductions in neural correlations are quite large for weak depression, $\gamma = 0.1$. We thus found that synaptic depression non-linearly decorrelates neural activities in the entire network with synaptic depression.

3.4.3 Rate correlation

We explained that depressing synapses reduces spiking correlations $A^s(\tau)$ and $C^s(\tau)$ at almost all τ in the previous section. We calculated rate correlation r_i using Eq. (3.48) to evaluate what effect synaptic depression had on the neural correlation between neural activities within a long time frame. When we calculated the firing rate correlation between a neuron with preferred orientation 0 rad and a neuron with preferred orientation $\pi/10$, we found that synaptic depression reduces rate correlations r_i by 98% for $\gamma = 1$.

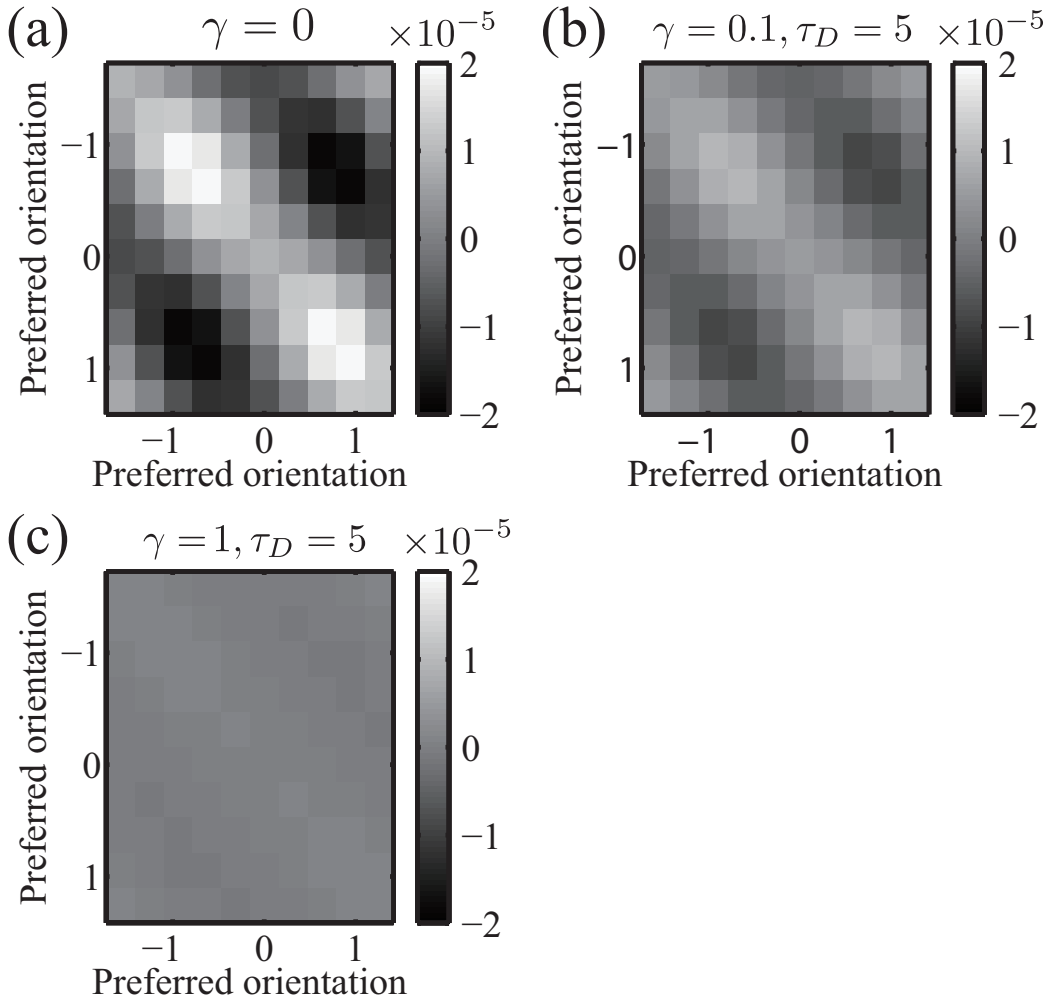

Fig. 3.4. (a) Grayscale plots of covariance matrix $\mathcal{Q}$ in absence of synaptic depression ($\gamma = 0$), (b) in presence of weak synaptic depression ($\gamma = 0.1$ and $\tau_D = 5$), and (c) strong synaptic depression ($\gamma = 1$ and $\tau_D = 5$).

Next, let us consider the effect of depressing synapses on all the pair-wise correlations of neural activities. The correlation theory in a network with synaptic depression enables

us to investigate entire rate correlation $\mathbf{Q}$, as shown in Fig. 3.4.

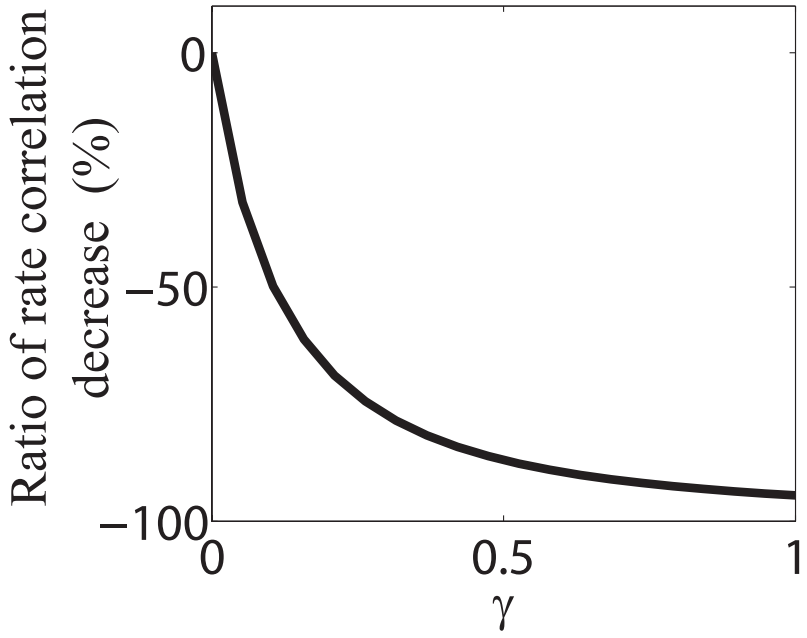

Fig. 3.5. Effects of synaptic depression on average of absolute value of rate correlations.

Here, to visualize the $\mathbf{Q}$ of neurons, let us introduce a $K \times K$ matrix, $\mathcal{Q}$, where $K = 10$ is the number of subpopulations in the neurons. Because the correlations between two neurons are only determined by the difference in their preferred orientations, the correlations between a neuron in the k th population of excitatory neurons and a neuron in the l th are the same. Thus, matrix $\mathbf{Q}$ can be written as $K \times K$ block matrix $\mathcal{Q}$. The elements of $\mathcal{Q}$, and $\mathcal{Q}_{kl}$, stand for the mean firing rate correlations between a neuron in the k th population of neurons and one in the lth:

$$\mathcal{Q}_{kl} = Q_{ij}, \tag{3.57}$$

where $\forall\ i$ is in the kth population and $\forall\ j$ is in the lth; $\mathcal{Q}$ does not contain any diagonal elements of $\mathbf{Q}$. Although matrix $\mathbf{Q}$, which is an $N \times N$ matrix, it is difficult to numerically calculate the entire matrix because of the substantial amount of time that would be required to do this. Note that our theoretical framework enables us to analytically calculate all pair-wise neural correlations. Figure 3.4 shows that the absolute values of all the pair-wise neural correlations greatly decrease depending on the strength of synaptic depression, γ. Thus, neural activities decorrelate due to depressing synapses in an entire network. Finally, we investigate how neural activities decorrelate by changing the strength of synaptic depression. Figure 3.5 indicates that the greater the strength of synaptic depression γ, the fewer the rate correlations.

3.4.4 Fisher information

To understand what effect synaptic depression has on Fisher information I, which depends on firing rates and rate correlations, let us consider the first term of Fisher information, $I_{\text{mean}} = \mathbf{f}'(\theta)^T \mathbf{Q}^{-1} \mathbf{f}'(\theta)$, because I_{mean} is foremost in our model (the second term of Fisher information, I_{cov}, is only about 0.7% of the Fisher information I). I_{mean} depends on the derivatives of mean firing rates $\mathbf{f}'$ and the inverse of covariance matrix $\mathbf{Q}^{-1}$. Because synaptic depression changes both $\mathbf{f}'$ and $\mathbf{Q}^{-1}$, we have to take both changes into account to consider how synaptic depression affects the amount of information.

We adjusted inputs h_i in Section 3.4.2 and 3.4.3, and maintained mean firing rates $\mathbf{f}$ (as shown in Fig. 3.6) to consider what effect synaptic depression had on neural correlations. This section consider the effects of synaptic depression on both firing rates and neural correlations; we set external inputs $h_i = h_i^0$, where $h_i^0 = e_0 \cos(2(\theta_i - \phi))$, $e_0 = 0.2$, and orientation stimuli $\phi = 0$. The response kernels of the discrete spike model are given by $\epsilon_{ij}(\tau) = [1 - \exp(-1/\tau_s)] \exp(-\tau/\tau_s)$, where $\tau_s = 2$. Synaptic depression generally reduces mean firing rates $\mathbf{f}$ and their slopes ($\mathbf{f}' = d\mathbf{f}/d\theta$), as shown in Figs. 3.6(a) and (b) (Abbott et al. 1997, Igarashi et al. 2010). These changes to the firing rates reduce $I_{\text{mean}} = \mathbf{f}'(\theta)^T \mathbf{Q}^{-1} \mathbf{f}'(\theta)$.

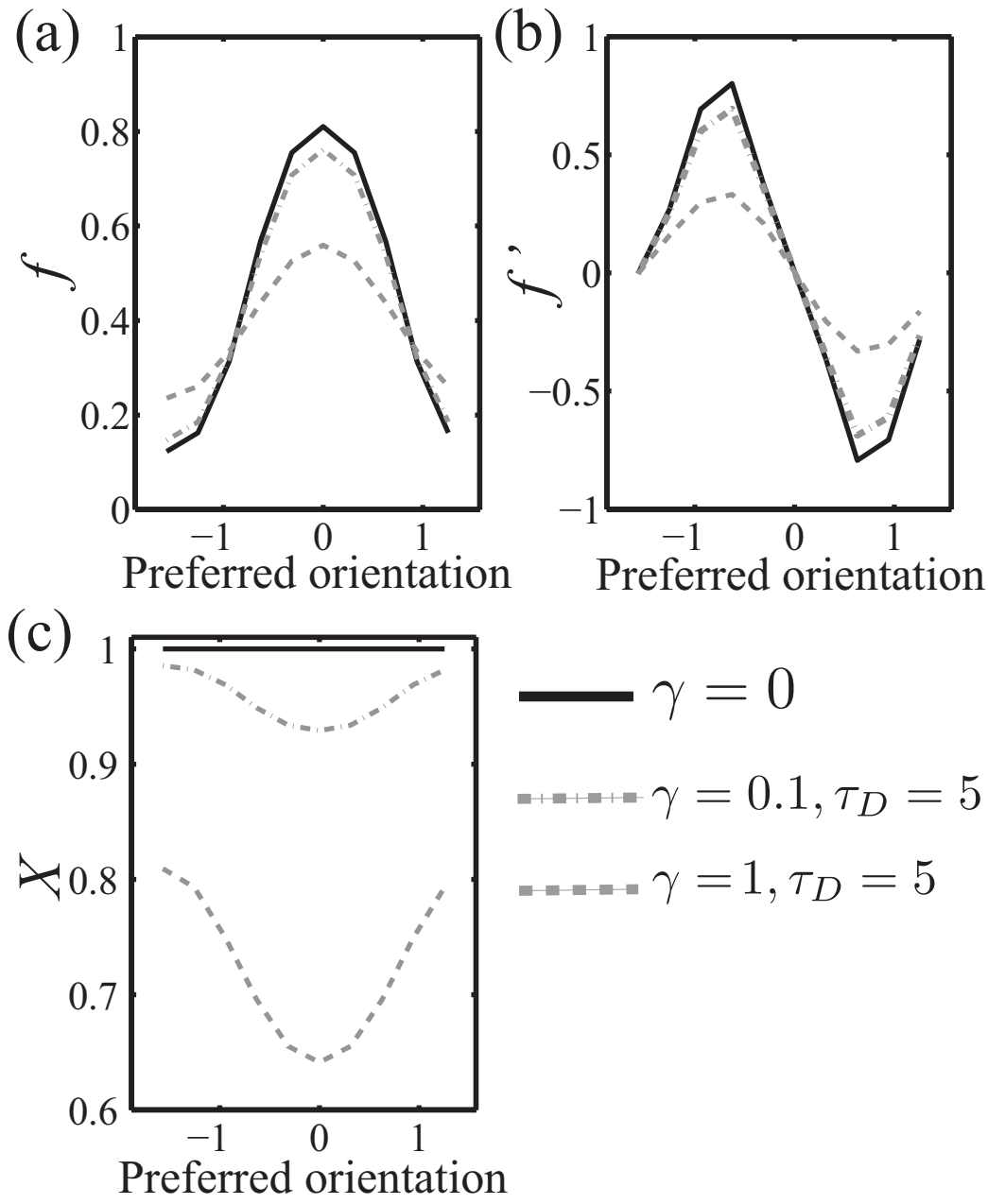

Fig. 3.6. (a) Mean firing rates, f, (b) derivatives of mean firing rates, f', and (c) mean synaptic efficacies, X, of V1 neurons with $J_0 = 0.5$ and $J_1 = 3$. Solid lines plot f, f', and X in absence of synaptic depression ($\gamma = 0$ and $\tau_D = 1$). Chain and dashed lines plot f, f', and X in presence of weak synaptic depression ($\gamma = 0.1$ and $\tau_D = 5$) and strong synaptic depression ($\gamma = 1$ and $\tau_D = 5$), respectively.

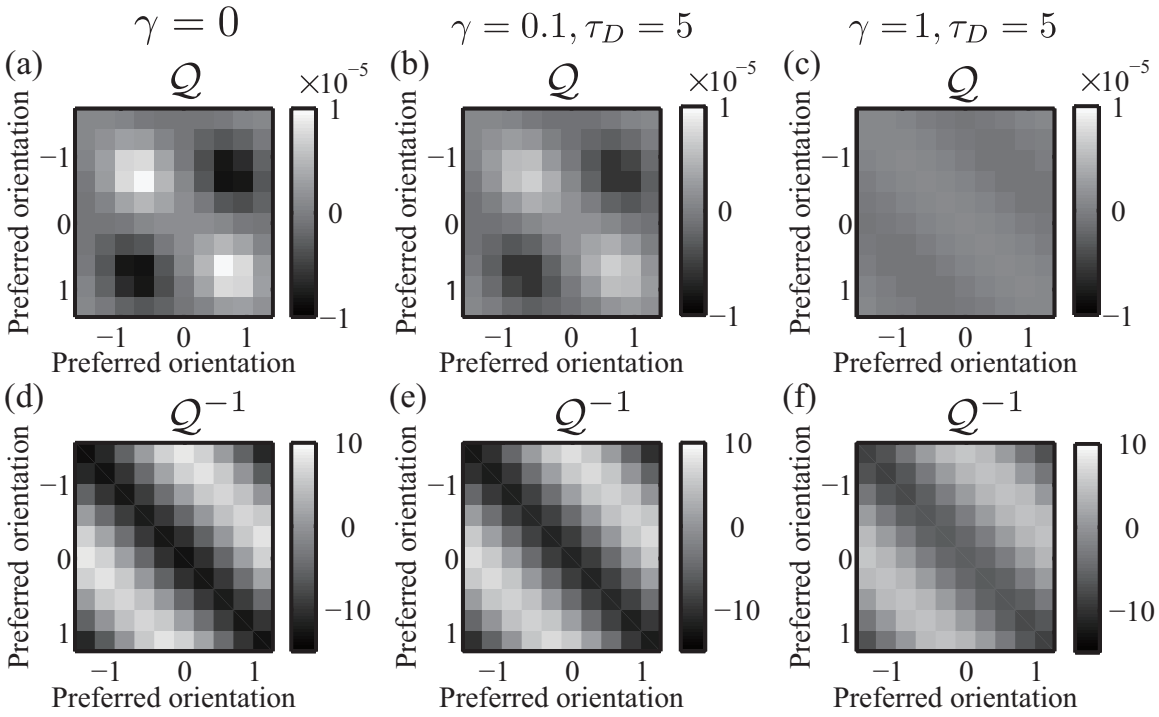

Fig. 3.7. Covariance matrix $\mathcal{Q}$ and those of inverse of covariance matrix $\mathcal{Q}^{-1}$. Note that off-diagonal elements of covariance matrix $\mathbf{Q}$ are written as $\mathcal{Q}$. (a)-(d): Plots of covariance matrix $\mathcal{Q}$ ((a), (b), and (c)) and inverse of covariance matrix $\mathcal{Q}^{-1}$ ((d), (e), and (f)) of V1 neurons in the absence ($\gamma = 0$) and presence of weak ($\gamma = 0.1$ and $\tau_D = 5$) and strong ($\gamma = 1$ and $\tau_D = 5$) synaptic depression, respectively. Synaptic strengths are $J_0 = 0.5$ and $J_1 = 3$. Diagonal elements are set to 0 to enable visualization.

Now, we shall consider how $\mathbf{Q}^{-1}$ affects Fisher information. Figures 3.7 (a)-(f) show the off-diagonal elements of covariance matrix $\mathbf{Q}$ and those of the inverse of covariance matrix $\mathbf{Q}^{-1}$. When locally positive correlations are induced by recurrent excitations (Figs. 3.7 (a)-(c)), the off-diagonal elements of $\mathbf{Q}^{-1}$ near the diagonal elements are negative (Figs. 3.7 (d)-(f)). As demonstrated by Eq. (3.53), we can understand that these locally negative off-diagonal elements decrease Fisher information if the tuning curves, $\mathbf{f}$, are fixed. Locally positive correlations thus decrease Fisher information (Sompolinsky et al. 2001). Next, let us investigate how synaptic depression affects $\mathbf{Q}^{-1}$. As discussed in Section 3.4.3, synaptic depression reduces rate correlations $\mathbf{Q}$ (Figs. 3.7 (a)-(c)). Neural decorrelation also leads to an increase in locally negative off-diagonal elements, as indicated in Figs. 3.7 (d)-(f), which increases the amount of information.

As a result, the effects of the derivatives of the tuning curves $\mathbf{f}'$ on Fisher information are the opposite of the effects of neural correlations. Whether Fisher information increases or not as a combinational effect is determined by which effects are stronger. We calculated the Fisher information to evaluate the effects of synaptic depression on information processing and found that, when we set the parameters for connections, $J_0 = 0.5$ and $J_1 = 3$, synaptic depression increased the amount of information depending on the strength of synaptic depression shown in Fig. 3.8. However, synaptic depression does not always increase Fisher information, because it depends on the synaptic strengths, J_0 and J_1. We also found that synaptic depression reduced Fisher information for the weak lateral-inhibitory interaction $J_1 = 1$ shown in Fig. 3.9. Thus, synaptic connections established the effect of synaptic depression.

3.5 Discussion

We constructed a theory of correlation in spiking neuron models with synaptic depression by expanding a previous theoretical framework (Ginzburg and Sompolinsky 1994, Meyer and van Vreeswijk 2002, Toyoizumi et al. 2008, Oizumi et al. 2010). This theory enables us to analytically calculate what effect synaptic depression, which rapidly changes neural interactions, had on neural correlations. Our study should opens up the way for theoretical studies on the effects of interaction changes on the linear response function in large stochastic networks.

We investigated how synaptic depression affects neural correlations in a ring attractor network with Mexican-hat-type connectivity by using our theoretical framework. We found that synaptic depression reduces neural cross-correlations in the ring

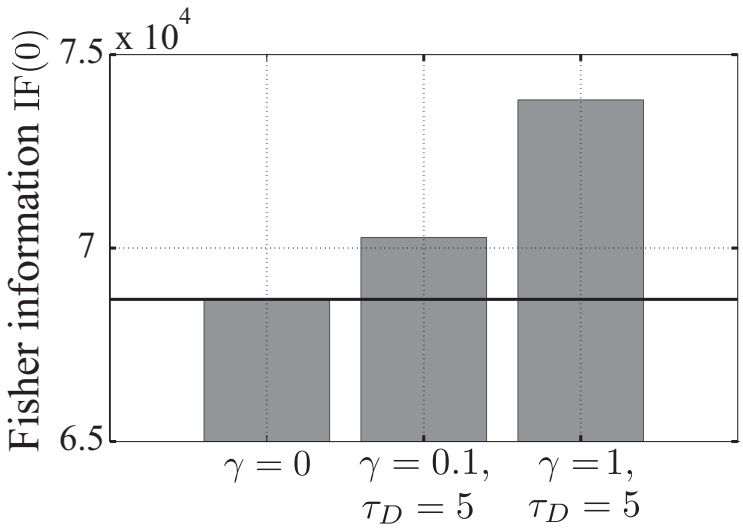

Fig. 3.8. Effects of synaptic depression on Fisher information. Fisher information increases depending on strength depression γ, when parameters of connections are $J_0 = 0.5$ and $J_1 = 3$

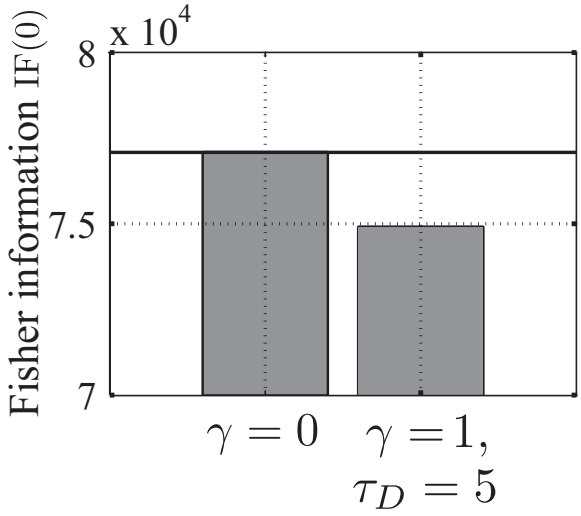

Fig. 3.9. Effects of synaptic depression on Fisher information. When we set uniform interaction, $J_0 = 0.5$, and weak lateral-inhibitory interaction, $J_1 = 1$, synaptic depression ($\gamma = 1$ and $\tau_D = 5$) decreases Fisher information by 2.8%.

network model as well as neural auto-correlations by using our theoretical framework (Goldman et al. 2002). The decorrelations of neural activities can improve the efficiency of a population of neurons encoding information (Abbott and Dayan 1999, Averbeck, Latham and Pouget 2006, Gutnisky and Dragoi 2008, Cohen and Maunsell 2009).

To evaluate how synaptic depression affects information processing, we analytically

calculated Fisher information, which quantifies the maximum amount of information on stimuli that can be extracted from noisy neural activities. We found that although synaptic depression generally reduces signal strength, viz., the mean firing rates, it can improve the efficiency of population coding. Some researchers have reported that short-term synaptic depression is a possible mechanism for the effects of belief adaptation to a stimulus with a fixed orientation in the primary visual cortex, because this brief adaptation leads to the depression of feed forward synapses and intracortical synapses (Kohn 2007, Chelaru et al. 2008). In fact, recent neurophysiological experiments have shown that, after belief adaptation, both firing rates and neural correlations decrease and Fisher information increases in the macaque primary visual cortex (Gutnisky and Dragoi 2008). These post-adaptation changes coincide with the effects of synaptic depression. Further investigations are needed to calculate Fisher information in the network of the primary visual cortex with synaptic depression (Chelaru et al. 2008) to enable the mechanism for decorrelation after brief adaptation to be studied.

Recent findings by Montani et al., and Ohiorhenuan and Victor have pointed out the relevance of higher order correlations that are larger than two in the cerebral cortex (Montani et al. 2009, Ohiorhenuan and Victor 2011). Macke et al. have theoretically proved that common inputs explain high-order correlations in a simple model of neural population activity (Macke et al., 2011), in which there were no recurrent connections and neural correlations were only determined by common inputs. In contrast, we did not consider common noisy inputs in our model for simplicity, which produced large high-order correlations, and focused on neural correlations which were produced only by recurrent synaptic connections. We therefore could analytically calculate the neural correlations and theoretically prove that the pair-wise correlations are scaled as $\sim O(1/N)$ and that high-order correlations are less than the order of $1/N$ in a network with synaptic depression, where N is the number of neurons. On the other hand, we cannot directly argue how synaptic depression affects the large higher-order correlations produced by common inputs in the framework of the mean-field theory. Further study will be to include common noisy inputs in the network and investigate by simulations what effect synaptic depression has on higher-correlations, which are produced by common inputs.

We have only investigated the role of synaptic depression in spike train decorrelation in this study, but other short-term processes such as spike rate adaptation (Liu and Wang 2001), synaptic facilitation (Lisman 1997, Tsodyks et al. 1998), and postsynaptic receptor dynamics could enable more general filtering of spike trains (Maass and Zador 1999). Mongillo et al. reported that working memory is sustained

by both synaptic depression and synaptic facilitation in the recurrent connections of neocortical networks (Mongillo et al. 2008). However, neural correlations, which affect the efficiency of a population of neurons to encode information, have not been taken into consideration in the network. Expanding our theoretical framework to spiking neural network models with both synaptic depression and facilitation and investigating how these synaptic plasticities affect Fisher information is an interesting issue that we intend to pursue.

Chapter 4

Higher-order correlation in a feed-forward network with inhomogeneous connectivity

4.1 Background

The widely observed complex features of population activity, such as the synchronization and concentration patterns of suspension, can be captured by not only the pairwise correlations but also by the higher-order correlations, which have a significant effect on the complicated physical processes and information processing (Heimel and Coolen 2001, Teramae and Tanaka, Saintillan and Shelley 2008). Electrophysiological experiments conducted in the field of neuroscience have recently shown that the manner in which information is represented using specific spiking and silence patterns over a group of neurons, is also understood both by the pairwise and higher-order correlated neural activities (Schneidman et al., 2006, Shlens et al., 2006, Ohiorhenuan et al., 2010, Ohiorhenuan and Victor 2011, Ganmor et al., 2011, Yu et al, 2011). However, very little is known about the relationships in the higher order correlations linking the role of information processing.

It is widely acknowledged that the detailed nature of a neural population code is determined by the dependencies among cells (Rieke et al, 1997, Riehle et al, 1997, Parisi 1998, Averbeck, Latham and Pouget 2006). Then, some researchers have characterized the functional specificity of the local connections in the primary visual cortex to better understand the complex relationship between the structure of a neural network and neural

population code (V1)(Alonso and Martinez 1998, Yoshimura et al, 2005, Ko et al., 2011). It would appear that these structured neural connectivities in V1 affect not only the firing rates and pairwise neural correlation but also the higher-order correlations structure in neuronal firing.

Previous studies have shown that both the pairwise correlated input, which is commonly generated from common inputs, and non-linear spiking thresholds are needed to produce higher-order correlations (Amari et al., 2003, Macke et al., 2011). However, very little is theoretically known about the relationships in a network of physical or structural (synaptic) connections linking the higher order correlations as the number of connections among a given number of neurons exponentially grows, because they used homogeneous neural networks. Therefore, the effect of inhomogeneous connections in cortical networks on the higher-order neural correlations remains an open challenge and is thus the topic of this paper.

We expanded the previous theoretical framework in this paper to a feed-forward network with inhomogeneous connectivity. We then used our structured network model and investigated how structural connection changes the neural activities, especially the structure of higher-order correlations structure among the neural population. We first focused on a comparisong of our theoretical results with the electro-physiological experiment reported by Ohiorhenuan *et al.*, who have recently reported on the structured higher-order correlations between neurons in V1 that receive random visual stimulus (Ohiorhenuan et al., 2010, Ohiorhenuan and Victor 2011), and show that our theoretical results are consistent with the experimental observations (Ohiorhenuan and Victor 2011).

It is assumed that visual stimulation clearly reorganizes the activity of structured V1 circuits by preferentially activating V1 neurons. We investigated the effect of external inputs on the higher order correlations of neural activity by changing the stimulus to the V1 network, and then made a theoretical prediction for the V1 network model. We show that external stimuli change the structure of the higher-order correlations among neurons and generate both sparse and synchronized neural activity due to the structures of synaptic connections. These dynamics enable 3rd-order correlations resulting from visual stimulation to carry stimulus-specific information.

4.2 Model

Let us consider a two-layer feed-forward network as shown in Fig. 4.1. We define $s_j = \{0, 1\}$ and $x_i = \{0, 1\}$ as the output of a Layer 1 and Layer 2 neuron, respectively. The

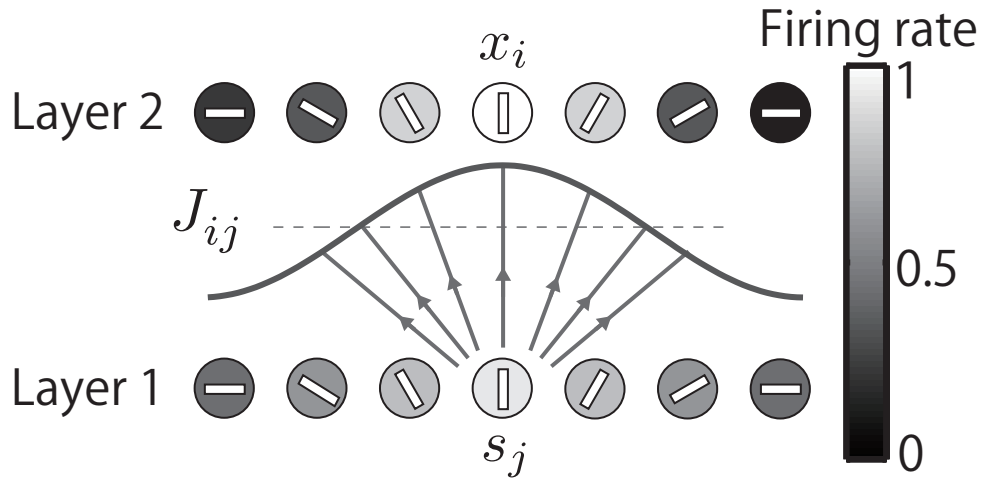

Fig. 4.1. Network architecture. The connections between the two layers, J_{ij}, consist of inhomogeneous feed-forward connections. The orientation of the bar indicates the preferred orientation and the gray scale of value in a circle shows the firing rate of a neuron.

state of the Layer 2 neuron x_i depends on the neural input u_i from the Layer 1 neurons:

$$x_i = \Theta(u_i), \tag{4.1}$$

$$u_i = \sum_j^N J_{ij} s_j + \eta + z_i - h, \tag{4.2}$$

where h is a threshold and Θ is a step function, which is nonlinear transformation. The non-linear spiking threshold generates higher-order correlations among neural firing $x_1, \ldots, x_N$. (Amari et al., 2003). η and z_i are fluctuations in inputs, and we assume that the two noise terms, z_i and η, are described by an identical Gaussian distributions with a mean of 0 and variances of λ and $1-\lambda$, respectively, i.e., $\eta \sim \mathcal{N}(0, \lambda)$ and $z_i \sim \mathcal{N}(0, 1-\lambda)$. We normalized the scale of the fluctuations such that $z_i + \eta$ is subject to the normal Gaussian distribution $\mathcal{N}(0, 1)$ (Amari et al., 2003). Let us explain the more detail of η. η is caused by common inputs (Amari et al., 2003, Macke et al., 2011) and, due to η, there are pairwise correlations between neural inputs. The pairwise correlated inputs and the non-linear spiking threshold induce statistical interactions at all orders of this model. The common fluctuating input also induces phase synchronization and previous theoretical studies have investigated the effects of only a weak common noise ($\lambda \to 0$) on phase synchronization (Teramae and Tanaka).

As shown in Fig. 4.1, each cell has a preferred feature, e.g., orientation, preferred spatial frequency (scale), and receptive field location. We then assume that the synaptic weight

between the two layers, J_{ij}, has translational symmetry and is determined on the basis of the difference between the preferred features, i.e.,

$$J_{ij} = J(\phi_i - \phi_j) = \sum_{k=0}^{K} \frac{J_k}{N} \cos 2k(\phi_i - \phi_j), \tag{4.3}$$

where ϕ_i represents a preferred feature of neuron i. A model with K = 0 reduces to a network with uniform connections, as demonstrated in a previously studied model (Amari et al., 2003, Macke et al., 2011). Furthermore, in the case of $K = 1$, the network model represents a two-layer feed-forward network of V1 neurons that modeled the supra-granular layers 2/3 (Layer 2) and granular layer 4 (Layer 1) (Hubel and Wiesel 1962, Ben-Yishai et al. 1995, Hamaguchi et al. 2005, Hamaguchi 2006, Priebe and Ferster 2008) (Fig. 4.1), where the neurons are parameterized by an angle ϕ, ranging from $-\pi/2$ to $+\pi/2$, that denotes their preferred orientations, and J_1 is a lateral-inhibitory connection. In a network with the inhomogeneous connectivity, columnar localized activity is produced when a grating stimulus is presented.

4.3 Theory of higher-order correlations

We constructed a theory of higher-order correlations in a structured network with common inputs and spiking non-linearities. We observed the activity of the Layer 1 neural field, s, through macroscopic variables (order parameters).

The order parameters are defined as $r_0 = \frac{1}{N}\sum_i s_i$, which represents the population firing rate,

$$r_k^c = \frac{1}{N} \sum_i \cos(2k\phi_i) s_i, \tag{4.4}$$

$$r_k^s = \frac{1}{N} \sum_i \sin(2k\phi_i) s_i \tag{4.5}$$

$$, \tag{4.6}$$

where $1 \leq k \leq K$; r_1^c and r_1^s denote the coefficients of the first Fourier mode of the spatial firing pattern, representing the eccentricity of the localized activity about $\phi = 0$ and $\pi/2$, respectively. The input to Layer 2 neuron i from the Layer 1 neurons, u_i, can

be represented by the following order parameters,

$$u_i = \gamma_i + \eta + z_i, \tag{4.7}$$

$$\gamma_i = J_0 r_0 + \sum_{k=1}^{K} J_k (r_k^c \cos(2k\phi_i) + r_k^s \sin(2k\phi_i)) - h. \tag{4.8}$$

Our feed-forward network model reproduces both inhomogeneous neural inputs and homogeneous properties of neural noise, which have been observed in neurophysiological experiments (Yu and Ferster 2010, Anderson et al. 2000). The point of pivotal importance in our model is that the localized neural input, γ_i, resulting from the inhomogeneous connectivity ($K \geq 1$), modulates the spiking nonlinearity to each Layer 2 neuron and gives rise to inhomogeneous neural correlations, even though the noise properties are uniform.

Depending on the common noise, η, not only the microscopic behavior but also the macroscopic state stochastically perturb in the network model, and thus, a probability distribution of order parameters can be constructed (Amari et al., 2003, Hamaguchi et al. 2005). Although most theoretical studies derive neural correlations based on the fluctuation-dissipation theory for investigating changes in the equilibrium order parameters, there are no equilibrium order parameters due to sufficiently weak externally applied perturbations (Ginzburg and Sompolinsky 1994), and thus, we cannot use the fluctuation-dissipation theory in the network model (Amari et al., 2003, Macke et al., 2011). Some researchers, therefore, calculate neural correlations from the probability distribution of the order parameters (Amari et al., 2003, Hamaguchi et al. 2005, Macke et al., 2011).

Here, we expanded the previous theoretical framework to higher-order correlations in a structured network model (Amari 2001, Macke et al., 2011). Let us consider the firing activities of arbitrarily chosen M neurons from Layer 2. Due to the homogeneous noise input, we can write the probability distribution of a binary M-dimensional vector $\boldsymbol{x} = \{x_1, x_2, \ldots, x_M\}$, $P(\boldsymbol{x})$, as

$$P(\boldsymbol{x}) = \int_{-\infty}^{\infty} d\eta p(\eta) L(x_1|\eta) L(x_2|\eta) \times \cdots \times L(x_M|\eta), \tag{4.9}$$

$$p(\eta) = \frac{1}{\sqrt{2\pi\lambda}} \exp\left(-\frac{\eta^2}{2\lambda}\right), \tag{4.10}$$

$$L(x_i|\eta) = (P(u_i < 0|\eta))^{(1-x_i)} (P(u_i > 0|\eta))^{x_i}. \tag{4.11}$$

Because the input u_i has a Gaussian distribution, it can be calculated as

$$P(u_i > 0|\eta) = \mathrm{erfc}\left(-\frac{\gamma_i + \eta}{\sqrt{1-\lambda}}\right). \tag{4.12}$$

Here, we define

$$\mathrm{erfc}(x) = \frac{1}{\sqrt{2\pi}} \int_x^\infty \exp(-u^2) du. \tag{4.13}$$

To derive higher-order correlations among neural activities, we expand the probability distribution, $P(\boldsymbol{x})$, as

$$\log P(\boldsymbol{x}) = \sum_i \theta_i x_i + \sum_{i<j} \theta_{ij} x_i x_j + \sum_{i<j<k} \theta_{ijk} x_i x_j x_k + \cdots + \theta_{1\ldots M} x_1 x_2 \ldots x_M - \Psi, \tag{4.14}$$

where Ψ is a normalizing factor and $\boldsymbol{\theta} = (\theta_i, \theta_{ij}, \theta_{ijk}, \ldots, \theta_{1\ldots M})$ are parameters to specify $P(\boldsymbol{x})$, which represents the interactions of M neurons. For example, when we set $M = 3$, we can derive these correlation parameters $\boldsymbol{\theta}$ from $P(\boldsymbol{x})$ as follows,

$$\theta_i = \log \frac{P(1,0,0)}{P(0,0,0)}, \tag{4.15}$$

$$\theta_{ij} = \log \frac{P(1,1,0)P(0,0,0)}{P(1,0,0)P(0,1,0)} \tag{4.16}$$

$$\theta_{ijk} = \log \frac{P(1,0,0)P(0,1,0)P(0,0,1)P(1,1,1)}{P(0,0,0)P(0,1,1)P(1,0,1)P(1,1,0)}. \tag{4.17}$$

In the case of $\theta_{ijk} > 0$, the probability of synchronous firing between the 3 neurons is presented at a significant level. Thus, these correlation parameters $\boldsymbol{\theta}$ can be derived from a full joint distribution $P(\boldsymbol{x})$, which can be analytically calculated in our model.

As previously described, we focused on comparing our theoretical results with those from the electrophysiological experiment in V1, where most neurons respond best to elongated light bars and are directionally selective (Hubel and Wiesel 1962). We considered a two-layer feed-forward network consisting of V1 neurons as a model of the orientation selectivity (Hubel and Wiesel 1962, Hamaguchi et al. 2005, Priebe and Ferster 2008) (Fig. 4.1, $K = 1$). We presumed that each laminar V1 network consists of G types of subpopulations, where the number of neurons in each subpopulation is N_G ($N = G \times N_G$) and all neurons in each subpopulation have the same preferred orientation, such that

$$\phi_i = -\pi/2 + g_i \pi / G, \tag{4.18}$$

where g_i represents the number of neuron i's subpopulation and we set $g_i = \lfloor i/N_G \rfloor$. We analytically calculated the neural correlations in the V1 network model and investigated the effect of lateral inhibition on the 3rd-order correlations between V1 neurons in supragranular layer 2/3. We then set $M = 3$ and derived these correlation parameters $\boldsymbol{\theta}$ from $P(\boldsymbol{x})$ as denoted above.

4.4 Stimulus-specific decomposition of the mutual information (SSI)

To evaluate the effects of higher order correlations on information processing, we calculate Stimulus-specific decomposition of the mutual information (SSI) which is delivered by higher-order correlations, especially 3rd order correlations, between neural population activities in V1 network model.

The basic quantity of information theory is information entropy, a measure of the uncertainty or randomness of a variable, such as neural firing state. Entropy can be intuitively, thought of a generation of variance. More concretely and correctly, entropy is the amount of information required, on average, to render the value of a variable and is measured in bits. The entropy $H(\Psi)$ of a grating stimulus ensemble Ψ is given by:

$$H(\Psi) = -\sum_{\psi \in \Psi} p(\psi) \log_2 p(\psi), \tag{4.19}$$

where ψ represents the orientation of a grating stimulus.

Mutual information, I_{mut}, is a measure of the informativeness of one variable about another, e.g., of a neural response X about a stimulus Ψ. It is the total entropy minus the conditional entropy:

$$I_{mut}(X, \Psi) = H(X) - H(X|\Psi) = H(\Psi) - H(\Psi|X) \tag{4.20}$$

$$= \sum_{\psi \in \Psi} p(\psi) \sum_{\boldsymbol{x} \in X} p(\boldsymbol{x}|\psi) \log \frac{p(\boldsymbol{x}|\psi)}{\boldsymbol{x}} \tag{4.21}$$

Uppercase characters Ψ and X represent the stimulus and response ensembles, while lowercase characters $(\psi, \boldsymbol{x})$ repsent a single value within the ensemble.

Since mutual information can be used to quantify the information which is represents by an whole response ensemble about an entire stimulus ensemble, we can not know about the precision with which specific stimuli within the ensemble are encoded from it. To address this, specific information and stimulus-specific information have been proposed (DeWeese and Meister 1999, Butts 2003).

Specific information is a mutual information decomposition that quantifies the decrease in uncertainty about the stimulus due to the observation of a given response:

$$I_{SI}(\boldsymbol{x}) = \sum_{\psi \in \Psi} p(\psi|\boldsymbol{x}) \log p(\psi|\boldsymbol{x}) - p(\psi) \log p(\psi) \tag{4.22}$$

The specific information has a unique and advantageous property in that it is additive (DeWeese and Meister 1999).

The stimulus specific information (SSI), which is calculated in this article, is a stimulus-specific development of the specific information (Butts 2003). The SSI is the average specific information associated with a given stimulus:

$$I_{SSI}(\psi) = \sum_{\boldsymbol{x}\in X} p(\boldsymbol{x}|\psi) I_{SI}(\boldsymbol{x}) \tag{4.23}$$

$$= \sum_{\boldsymbol{x}\in X} p(\boldsymbol{x}|\psi) \left[\sum_{\psi\in\Psi} p(\psi|\boldsymbol{x}) \log p(\psi|\boldsymbol{x}) - p(\psi) \log p(\psi) \right] \tag{4.24}$$

The SSI could be considered less stimulus-specific than the specific surprise, which is Mutual Information decomposition, since it relates to an observer's knowledge of the full stimulus ensemble (Butts 2003).

Calculating SSI both in the presence of higher-order correlations among neural activities and in the absence of 3rd-order correlations, we investigate the effects of higher-order correlations on sensory processing.

4.5 Results: Response to a random stimulus

Psychophysical experiments have shown that when primates see random stimuli, negative triplet correlations between the neural activities in V1. This indicates that the probability of synchronous firing between the three neurons is present at a significant level, creating sparser codes by increasing the periods of total quiescence, and thus, concentrating information into briefer periods of common activity (Ohiorhenuan et al., 2010, Ohiorhenuan and Victor 2011).

Previous theoretical studies have focused on the mechanism of the negative 3rd order correlations (Macke et al., 2011). They show that threshold nonlinearity reproduces these observed 3rd-order correlations between neural activities features for random visual stimuli when using a homogeneous network model (Macke et al., 2011). However, the effects of inhomogeneous connectivities, which were observed in V1 (Anderson et al. 2000), on the 3rd-order neural correlations remain unknown. We investigated how the structured connections affect the 3rd-order correlations by using a structured network model for this research.

We simulated the V1 neuron response to a random stimulus ($r_0 = 0.5$, $r_1^s = r_1^c = 0$) and compared the 3rd-order correlations in the homogeneous network ($J_1 = 0$) with those in the network with a lateral-inhibitory connectivity ($J_1 = 3$) (Fig. 4.2). We used a

two-layer feed-forward network in the simulation, where each layer was constructed of $N = 200$ neurons ($N_G = 10$, $G = 20$), and set a variance of η, $\lambda = 0.5$, a threshold, $h = 0.25$, and a uniform interaction, $J_0 = -0.25$.

We found that the firing correlations obtained in the simulations under these conditions coincided with our theoretical results (Figs. 4.2 and 4.3), which provides a powerful way for interpreting the role of neuronal parameters, such as the inhomogeneous connection. We also found that although a lateral-inhibitory connection increases the 3rd-order neural correlation, a common input model could lead to a negative triple interaction for all combinations when there is random visual stimulus, thus creating sparser codes by increasing the periods of total quiescence. These results are consistent with the experimental observations, as well as with those in a previous study using a homogeneous network (Macke et al., 2011).

In addition to the negative 3rd-order correlations among neural activities, the electrophysiological experiments in V1 have shown that while the firing rates are negatively correlated with the 3rd-order correlations, the 2nd-order correlations have a strong correlation with the 3rd-order correlations (Ohiorhenuan et al., 2010, Ohiorhenuan and Victor 2011). Since they present the visual stimulus of a binary checkerboard stimulus, pseudorandom in space and time, these correlative relationships between statistics are attributed to the structured network or neural dynamics characteristics, such as the threshold nonlinearity.

We calculated the relationship for the firing rates, 2nd-order correlations, and 3rd-order correlations among neurons using the V1 network model. We found that while the 3rd-order correlations are higher when the total firing rates among the three neurons are high, the 3rd-order correlations are lower when the pairwise correlation is high, as shown in Figs. 4.2 (e) and (f). This indicates that the inhomogeneous connectivity has an insignificant effect on the correlative relationships for the firing rates, 2nd-order correlations, and 3rd-order correlations among neurons, which are induced by threshold nonlinearity, for random stimuli. These theoretical results in a structured V1 network model, which are similar to the experimental observations (c. f. (Ohiorhenuan and Victor 2011), Fig. 4) and the previous theoretical results in a homogeneous network model (Macke et al., 2011), promote that spiking nonlinearity is necessary for the high-order correlation, which are observed in V1 (Amari et al., 2003, Macke et al., 2011).

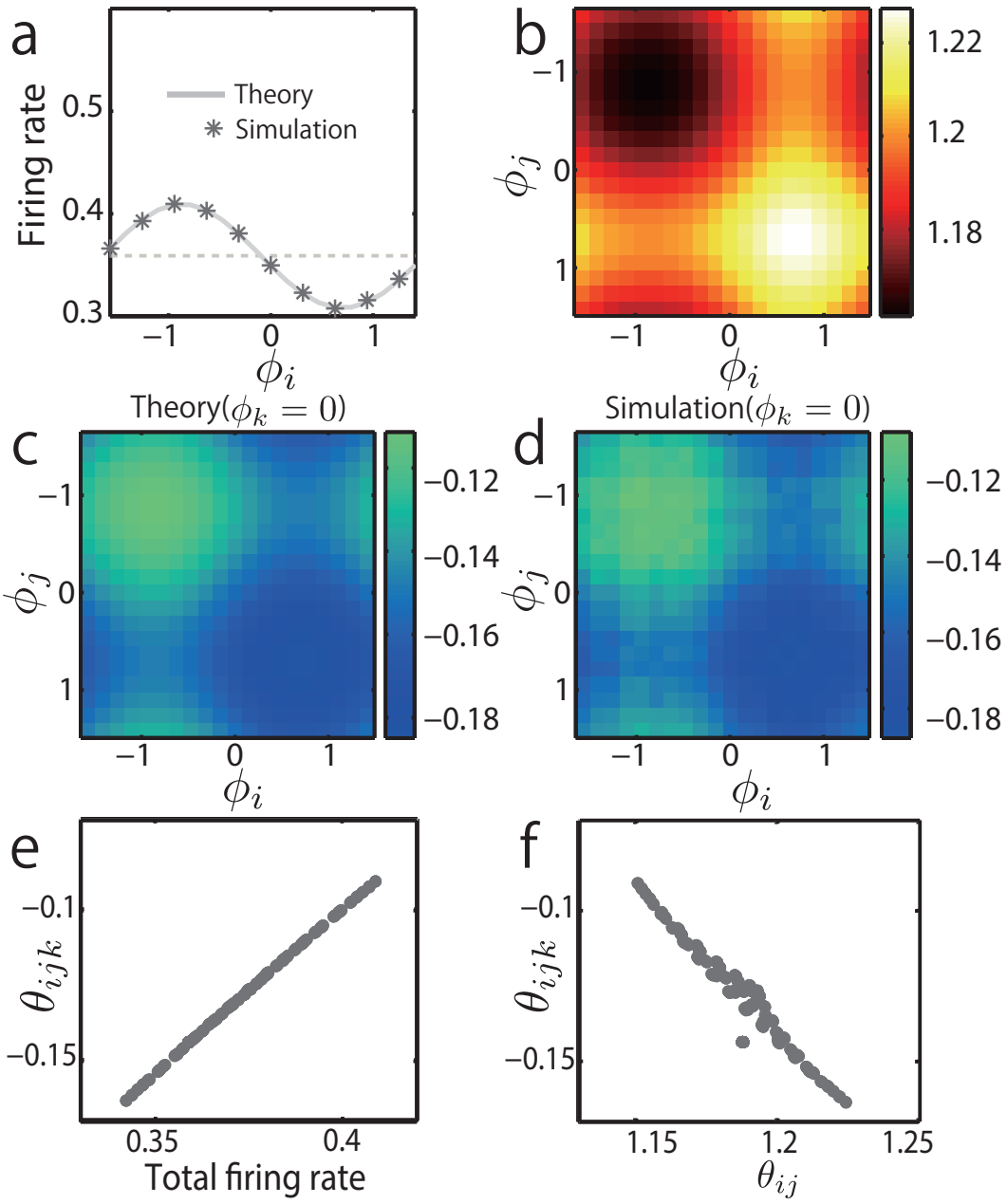

Fig. 4.2. Responses to a random stimulus ($r_1^c = -0.01$, $r_1^s = -0.04$) in the V1 network with MH-type connections ($J_1 = 3$). (a) Firing rates. (b) Pair-wise correlation, θ_{ij}, in the V1 network. (c), (d) θ_{ijk} in the V1 network obtained from theory compared with theoretical simulations. Here, we set $\phi_k = 0$. (e) θ_{ijk} is strongly correlated with the total firing rate. (f) Here, we set $\phi_k = 0$. θ_{ijk} is negatively correlated with θ_{ij}.

4.6 Results: Prediction of responses to a grating stimulus

Although higher correlations among neurons are uniform in a homogeneous feed-forward network regardless of the external stimulus (Amari et al., 2003, Macke et al., 2011), it is believed that visual stimulation clearly reorganizes the structured V1 circuit activity by preferentially activating the V1 neurons. We investigated the effect of a grating stimulus (direction $\psi = 0$) on the neural activity pattern and made a theoretical prediction for the V1 network model (lateral-inhibitory interaction $J_1 = 3$). Fig. 4.3(a) shows the network neurons activity response plotted as a function of their preferred stimulus angle in response to light bars (direction $\psi = 0$). The preferred orientation of the maximum neural response is consistent with the stimulus direction $\psi = 0$, meaning this network model can achieve orientation selectivity. The pairwise correlation structure, θ_{ij}, has a multimodal distribution and is neither Gaussian nor table-shaped due to the inhomogeneous input of the V1 neuron, u, as shown in Fig. 4.3(b) (Hamaguchi et al. 2005). As u has a unimodal distribution, u crosses the threshold at two points ($\phi = \pm\pi/4$) for a grating stimulus, and there are four local minimum values for the pairwise correlation, as shown in Fig. 4.3(b).

We then calculated the 3rd-order correlated activities driven by the light bars (direction $\psi = 0$). We found that the 3rd-order correlations structure among the V1 neurons had a multimodal distribution in response to a grating stimulus $\psi = 0$, $r_1^c = 0.27$, as shown in Fig. 4.3(c).

Of particular interest are the two types of triplet neural activity patterns with a preferred orientation ($\phi_i = \phi_j = \phi_k = 0$ and $\phi_i = \phi_j = \pi/2,\ \phi_k = 0$); the former groups have the same preferred orientation as the stimulus while the latter have an orthogonal preferred orientation. Unlike the responses to the random stimulus, the 3rd-order correlations among the neurons that have the same preferred orientation ($\phi_i = \phi_j = \phi_k = 0$) are positive when the coefficients of the first Fourier mode of the spatial firing pattern $r_1^c > 0.15$, as shown in Fig. 4.3(d). In contrast, the 3rd-order correlated correlations among the neurons with preferred orientations $\phi_i = \phi_j = \pi/2,\ \phi_k = 0$ are negative and decrease when r_1^c increases. This indicates that the neurons with an orthogonal preferred orientation displayed fewer triplet events than predicted from their pairwise interactions, while there was more synchrony than expected from the pairwise interactions alone among the neurons with a preferred orientation along the direction of the light bars. Thus, our theoretical results indicate that by changing the structure of higher-order correlations among neurons and generating both sparse and synchronized neural activity, the 3rd-order correlations

resulting from visual stimulation can carry stimulus-specific information.

Using our theory, we predicted the relationships among various statistics, including 3rd-order correlations, 2nd-order correlations, and firing rates, in the case of a grating stimulus. Similar to the case of a random stimulus, the number of triplet events is strongly correlated with the firing rate, as shown in Fig. 4.3(e). In contrast to such a relationship, Fig. 4.3(f) shows that the 3rd-order correlations are not correlated with the strength of the pairwise interactions due to their multimodal distribution (Figs. 4.3(b), (c)). Our theory thus predicts that a grating stimulation reorganizes the structured neural correlations and the activity of V1 circuits.

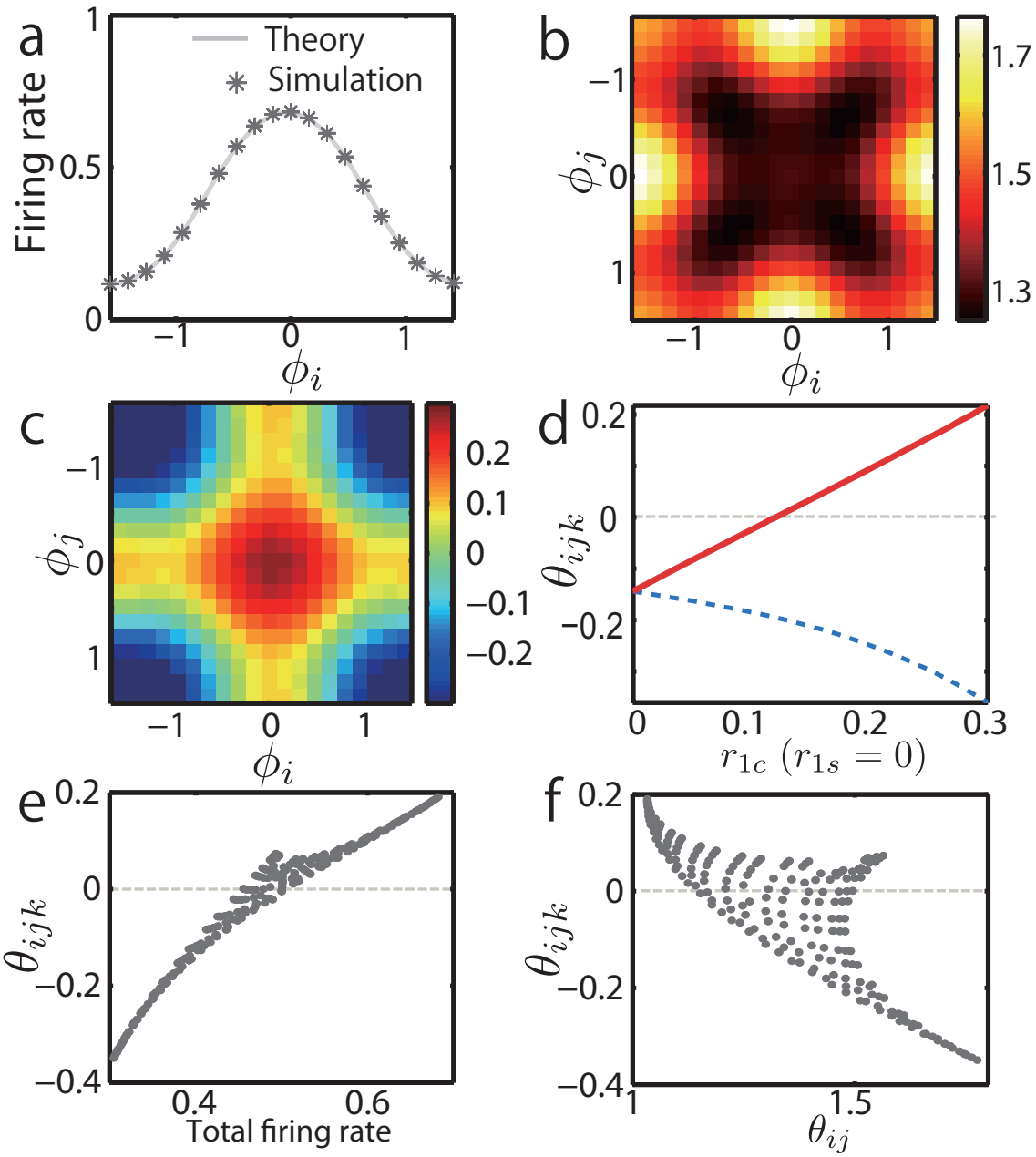

Fig. 4.3. Responses to a grating stimulus (direction $\psi = 0$, $r_1^c = 0.27$, $r_1^s = 0$) in the V1 network model ($J_0 = -0.2$, $J_1 = 3$). (a) Firing rates. (b) Pair-wise correlation, θ_{ij}. (c) The distribution of the 3rd-order correlation, θ_{ijk}, is a multimodal distribution. Here, we set $\phi_k = \psi = 0$. (d) The coefficients of the first Fourier mode of the input pattern (r_1^c) increase θ_{ijk} ($\phi_i = \phi_j = \phi_k = \psi = 0$, solid line) and decrease θ_{ijk} ($\phi_i = \phi_j = \frac{\pi}{2}$, $\phi_k = 0$, dotted line). (e) θ_{ijk} is strongly correlated with the total firing rate. (f) Here, we set $\phi_k = 0$. If $\theta_{ijk} > 0$, the relationship between θ_{ij} and θ_{ijk} is uncorrelated, but if $\theta_{ijk} < 0$, then θ_{ijk} is negatively correlated with θ_{ij}.

4.7 Results: Information theory for higher order correlations

In the previous section, we show that structured neural connections modulate spiking nonlinearity and induce generating both sparse and synchronized neural activity depending on external inputs. As a result, the 3rd-order correlations resulting from visual stimulation can carry stimulus-specific information.

To validate this, we investigate the precision with which specific stimuli within the highly correlated neural ensemble are encoded, using stimulus-specific decomposition of the mutual information (SSI). Similar to the previous section, we focus on the triplet neural activity patterns with a preferred orientation ($\phi_i = \phi_j = \phi_k = 0$). Changing the stimulus orientation ψ from $-\pi/2$ to $\pi/2 - \pi/G$, we analytically calculate the joint probability distribution, $P(\boldsymbol{x})$, and derive correlation parameters $\boldsymbol{\theta}$ from $P(\boldsymbol{x})$.

In this section, we calculate two types of SSI in each stimulus orientation ψ. First, we directly calculate SSI from the above joint probability distribution, $P(\boldsymbol{x})$, which include 3rd order correlations among neural activities, as shown in black line of Fig4.4. Second, we set $\theta_3 = 0$ and do inverse transformation from the adjusted correlation parameters to joint probability distribution, $P'(\boldsymbol{x})$. Then, we calculate the SSI as indicated in gray line of Fig4.4.

From the results, we found that $I_{SSI}(\psi)$ in the case of $\theta_3 \neq 0$ is larger than $\theta_3 = 0$. This results indicate that the 3rd-order correlations resulting from visual stimulation carry stimulus-specific information when neurons have the same preferred orientation as external grating stimulus, i.e., $\phi_i = \phi_j = \phi_k = \psi = 0$. Figs 4.5 show the effects of common noise on SSI. We found that although common noise decrease SSI due to the neural correlations (Averbeck, Latham and Pouget 2006), comparatively-high is the SSI of triplet neurons which have the same preferred orientation as external grating stimulus, due to 3rd-order neural correlations.

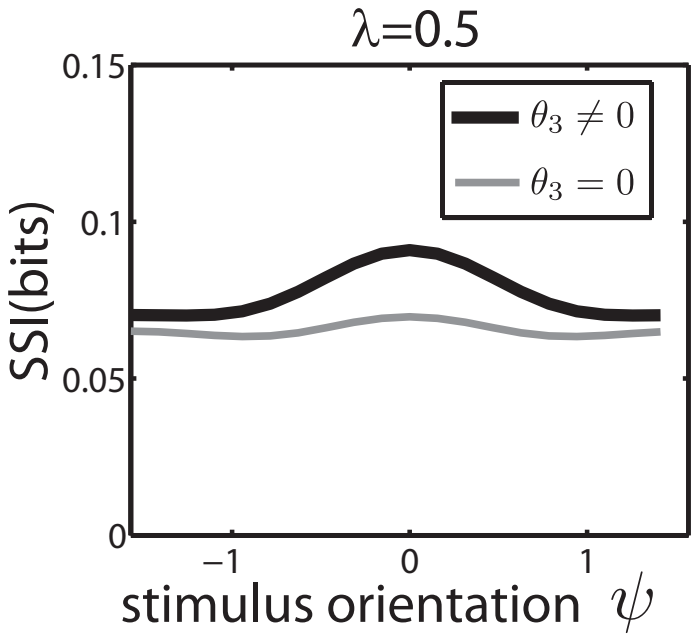

Fig. 4.4. $I_{SSI}(\psi)$ of three neurons ($\phi_i = \phi_j = \phi_k = \psi = 0$) to a grating stimulus (stimulus orientation $-\pi/2 \leq \psi \leq \pi/2 - \pi/G$) in the V1 network with MH-type connections ($J_1 = 3$, $\lambda = 0.5$). We compare $I_{SSI}(\psi)$ in the case of $\theta_3 = 0$ and $\theta_3 \neq 0$ and found that $I_{SSI}(\psi)$ in the case of $\theta_3 \neq 0$ is larger than $\theta_3 = 0$.

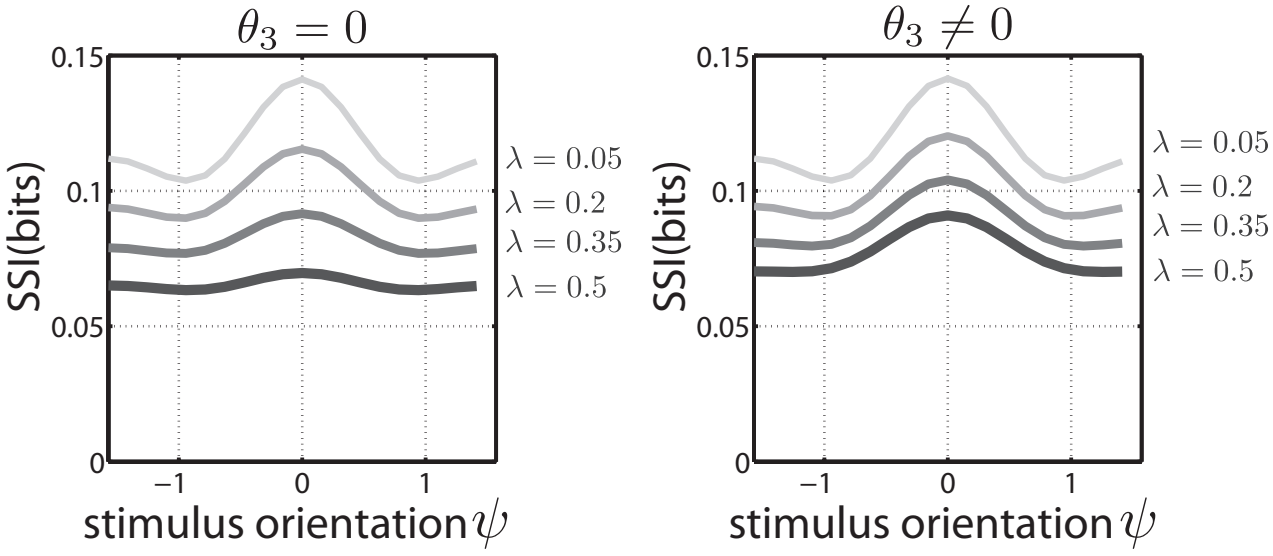

Fig. 4.5. $I_{SSI}(\psi)$ of three neurons ($\phi_i = \phi_j = \phi_k = 0$) to a grating stimulus (stimulus orientation $-\pi/2 \leq \psi \leq \pi/2 - \pi/G$) in the V1 network with MH-type connections ($J_1 = 3$). Although common noise (λ represents the variance of common noise) decreases I_{SSI}, $I_{SSI}(\psi = 0)$ relatively higher due to 3rd-order correlations.

4.8 Summary

We constructed a parsimonious structured network with common inputs and spiking nonlinearities as a model of orientation selectivity and propose decisive experiments with grating stimulus in primary visual cortex to test the effect of inhomogeneous connectivity on higher-order correlations. Unlike a homogeneous network model (Macke et al., 2011), inhomogeneous connections provide not only the tuning curve of firing rates but also the relationships among the statistics observed in the neurophysiological experiments in V1 (Ohiorhenuan and Victor 2011). It is noteworthy that the functional specificity of the network can dynamically control the structure of higher-order correlations and can generate both sparse and synchronized neural activity. We expect our study to pave the way for theoretical studies on the effects of structured interactions on higher-order correlated neural activity and information processing in the brain, but also promote a theory of how a finite common noise and higher-order correlations induce the phase synchronization of a general class of limit cycle oscillators.

Chapter 5

Conclusion

Perception is highly robust to the presence of sensory noise and adapt rapidly to changes in incoming stimuli (Dragoi et al. 2002, Simoncelli 2003). How to be robust and adapt rapidly to the external stimulus and to optimize neuronal performance have been intensely debated. Actually, 400-ms brief adaptation to a grating of fixed orientation improves the accuracy of a population code to optimize neuronal performance during natural viewing in macaque primary visual cortex (Gutnisky and Dragoi 2008). This result partly coincides with psychophysical data showing that orientation discrimination performance is improved after iso-orientation adaptation (Clifford et al. 2001). How to adapt rapidly to the external stimulus and optimize neuronal performance has been intensely debated. A possible mechanism is short-term synaptic plasticity, which occurs over milliseconds to minutes (Zucker and Regehr 2002) and allows synapses to perform critical computational functions in neural circuits. An advantage of the synaptic computation is to rapidly compute information processing because this is local computation and does not need to sum up their individual information. However, because of their dynamical synapses, it is difficult to evaluate their macroscopic effects on information processing. In the first-half of paper, we construct the theoretical framework for investigating the role of synaptic plasticity in adjusting information processing to external stimulus. To evaluate the effect of synaptic depression on the estimation of information conveyed by the firing rates of neural populations, we analytically calculated the Fisher information, using the tuning curves and neural correlations in neural network models with synaptic depression obtained in the Chapter 2 and 3.

In Chapter 2, we have explored the macroscopic properties of two types of stochastic binary neural networks with synaptic depression: a network with homogeneous connectivity and a ring attractor network with Mexican hat type connectivity. Although a stochas-

tic binary neural network model with synaptic depression cannot be analyzed owing to the asymmetry of connections by the conventional equilibrium statistical-mechanical approach, we derive the microscopic dynamical mean field equations for the network model. Because in the equations the averaged product of the two stochastic variables is decoupled as the product of their averages, they must be independent. We proved the independence and derived the microscopic equations in this paper, assuming that the synaptic weight J_{ij} is of the order of $1/N$ with respect to the number of neurons N. Using the microscopic mean field equations, we derived macroscopic steady-state equations for these networks and investigated the stability of the steady-state solutions obtained. The results coincided with those of a simulation. We conclude that the presence of synaptic depression leads to oscillatory instability and that various oscillatory states appear depending on the strength of the interneuron connections. Synaptic depression thus causes the diversity of dynamic states in large networks of spiking neurons.

In Chapter 3, we extended a previous theoretical framework to a theory of correlation in spiking neuron models with synaptic depression. This theory enables us to analytically calculate the effect of synaptic depression on neural correlations. Some previous studies, in which neural correlations were computed in rate neural network model, relied on numerical methods because of the difficulty of analytically computing correlations, that take a substantial amount of time to calculate (Series et al. 2004, Cortes et al. 2010). Our theoretical framework greatly reduced this time cost and enables us to extensively investigate the various parameters of the neural network model with short-term synaptic depression.

As previously indicated, using the tuning curves and neural correlations in neural network models with synaptic depression obtained in the Chapter 2 and 3, we analytically calculated the Fisher information to elucidate how synaptic depression affects the coding efficiency in the latter part of Chapter 3. We found the parameter regions where, although synaptic depression reduces coding accuracy on the single neuron level, synaptic depression increases the efficacy of information processing on the population level by a reduction of the neural correlations. This theoretical framework has broad utility and can be applied to other synaptic plasticity, such as spike rate adaptation (Liu and Wang 2001), synaptic facilitation (Lisman 1997, Tsodyks et al. 1998) and postsynaptic receptor dynamics cold allow more general filtering of spike trains (Maass and Zador 1999), because our theoretical framework draws on the activity-dependent quality of synaptic plasticity. Our approach thus provides a powerful way of studying how synaptic plasticity affects neural correlation and accuracy of population code in a realistic network model of spiking neurons.

In the Chapter 2 and 3, we discuss only about the sensory information transmitted by firing rates and pair-wise correlations between neurons. However, the widely observed complex features of population activity, such as synchronization and concentration patterns of suspension, can be captured not only by pairwise correlations but also by higher-order correlations, which have significant effects on complicated physical processes and information processing. In neuroscience, electrophysiological experiments have recently shown that the manner in which information is represented by specific patterns of spiking and silence over a group of neurons, is also understood both by the pairwise and higher-order correlated neural activities. But, very little is known about the relationships the higher-order correlations linking the role of information procening, that is, whether higher-order correlations between neuronal activities could allow neurons to robustly and rapidly transmit sensory or motion information.

In Chapter 4, we investigated a parsimonious structured network with common inputs and spiking non-linearities to investigate the effects of structured connectivities on higher-order correlations, which are recently observed in various brain regions. Although in the previous chapter we derive neural correlations based on the fluctuation-dissipation theory for investigating changes in the equilibrium order parameters, due to sufficiently weak externally applied perturbations (Ginzburg and Sompolinsky 1994), this network model cannot reproduce there are no equilibrium order parameters and we cannot apply the fluctuation-dissipation theory to network model (Amari et al., 2003, Macke et al., 2011). We then constructed a parsimonious structured network with common inputs and spiking non-linearities as a model of orientation selectivity and theoretically investigate the effects of structured connectivity on higher-order correlations. Unlike a homogeneous network, a network with heterogeneous connections can provide not only a tuning curve of firing rates but also a relationship among the statistics gathered from neurophysiological experiments in the primary visual cortex. We found that the heterogeneous structure of the network can dynamically control the structure of higher-order correlations and can generate both sparse and synchronized neural activity. Due to these dynamics, the 3rd-order correlations resulting from visual stimulation can carry stimulus-specific information. The theoretical frameworks developed in this thesis will provide a powerful tool to elucidate the role of structured connectivities in neural information processing in the brain.

The recent development of experimental techniques enable us to simultaneously record the activity of large numbers of neurons. These electro-physiological data are a mine of treasure which will give great insight about principle of information processing in the brain, such as higher-order correlations. Unfortunately, however, we think most treasures

are still buried. To discover them and fully understand information processing them, not only analyzing the electrophysiological data but also constructing a network model by using experimental data as constraints are needed. By analyzing both actual data and network model with the theoretical frameworks in this thesis, we aim to reveal mysterious mechanisms of information processing in the brain.

Appendix A

Dimensionality reduction for stability analysis

In §2.5.3, we showed that a few eigenvalues consisting of low-frequency perturbations affected the stability of the system. This means that only low-frequency perturbations affect the stability of the system. In this Appendix, we compare the eigenvalues of the Jacobian matrix in Fourier space [eq. (2.60)] for high- and low-frequency perturbations with those for low-frequency perturbations, as indicated in Figs. A.1 and A.2. Figure. A.1(b) shows the distributions of eigenvalues for the Jacobian matrix [eq. 2.60] for perturbations $\delta\hat{m}_k$ and $\delta\hat{X}_k$ $(-5\times10^2 \leq k \leq 5\times10^2-1)$ in a ring network with $\gamma = 1.5$ and $\tau = 3$, similar to in Fig. 2.8(b). Figures. A.1(d) and A.1(e) show the distributions for low-frequency perturbations, namely, $\delta\hat{m}_k$ and $\delta\hat{X}_k$ $(-5\times10 \leq k \leq 5\times10-1)$, and $\delta\hat{m}_k$ and $\delta\hat{X}_k$ $(-5 \leq k \leq 5-1)$, respectively. Figure. A.2 shows a comparison for a ring network with $\gamma = 2.5$ and $\tau = 3$.

Although we did not approximate the distributions in Fig. A.1(b) by the distributions shown in Fig. A.1(d), we found that the maximum eigenvalue of the Jacobian matrix for perturbations $\delta\hat{m}_k$ and $\delta\hat{X}_k$ $(-5\times10 \leq k \leq 5\times10-1)$ coincided with that of the Jacobian matrix for perturbations $\delta\hat{m}_k$ and $\delta\hat{X}_k$ $(-5\times10^2 \leq k \leq 5\times10^2-1)$. However, the results of stability analysis for perturbations $\delta\hat{m}_k$ and $\delta\hat{X}_k$ $(-5 \leq k \leq 5-1)$ and those for perturbations $\delta\hat{m}_k$ and $\delta\hat{X}_k$ $(-5\times10^2 \leq k \leq 5\times10^2-1)$ differed in the maximum eigenvalue of the Jacobian matrix because the lateral-inhibitory interaction (J_1) was relatively strong [Figs. A.1(b) and A.1(f)]. In contrast to the stability analysis for $\delta\hat{m}_k$ and $\delta\hat{X}_k$ $(-5\times10 \leq k \leq 5\times10-1)$, we obtained different results for the stability analysis. We obtained the same results of stability analysis for $\gamma = 2.5$ and $\tau = 3$, as shown in Fig. A.2.

These results show that high-frequency perturbations m_k and X_k did not affect the stability of inhomogeneous steady-state solutions because J_1 was relatively weak. Therefore, when there is a weak lateral-inhibition, we can reduce the dimensions for the stability analysis since we do not need to take into account high-frequency perturbations. This reduction of dimensionality enables rapid analysis of the stability of steady-state solutions for a ring network with synaptic depression.

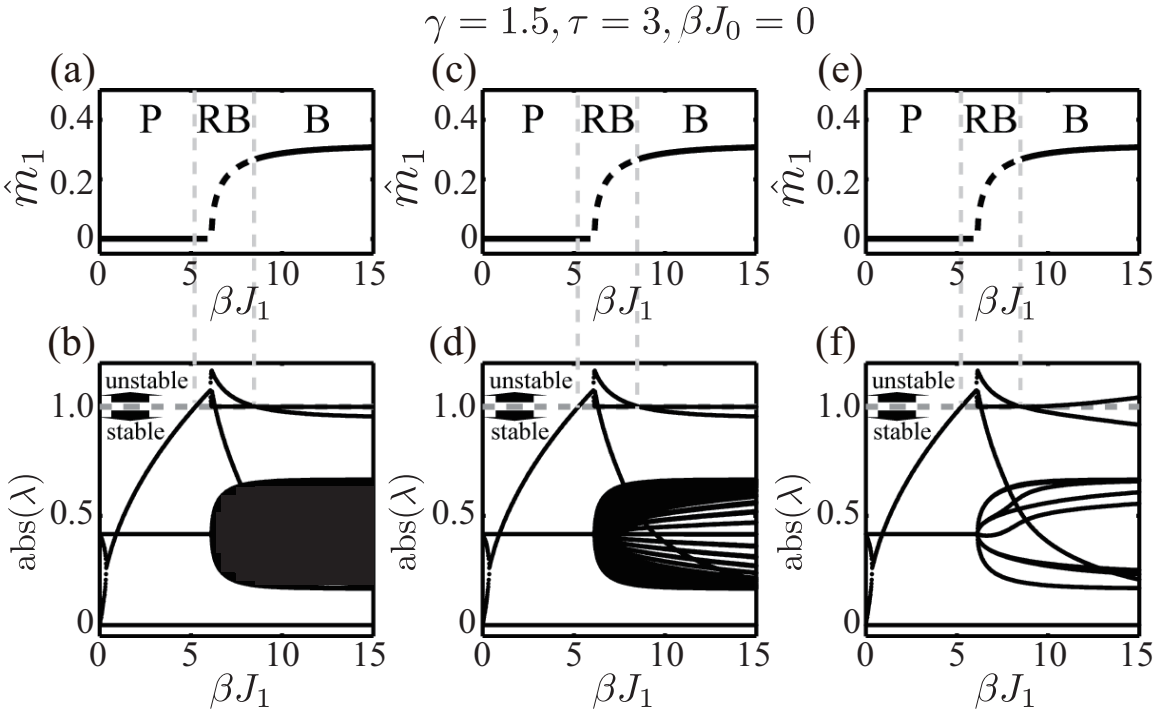

Fig. A.1. Solid and dashed lines in (a), (c), and (e) respectively represent stable and unstable solutions to the amplitude of localized activity, $\hat{m}_1$. (b), (d), (f) Distribution of eigenvalues for Jacobian matrix H [eq. 2.60] for perturbations $\delta\hat{m}_k$ and $\delta\hat{X}_k$ $(-K \leq k \leq K-1)$. (b) $K = 5 \times 10^2$. The size of the Jacobian matrix H is 2000×2000. (d) $K = 5 \times 10$. The size of the Jacobian matrix H is 200×200. (f) $K = 5$. The size of the Jacobian matrix H is 20×20.

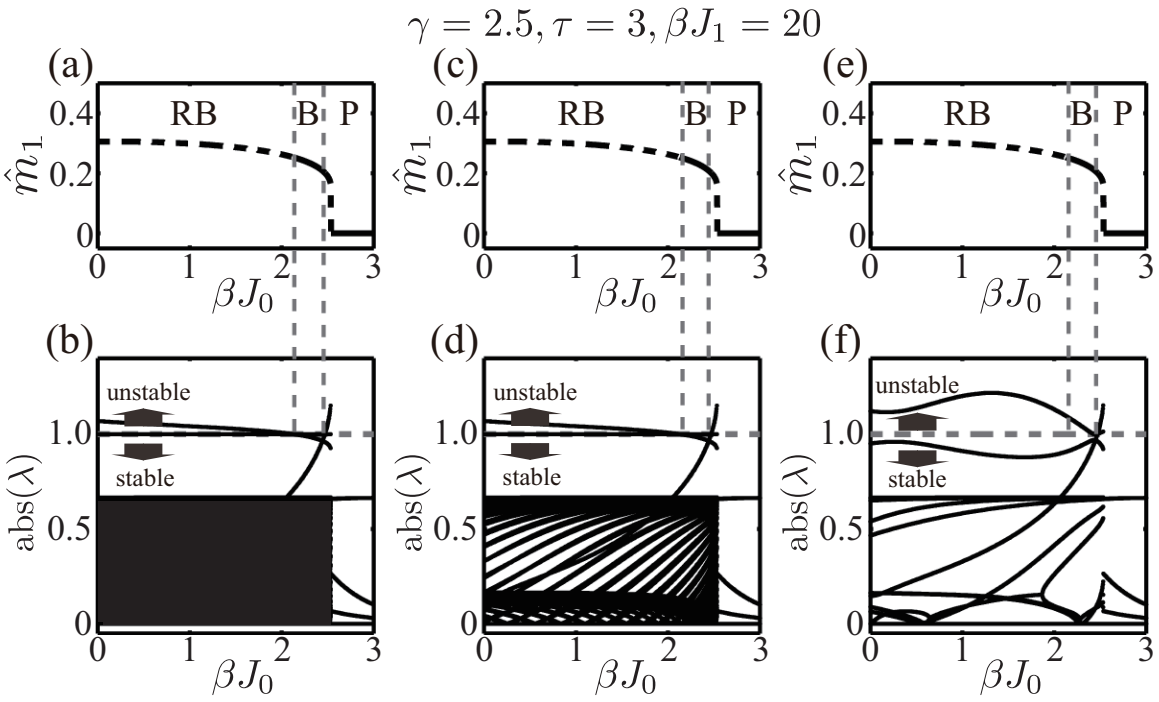

Fig. A.2. Solid and dashed lines in (a), (c) and (e) respectively represent stable and unstable solutions to the amplitude of localized activity $\hat{m}_1$. (b), (d), (f) Distribution of eigenvalues for the Jacobian matrix H [eq. 2.60] for perturbations $\delta\hat{m}_k$ and $\delta\hat{X}_k$ $(-K \leq k \leq K-1)$. (b) $K = 5 \times 10^2$. The size of the Jacobian matrix H is 2000×2000. (d) $K = 5 \times 10$. The size of the Jacobian matrix H is 200×200. (f) $K = 5$. The size of the Jacobian matrix H is 20×20.

Appendix B

The order of input correlations

We prove that $\langle(\delta u_i)^2\rangle$ is the order of $1/N$ in this appendix. Using Eqs. (3.25), (3.28), and (3.29), we can write $\langle(\delta u_i)^2\rangle$ as

$$\begin{aligned}\langle(\delta u_i)^2\rangle = \Bigg\langle \sum_{\tau,\tau'}^{\infty}\sum_{j\neq i}\sum_{k\neq i} 2J_{ij}\epsilon_{ij}(\tau)2J_{ik}\epsilon_{ik}(\tau') \\ \times \delta(x_j(t-\tau)S_j(t-\tau))\delta(x_k(t-\tau')S_k(t-\tau'))\Bigg\rangle, \\ = \sum_{\tau,\tau'}^{\infty}\sum_{j\neq i}\sum_{k\neq i,j} 2J_{ij}\epsilon_{ij}(\tau)2J_{ik}\epsilon_{ik}(\tau')Z_{jk}(t-\tau,t-\tau') \\ + \sum_{\tau,\tau'}^{\infty}\sum_{j\neq i} 4J_{ij}^2\epsilon_{ij}(\tau)\epsilon_{ij}(\tau')Z_j(t-\tau,t-\tau'). \quad \text{(B.1)}\end{aligned}$$

First, we consider the order of the first term in Eq. (B.1). When each neuron is connected to a number of neurons of order N and connections J_{ij} are all of order $1/N$, $\sum_{\tau,\tau'}^{\infty}\sum_{j\neq i}\sum_{k\neq i,j} 2J_{ij}\epsilon_{ij}(\tau)2J_{ik}\epsilon_{ik}(\tau')$ are of order 1 and the order of the first term in Eq. (B.1) is determined by $Z_{jk}(t-\tau,t-\tau')$. Using Eq. (3.29), we found $Z_{jk}(t-\tau,t-\tau')(j\neq k)$ is the same order of $1/N$ as C^s_{jk}. Thus, the order of the first term in Eq. (B.1) is $1/N$. Next, we discuss the order or the second term in Eq. (B.1). Similarly, because $J_{ij}^2\epsilon_{ij}(\tau)\epsilon_{ij}(\tau')$ are of order $1/N$ and the order of $Z_j(t-\tau,t-\tau')$ is no more than the order of $O(1)$, the second term in Eq. (B.1) is also on the order of $1/N$. Hence, the order of $\langle(\delta u_i)^2\rangle$ is $1/N$.

B.1 Equal-time correlation functions

Here, we describe the details on calculating equal-time correlation functions. A important point in the calculations is that we ignore high-order correlations, which are no more than the order of $1/N$, to derive a set of closed equations for correlation functions.

First, we derive the equal-time cross-correlation functions between $S_i(t)$ and $S_j(t)(j \neq i)$ at equilibrium, $C^s_{ij}(0)$, [Eq. (3.25)]. By expanding $g[u_i(t)]$ around the noise average of $\langle u_i \rangle$ [Eq. (3.24)], we obtain

$$C^s_{ij}(0) = g'(\langle u_i \rangle) g'(\langle u_j \rangle) \langle \delta u_i \delta u_j \rangle, \tag{B.2}$$

where $\langle \delta u_i \delta u_j \rangle$ is

$$\begin{aligned}\langle \delta u_i \delta u_j \rangle = &\sum_{\tau,\tau'}^{\infty} \sum_{k \neq i} \sum_{l \neq j,k} 2J_{ik}\epsilon_{ik}(\tau) 2J_{jl}\epsilon_{jl}(\tau') Z_{kl}(\tau - \tau') \\ &+ \sum_{\tau,\tau'}^{\infty} \sum_{k \neq i} 2J_{ik}\epsilon_{ik}(\tau) 2J_{jk}\epsilon_{jk}(\tau') Z_k(\tau - \tau'),\end{aligned} \tag{B.3}$$

because

$$\delta u_i(t) = \sum_{\tau=1}^{\infty} \sum_{j \neq i} J_{ij}\epsilon_{ij}(\tau) 2\delta(x_j(t-\tau) S_j(t-\tau)). \tag{B.4}$$

Substituting Eq. (B.3) into Eq. (B.2) gives [Eq. (3.25)].

We then evaluate $Z_{kl}(\tau)$ and $Z_k(\tau)$ as discussed above. $Z_{kl}(t, t+\tau)$ can be written as

$$\begin{aligned}Z_{kl}(t, t+\tau) &= \langle \delta(x_k(t) S_k(t)) \delta(x_l(t+\tau) S_l(t+\tau)) \rangle, \\ &= \langle x_k(t) S_k(t) x_l(t+\tau) S_l(t+\tau) \rangle \\ &\quad - \langle x_k(t) S_k(t) \rangle \langle x_l(t+\tau) S_l(t+\tau) \rangle, \\ &= \Big\langle [\delta x_k(t) + \langle x_k(t) \rangle][\delta S_k(t) + \langle S_k(t) \rangle] \\ &\quad \times [\delta x_l(t+\tau) + \langle x_l(t+\tau) \rangle] \\ &\quad \times [\delta S_l(t+\tau) + \langle S_l(t+\tau) \rangle] \Big\rangle \\ &\quad - \langle [\delta x_k(t) + \langle x_k(t) \rangle][\delta S_k(t) + \langle S_k(t) \rangle] \rangle \\ &= C^s_{kl}(t, t+\tau) \langle x_k(t) \rangle \langle x_l(t+\tau) \rangle \\ &\quad + C^{sx}_{kl}(t, t+\tau) \langle x_k(t) \rangle \langle S_l(t+\tau) \rangle \\ &\quad + C^{xs}_{kl}(t, t+\tau) \langle S_k(t) \rangle \langle x_l(t+\tau) \rangle \\ &\quad + C^{x}_{kl}(t, t+\tau) \langle S_k(t) \rangle \langle S_l(t+\tau) \rangle.\end{aligned} \tag{B.5}$$

We ignore three-point cross-correlations and four-point cross-correlations. Taking limit $t \to \infty$ yields Eq. (3.28). For $k = l$ in Eq. (3.28), we obtain Eq. (3.29).

Next, let us consider equal-time cross-correlation functions between S_i and x_j, $C_{ij}^{sx}(0)$. Similar to the approach we took in the previous section, we expanded $g[u_i(t)]$ around $\langle u_i \rangle$ and substituted it into Eq. (3.3) to obtain

$$\begin{aligned} C_{ij}^{sx}(t,t) = \Big\langle g'(\langle u_i(t) \rangle) \delta u_i(t) \\ \left\{ \left(1 - \frac{1}{\tau_d} \right) \delta x_j(t-1) - U \delta [x_j(t-1) S_j(t-1)] \right\} \Big\rangle, \\ = \sum_{\tau=1}^{\infty} \sum_{k \neq i,j} \tilde{J}_{ik}(\tau) \Bigg\{ \left(1 - \frac{1}{\tau_d} \right) \\ \times \langle \delta(x_k(t-\tau) S_k(t-\tau)) \delta x_j(t-1) \rangle - U Z_{kj}(t-\tau, t-1) \Bigg\}, \end{aligned} \tag{B.6}$$

where we denote $\tilde{J}_{ik}(\tau) = 2g'(\langle u_i \rangle) J_{ik} \epsilon_{ik}(\tau)$ and use Eq. (3.27). Taking limit $t \to \infty$ gives

$$\begin{aligned} C_{ij}^{sx}(0) = \lim_{t \to \infty} \sum_{\tau=1}^{\infty} \sum_{k \neq i,j} \tilde{J}_{ik}(\tau) \Bigg\{ \left(1 - \frac{1}{\tau_d} \right) \\ \times \langle \delta(x_k(t-\tau) S_k(t-\tau)) \delta x_j(t-1) \rangle - U Z_{kj}(\tau - 1) \Bigg\}, \end{aligned} \tag{B.7}$$

To derive a set of closed equations for correlation functions, which is described by Eqs. (3.19) and (3.20), we evaluate $\lim_{t \to \infty} \langle \delta(x_k(t-\tau) S_k(t-\tau)) \delta x_j(t-1) \rangle$ as

$$\begin{aligned} \lim_{t \to \infty} \langle \delta(x_k(t-\tau) S_k(t-\tau)) \delta x_i(t-1) \rangle \\ = \lim_{t \to \infty} \langle x_k(t-\tau) S_k(t-\tau) \delta x_i(t-1) \rangle \\ = \lim_{t \to \infty} \Big\langle (\delta(x_k(t-\tau)) + \langle x_k(t-\tau) \rangle)(\delta(S_k(t-\tau)) \\ + \langle S_k(t-\tau) \rangle) \delta x_i(t-1) \Big\rangle \\ = \langle x_k \rangle C_{ki}^{sx}(\tau - 1) + \langle S_k \rangle C_{ki}^{x}(\tau - 1). \end{aligned} \tag{B.8}$$

Substituting Eq. (B.8) into Eq. (B.7) gives Eq. (3.30). Since $C_{ij}^{xs}(t,t) = C_{ji}^{sx}(t,t)$, we can also obtain $C_{ji}^{sx}(0)$ from Eq. (3.30).

Finally, we derive equal-time cross-correlation functions between x_i and x_j, $C_{ij}^{x}(0)$.

Substituting Eq.(3.3) into Eq.(3.18) and taking limit $t \to \infty$ gives

$$
\begin{aligned}
&C_{ij}^{x}(0) \\
&\quad = \lim_{t\to\infty} \left\{ \left(1 - \frac{1}{\tau_d}\right) \delta x_i(t-1) - U\delta[x_i(t-1)S_i(t-1)] \right\} \\
&\qquad \left\{ \left(1 - \frac{1}{\tau_d}\right) \delta x_j(t-1) - U\delta[x_j(t-1)S_j(t-1)] \right\} \\
&\quad = \lim_{t\to\infty} \Bigg\{ \left(1 - \frac{1}{\tau_d}\right)^2 C_{ij}^{x}(t-1,t-1) + U^2 Z_{ij}(t-1,t-1) \\
&\qquad - U\left(1 - \frac{1}{\tau_d}\right) \Big[\langle \delta(x_i(t-1)S_i(t-1))\delta x_j(t-1)\rangle \\
&\qquad\qquad + \langle \delta(x_j(t-1)S_j(t-1))\delta x_i(t-1)\rangle \Big] \Bigg\}. \qquad \text{(B.9)}
\end{aligned}
$$

Substituting Eq. (B.8) into Eq. (B.9), we obtain Eq. (3.31).

B.2 Adjustment of external inputs

We first explain why we have to maintain the firing rate, $\langle S_i \rangle$, in order to study how synaptic depression affects neural correlations in this appendix. While the change in instantaneous firing rates affects neural correlations (Eq. (3.21)), input h_i only has an indirect effect on neural correlations via the instantaneous firing rates. We thus adjust the strength of input and maintain the firing rate to study what effects synaptic depression has on neural correlations.

We then derive the external inputs to neurons, h_i. To begin with, we simply emulate noisy orientation selective inputs to the neurons (Fig. 3.1(a)). We respectively define h_i^0 and $\langle S_i^0 \rangle$ as the input and instantaneous firing rate in the absence of synaptic depression, i.e., $\gamma = 0$. To keep $\langle S_i \rangle$ in the presence of synaptic depression γ the same as $\langle S_i^0 \rangle$ by changing h_i, we derive the following equation from the self-consistent equation (3.16).

$$
\begin{aligned}
&g\left\{ \sum_{\tau=1}^{\infty} \sum_{j\neq i} J_{ij}\epsilon_{ij}(\tau) \left(2\frac{\langle S_j^0 \rangle}{1+\gamma\langle S_j^0 \rangle} - 1 \right) + h_i + u_r \right\} \\
&\qquad = g\left\{ \sum_{\tau=1}^{\infty} \sum_{j\neq i} J_{ij}\epsilon_{ij}(\tau) \left(2\langle S_j^0 \rangle - 1 \right) + h_i^0 + u_r \right\}. \qquad \text{(B.10)}
\end{aligned}
$$

Since the escape function, g, monotonically increases, Eq. (B.10) can be written as Eq. (3.56) . Using Eq. (3.56), we adjust external inputs h_i and the instantaneous firing rates

for $\gamma = 0$ to the same as those for $\gamma = 0.1$ and 1 shown in Fig. 3.1. Note from Eq. (3.47) that, instantaneous firing rate $\langle S_i \rangle$ and instantaneous synaptic efficacy $\langle x_i \rangle$ are the same as mean firing rate f_i and mean synaptic efficacy X_i, respectively, at equilibrium.

Bibliography

(Abbott et al. 1997) L. Abbott, J. Varela, K. Sen, and S. Nelson: Synaptic depression and cortical gain control, Science **275** (1997) 221.

(Abbott and Dayan 1999) L. F. Abbott and P. Dayan: The effect of correlated variability on the accuracy of a population code, Neural Comput. **11** (1999) 91.

(Abbott and Regehr 2004) L. Abbott and W. Regehr: Synaptic computation, Nature **431** (2004) 796.

(Alonso and Martinez 1998) J. M. Alonso and L. M. Martinez, Functional connectivity between simple cells and complex cells in cat striate cortex Nat. Neurosci. **1**(5), 395 (1998).

(Amari 2001) S. Amari, IEEE Trans. Inf. Theory, **47**(5), 1701 (2001).

(Amari et al., 2003) Amari, S.-I., Nakahara, H., Wu, S., and Sakai, Y. (2003). Synchronous firing and higher-order interactions in neuron pool. Neural computation, 15(1), 127-42.

(Anderson et al. 2000) Anderson, J. S., Lampl, I., Gillespie, D. C., and Ferster, D. (2000). The contribution of noise to contrast invariance of orientation tuning in cat visual cortex. Science, 290(5498), 1968-72.

(Averbeck, Latham and Pouget 2006) B. B. Averbeck, P. E. Latham and A. Pouget: Neural correlations, population coding and computation, Nature Rev. Neurosci. **7** (2006) 358.

(Benucci et al. 2007) A. Benucci, R. A. Frazor, and M. Carandini: Standing waves and traveling waves distinguish two circuits in visuail cortex, Neuron **55** (2007) 103.

(Ben-Yishai et al. 1995) R. Ben-Yishai, R. Bar-Or, and H. Sompolinsky: Theory of orientation tuning in visual cortex, Proc. Natl. Acad. Sci. U.S.A. **92** (1995) 3844.

(Britten et al. 1992) K. H. Britten, M. N. Shadlen, W. T. Newsome and J. A. Movshon: The analysis of visual motion: A comparison of neuronal and psychophysical performance, J. Neurosci **12** (1992) 4745.

(Brown and Milner 2003) R. E. Brown and P. M. Milner: The legacy of Donald O. Hebb: more than the Hebb synapse, Nature Rev. Neurosci. **4** (2003) 1013.

(Burrone and Murthy 2003) J. Burrone, J and V. N. Murthy: Synaptic gain control and homeostasis, Curr. Opin. Neurobiol. **13**, (2003) 560.

(Butts 2003) How much information is associated with a particular stimulus?, Network Comput. Neural Syst., **14**, (2003) 177-187.

(Buzsaki 2006) G. Buzsaki: *Rhythms of the Brain* (Oxford University Press, NY, 2006) p.111.

(Celebrini and Newsome 1994) M. I. Celebrini and W. T. Newsome: Neuronal and psychophysical sensitivity to motion signals in extractriate area MST of the macaque monkey, J. Neurosci. **14** (1994) 4109.

(Chelaru et al. 2008) M. I. Chelaru and V. Dragoi: Asymmetric synaptic depression in cortical networks, Cereb. Cortex **18** (2008) 771.

(Clifford et al. 2001) C. W. G. Clifford, A. M. Wyatt, D. H. Arnold, S. T. Smith and P. Wenderoth: Orthogonal adaptation improves orientation discrimination, Vision Research **41** (2001) 151.

(Cohen and Maunsell 2009) M. R. Cohen and J. H. R. Maunsell: Attention improves performance primarily by reducing interneuronal correlation, Nature Neurosci. **12** 1594 (2009).

(Compte et al. 2000) A. Compte, N. Brunel, P. Goldman-Rakic, and X. Wang: Synaptic mechanisms and network dynamics underlying spatial working memory in a cortical network model, Cerebral Cortex **10** (2000) 910.

(Cortes et al. 2010) J. M. Cortes, D. Marinazzo, P. Series, M. W. Oram, T. J. Sejnowski and M. C. W. van Rossum: Neural adaptation reduces energy cost while preserving coding accuracy, *Society for Neuroscience Annual Meeting 2010 Abstract.*

(Dayan and Abbott 2001) P. Dayan and L. F. Abbott *Theoretical Neuroscience* (The MIT Press, Cambridge, 2001).

(DeWeese and Meister 1999) M. R. DeWeese and M. Meiseter: How to measure the information gained from one symbol, Network **10**, (1999), 325-40.

(Dobrunz and Stevens 1999) L. E. Dobrunz and C. F. Stevens: Response of Hippocampal Synapses to Natural Stimulation Patterns, Neuron **22** 157 (1999).

(Dragoi et al. 2000) V. Dragoi, J. Sharma and M. Sur: Adaptation-induced plasticity of orientation tuning in adult visual cortex, Neuron **28** (2000) 287.

(Dragoi et al. 2002) V. Dragoi, J. Sharma, E. K. Miller and M. Sur: Dynamics of neuronal sensitivity in visual cortex and local feature discrimination, Nature Neurosci. **5** (2002) 883.

(Ecker et al. 2010) A. S. Ecker, P. Berens, G. A. Keliris, M. Bethge, N. K. Logothetis

and A. S. Tolias: Decorrelated neuronal firing in cortical microcircuits, Science **327** (2010) 584.

(Ganmor et al., 2011) Ganmor, E., Segev, R., and Schneidman, E. (2011). Sparse low-order interaction network underlies a highly correlated and learnable neural population code. Proceedings of the National Academy of Sciences of the United States of America, 108(23), 9679-84.

(Gawne and Richmond 1993) T. J. Gawane and B. J. Richmond: How independent are the messages temporal carried by adjacent inferior temporal cortical neurons? J. Neurophysiol. **13** (1993) 2758.

(Georgopoulos et al. 1986) A. P. Georgopoulos, A. B. Schwartz and R. E. Kettner: Neuronal population coding of movement direction, Science **233** (1986) 1416.

(Gerstner and Hemmen 1992) W. Gerstner and J. L. van Hemmen: Associative memory in a network of 'spiking' neurons, Nework **3** (1992) 139.

(Gerstner and Kistler 2002) W. Gerstner and W. Kistler: *Spiking Neuron Models* Cambridge University Press, NY, 2002.

(Gilbert and Wiesel 1989) Gilbert, D., and Wiesel, T. N. (1989). Columnar Specificity of Intrinsic Horizontal Connections in Cat Visual Cortex and Corticocortical. Journal of Neuroscience, 9(7), 2432-2442.

(Ginzburg and Sompolinsky 1994) I. Ginzburg and H. Sompolinsky: Theory of correlations in stochastic neural networks, Phys. Rev. E **50** (1994) 3171.

(Goldman et al. 2002) M S. Goldman, P. Maldoato, and L. F. Abbot: Redundancy reduction and sustained riring with stochastic depressing synapses, J. Neurosci. **22** (2002).

(Glauber 1963) R. J. Glauber: Time - Dependent Statistics of the Ising Model, J. Math. Phys. **4**(2) 294 (1963).

(Gray 1999) C. M. Gray: The temporal correlation hypothesis of visual feature integration: Still alive and well, Neuron **24** (1999) 31.

(Gutnisky and Dragoi 2008) D. A. Gutnisky and V. Dragoi: Adaptive coding of visual information in neural populations, Nature **452** (2008) 220.

(Hamaguchi et al. 2005) Hamaguchi, K., Okada, M., Yamana, M., and Aihara, K. (2005). Correlated firing in a feedforward network with Mexican-hat-type connectivity. Neural computation, 17(9), 2034-2059.

(Hamaguchi 2006) K. Hamaguchi, J. P. L. Hatchett, and M. Okada: Analytic solution of neural network with disordered lateral inhibition, Phys. Rev. E **73** (2006) 051104.

(Hamaguchi et al. 2008) K. Hamaguchi, H. Urano, and M. Okada: Effect of asymmetry in a binary state on the collective behavior of a system with spatially modulated

interaction and quenched randomness, Phys. Rev. E **78** (2008) 051124.

(Han et al. 2008) F. Han, N. Caporale, and Y. Dan: Reverberation of recent visual experience in spontaneous cortical waves Neuron **60** (2008) 321.

(Hansel and Sompolinsky 1998) D. Hansel and H. Sompolinsky: *Methods in Neural Modeling* (MIT Press, Cambridge, 1998) 2nd ed., p. 499.

(Heimel and Coolen 2001) J. Heimel and A. Coolen: Generating functional analysis of the dynamics of the batch minority game with random external information. Phys. Rev. E, **63**(5), 1 (2001).

(Hubel and Wiesel 1962) D. H. Hubel and T. N. Wiesel: Receptive fields, binocular interaction and functional architecture in the cat's visual cortex, J. Physiol. **160** (1962) 106.

(Igarashi et al. 2009) Y. Igarashi, M. Oizumi, Y. Otsubo, K. Nagata, and M. Okada: Statistical mechanics of attractor neural network models with synaptic depression, J. Phys. Conf. Ser. **197** (2009) 012018.

(Igarashi et al. 2010) Y. Igarashi, M. Oizumi and M. Okada: Mean field analysis of stochastic neural network models with synaptic depression, J. Phys. Soc. Jpn. **79** (2010) 084001.

(Igarashi et al. 2012) Y. Igarashi, M. Oizumi and M. Okada,
Theory of correlation in a network with synaptic depression.
Physical Review E **85**, 016108, 2012.

(Kay 1993) S. M. Kay: *Fundamentals of Statistical Signal Processing: Estimation Theory* Cambridge University Press, Prentice-Hall, Englewood Cliffs, NJ, 1993.

(Kenet et al. 2003) T. Kenet, D. Bibitchkov, M. Tsodyks, A. Grinvald, and A. Arieli: Spontaneously emerging cortical representations of visual attributes, Nature **425** (2003) 954.

(Kilpatrick and Bressloff 2010) Z. P. Kilpatrick and P. C. Bressloff: Effects of synaptic depression and adaptation on spatiotemporal dynamics of an excitatory neuronal network, Physica D **239** (2010) 547.

(Kilpatrick and Bressloff 2010) Z. P. Kilpatrick and P. C. Bressloff: Spatially structured oscillations in a two-dimensional excitatory neuronal network with synaptic depression, J. Comput. Neurosci. **28** (2010) 193.

(Kohn 2007) A. Kohn: Visual Adaptation: Physiology, Mechanisms, and Functional Benefits, J. Neurophysiol. **97** (2007) 3155.

(Ko et al., 2011) Ko Ho, Hofer Sonja, Pichler Bruno, Buchanan Katherine, Sjostrom Jes-

per, Mrsic-Flogel Thomas D. T D, xcitatory cortical neurons form fine-scale functional networks, Nature, **1**(473), 7345 (2011).

(Kriener et al. 2008) B. Kriener, T. Tetzlaff, A. Aertsen, M. Diesmann and S. Rotter: Correlations and population dynamics in cortical networks, Neural Comput. **20** (2008) 2185.

(Kuramoto 2003) Y. Kuramoto: *Chemical Oscillations, Waves, and Turbulence* (Dover Publications, NY, 2003) p.122.

(Lee et al. 1988) C. Lee, W. H. Rohrer and D. L. Sparks: Population coding of saccadic eye movements by neurons in the superior colliculus, Nature **332** (1988) 357.

(Lisman 1997) J. E. Lisman: Bursts as a unit of neural information: making unreliable synapses reliable, Trends Neurosci. **20** (1997) 383.

(Liu and Wang 2001) Y. H. Liu and X. J. Wang Spike-frequency adaptation of a generalized leaky integrate-and-fire model neuron, J. Comput. Neurosci. **10** (2001) 25.

(Lynch 2004) M. A. Lynch: Long-term potentiation and memory, Physiol. Rev. **84** (2004) 87.

(Maass and Zador 1999) W. Maass and A. M. Zador: Dynamic stochastic synapses as computational units, Neural Comput **11** (1999) 903.

(Macke et al. 2009) J. H. Macke, P. Berens, A. S. Ecker and A. S. Tolias: Generating spike trains with specified correlation coefficients, Neural Comput. **21** (2009) 397.

(Macke et al., 2011) Macke, J., Opper, M., and Bethge, M. (2011). Common Input Explains Higher-Order Correlations and Entropy in a Simple Model of Neural Population Activity. Physical Review Letters, 106, 1-4.

(Marino et al. 2005) J. Marino, J. Schummers, D. C. Lyon, L. Schwabe, O. Beck, P. Wiesing, K. Obermayer and M. Sur: Invariant computations in local cortical networks with balanced excitation and inhibition, Nature Neurosci. **8** (2005) 194.

(Matsumoto et al. 2007) N. Matsumoto, D. Ide, M. Watanabe, and M. Okada: Retrieval property of attractor network with synaptic depression, J. Phys. Soc. Jpn. **76** (2007) 084005.

(Meyer and van Vreeswijk 2002) C. Meyer and C. van Vreeswijk: Temporal correlations in stochastic networks of spiking neurons, Neural Comput. **14** (2001) 369.

(Mongillo et al. 2008) G. Mongillo, O. Barak and M. Tsodyks Synaptic theory of working memory, Science **319** (2008) 1543.

(Montani et al. 2009) Montani, F., Ince, R. a a, Senatore, R., Arabzadeh, E., Diamond, M. E., and Panzeri, S: The impact of high-order interactions on the rate of synchronous discharge and information transmission in somatosensory cortex. Philosophical trans-

actions. Series A, Mathematical, physical, and engineering sciences, **367(1901)** (2009) 3297-310.

(Morris 2003) R. G. Morris: Long-term potentiation and memory, Phil. Trans. R. Soc. Lond. B **358** (2003) 643.

(Newsome et al. 1989) W. T. Newsome, K. H. Britten and J. A. Movshon: Neuronal correlates of a perceptual decision, Nature **341** (1989) 52.

(Ohiorhenuan et al., 2010) Ohiorhenuan, I. E., Mechler, F., Purpura, K. P., Schmid, A. M., Hu, Q., and Victor, J. D. (2010). Sparse coding and high-order correlations in fine-scale cortical networks. Nature, 466(7306), 617-621.

(Ohiorhenuan and Victor 2011) Ohiorhenuan, I. E., and Victor, J. D. (2011). Information-geometric measure of 3-neuron firing patterns characterizes scale-dependence in cortical networks. Journal of computational neuroscience, 30(1), 125-41.

(Oizumi et al. 2010) M. Oizumi, K. Miura and M. Okada: Analytical investigation of the effects of lateral connections on the accuracy of population coding, Phys. Rev. E **81** (2010) 051905.

(Paradiso 1988) M. A. Paradiso: A theory for the use of visual orientation information which exploits the columnar structure of striate cortex, Biol. Cybern. **58** (1988) 35.

(Parisi 1998) G. Parisi *Statistical Field Theory* (Perseus Books Group), 1998.

(Perkel et al. 1967) D. H. Perkel, G. L. Gerstein and G. P. Moore: Neuronal spike trains and stochastic point processes, Biophys. J. **7** (1967) 391.

(Philips 1974) W. A. Philips: On the distinction between sensory storage and short-term visual memory, Percept. Psychophys. **16** (1974) 283.

(Priebe and Ferster 2008) N. J. Priebe and D. Ferster, Inhibition, spike threshold, and stimulus selectivity in primary visual cortex Neuron, 57(4), 482-97.

(Renart et al. 2010) A. Renart, J. de la Rocha, P. Bartho, L. Hollender, N. Parga, A. Reyes and K. D. Harris: The asynchronous state in cortical circuits, Scinece **327** (2010) 587.

(Riehle et al, 1997) Riehle, Alexa, Grun, S., Diesmann, M., and Aertsen, A. (1997). Spike Synchronization and Rate Modulation Differentially Involved in Motor Cortical Function. Science, 278(5345), 1950-1953.

(Rieke et al, 1997) Rieke, F., Warland D., Deruytervansteveninck R., and W. Bialek Spikes: Exploring the Neural Code. *T*he MIT Press, June 1999.

(Rothman et al. 2009) J. Rothman, L. Cathala, V. Steuber, and R. Silver: Synaptic depression enables neuronal gain control, Nature **457** (2009) 1015.

(Roxin, Brunel and Hansel 2005) A. Roxin, N. Brunel, and D. Hansel: Role of delays in

shaping spatiotemporal dynamics of neuronal activity in large networks, Phys. Rev. Lett. **94** (2005) 238103.

(Saintillan and Shelley 2008) D. Saintillan, D. and M. Shelley, Instabilities and Pattern Formation in Active Particle Suspensions: Kinetic Theory and Continuum Simulations. Phys. Rev. Lett., **100**(17), 1-4 (2008).

(Salzman et al. 1992) C. D. Salzman, C. M. Murasugi, K. H. Britten and W. T. Newsome: Microstimulation in visual area MT: Effects on direction discrimination Performance, J. Neurosci. **12** (1992) 2331.

(Schneidman et al., 2006) Schneidman, E., Berry, M. J., Segev, R., and Bialek, W. (2006). Weak pairwise correlations imply strongly correlated network states in a neural population. Nature, **440**(7087), 1007 (2006).

(Schwartz et al. 2007) O. Schwartz, A. Hsu and P. Dayan: Space and time in visual context, Nature Rev. Neurosci. **8** (2007) 522.

(Series et al. 2004) P. Series, P. E. Latham and A. Pouget: Tuning curve sharpening for orientation selectivity: coding efficiency and the impact of correlations, Nat. Neurosci. **7** (2004) 1129.

(Seung and Sompolinsky 1993) H. S. Seung and H. Sompolinsky: Simple models for reading neuronal population codes, Proc. Natl. Acac. Sci. USA **90** (1993) 10749.

(Shadlen and Newsome 1998) M. N. Shadlen and W. T. Newsome: The variable discharge of cortical neurons: Implications for connectivity, computation, and information Coding, J. Neurosci. **18** (1998) 3870.

(Sherrington and Kirkpatrick 1975) D. Sherrington and S. Kirkpatrick: Solvable model of a Spin-Glass, Phys. Rev. Lett. **35** (1975) 1792.

(Shlens et al., 2006) Shlens, J., Field, G. D., Gauthier, J. L., Grivich, M. I., Petrusca, D., Sher, A., Litke, A. M., *et al.* (2006). The structure of multi-neuron firing patterns in primate retina. J. Neurosci. **26**(32), 8254 (2006).

(Simoncelli 2003) E. P. Simoncelli: Vision and the statistics of the visual environment, Curr. Opin. Neurobiol. **13** (2003) 144?149.

(Singer 1999) W. Singer: Neuronal Synchrony: A versatile code for the definition of relations, neuron **24** (1999) 49.

(Sompolinsky et al. 2001) H. Sompolinsky, H. Yoon, K. Kang and M. Shamir: Population coding in neuronal systems with correlated noise, Phys. Rev. E **64** (2001) 051904.

(Stimberg et al. 2009) M. Stimberg, K. Wimmer, R. Martin, L. Schwabe, J. Marino, J. Schummers, D. C. Lyon, M. Sur and K. Obermayer: The operating regime of local computations in primary visual cortex, Cereb. Cortex **19** (2009) 2166.

(Suzuki and Kubo 1968) M. Suzuki and R. Kubo: Dynamics of the Ising model near the critical point. I, J. Phys. Soc. Jpn. **24**(1) 51 (1968).

(Teich and Qian 2003) A. F. Teich and N. Qian: Learning and adaptation in a recurrent model of V1 orientation selectivity, J. Neurophysiol. **89** (2003) 2086.

(Teramae and Tanaka) J. Teramae and D. Tanaka: "Noise induced phase synchronization of a general class of limit cycle oscillators" Prog. Theor. Phys. Suppl., **161**, 360 (2006).

(Thomson and Deuchars 1994) A. Thomson and J. Deuchars: Temporal and spatial properties of local circuits in neocortex, Trends Neurosci. **17** (1994) 119.

(Toyoizumi et al. 2008) T. Toyoizumi, K. R. Rad and L. Paninski: Mean-field approximations for coupled populations of generalized linear model spiking neurons with Markov refractoriness, Neural Comput. **21** (2009) 1203.

(Tsodyks and Markram 1997) M. Tsodyks and H. Markram: The neural code between neocortical pyramidal neurons depends on neurotransmitter release probability, Proc. Natl. Acad. Sci. U.S.A. **94** (1997) 719.

(Tsodyks et al. 1998) M. Tsodyks, K. Pawelzik, and H. Markram: Neural networks with dynamic synapses, Neural Comput. **10** (1998) 821.

(Tsodyks and Gilbert 2004) M. Tsodyks and C. Gilbert: Neural networks and perceptual learning, Nature **431** (2004) 775.

(Tulving and Schacter 1990) E. Tulving and D. L. Schacter: Priming and human memory systems, Science **247** (1990) 301.

(Turrigiano et al. 1998) G. G. Turrigiano, K. R. Leslie, N. S. Desai, L. C. Rutherford and S. B. Nelson: Activity-dependent scaling of quantal amplitude in neocortical neurons, Nature **391** (1998) 892.

(Turrigiano and Nelson 2004) G. G. Turrigiano and S. B. Nelson: Homeostatic plasticity in the developing nervous system. Nature Rev. Neurosci. **5** (2004) 97.

(Varela et al., 1997) J. A. Varela, K. Sen, J. Gibson, J. Fost, L. F. Abbott and S. B. Nelson: A Quantitative Description of Short-Term Plasticity at Excitatory Synapses in Layer 2 / 3 of Rat Primary Visual Cortex, J. Neurosci. **17**(20), 7926 (1997).

(Xu et al. 2007) W. Xu, X. Huang, K. Takagaki, and J. Wu: Compression and reflection of visually evoked cortical waves, Neuron **55** (2007) 119.

(York and van Rossum 2009) L. C. York and M. van Rossum: Recurrent networks with short term synaptic depression, J. Comput. Neurosci. **27** (2009) 607.

(Yoshimura et al, 2005) Yoshimura Yumiko, Dantzker Jami L. M., Callaway Edward M., Excitatory cortical neurons form fine-scale functional networks Nature, **1**(433), 7028 (2005).

(Yu and Ferster 2010) Yu, J., and Ferster, D. (2010). Membrane potential synchrony in primary visual cortex during sensory stimulation.Neuron, 68(6), 1187-201.

(Yu et al, 2011) S. Yu, H. Yang, H. Nakahara, G. S. Santos, D. Nikolic, and D, Plenz, The Journal of Neuroscience, **31**(48), 17514 (2011).

(Zohary et al 1994) E. Zohary, M. N. Shadlen and W. T. Newsome: Correlated neuronal discharge rate and its implications for psychophysical performance. Nature **370** (1994) 149.

(Zucker and Regehr 2002) R. S. Zucker and W. G. Regehr: Short-term synaptic plasticity, Annu. Rev. Physiol. **64** (2002) 355.

List of Publications

Peer Reviewed Papers

Y. Igarashi, M. Oizumi, Y. Otsubo, K. Nagata and M. Okada,
Statistical mechanics of attractor neural network models with synaptic depression,
Journal of Physics Conference Series **197**, 012018, 2009

Y. Igarashi, M. Oizumi and M. Okada,
Mean Field Analysis of Stochastic Neural Network Models with Synaptic Depression.
Journal of the Physical Society of Japan **79**, 084001, 2010.

Y. Igarashi, M. Oizumi and M. Okada,
Theory of correlation in a network with synaptic depression.
Physical Review E **85**, 016108, 2012.

Y. Katori, Y. Igarashi, M. Okada, and K. Aihara,
Stability Analysis of Stochastic Neural Network with Depression and Facilitation Synapses.
Journal of the Physical Society of Japan, **81**, 114007 2012.

R. Karakida, Y. Igarashi, K. Nagata, and M. Okada,
Inter-Layer Correlation in a Feed-Forward Network with Intra-Layer Common Noise
Journal of the Physical Society of Japan **82**, 064007, 2013.

I. Yamashita, K. Katahira, Y. Igarashi, K. Okanoya and M. Okada,
Recurrent network for multisensory integration-identification of common sources of audiovisual stimuli
Frontier in computational neuroscience, doi:10.3389 fncom.2013.00101, 2013

International conference

M. Okada, Y. Igarashi, Y. Otsubo, K. Nagata, M. Oizumi,
Statistical mechanics of attractor neural network models with synaptic depression,
International Workshop on Statistical- Mechanical Informatics 2009, Kyoto, September, 2009.

Y. Igarashi, M. Oizumi and M. Okada,
Theory of correlation in a network with short-term synaptic plasticity,
Computational and Systems Neuroscience (Cosyne) 2011, Salt City, USA, Feburary 24, 2011.

Y. Katori, Y. Igarashi, M. Okada, K. Aihara,
Stability Analysis on Stochastic Neural Network with Dynamic Synapses,
The 2nd International Symposium on Innovative Mathematical Modelling, Tokyo, May 15, 2012.

Y. Igarashi and M. Okada,
Higher order correlation in a feedforward networkwith lateral inhibition,
Sensory Coding and Natural Environment (SCNE) 2012, IST Austria, Klosterneuburg, Austria, September 10, 2012.

Y. Igarashi and M. Okada,
Theory of higher-order correlations neural network with columnar structure,
Computational and Systems Neuroscience (Cosyne) 2013, Salt Lake City, USA, March 1, 2013.